UNIVERSITÁ DEGLI STUDI DI PARMA

Dottorato di ricerca in Ingegneria Civile

Ciclo XXIII

Finite Element Analysis and Laboratory Investigation of Reinforced Road Pavements

Coordinatore:

Chiar.mo Prof. Gianfranco Forlani

Tutor:

Chiar.mo Prof. Antonio Montepara

Dottorando: **Valentina Rota**

Index.

Introduction and Literature Review.

In Italy most of the vehicular traffic is absorbed from the road infrastructures, both for commercial interchanges and for private passengers. Annually, the Italian Government ("Ministero delle Infrastrutture e dei Trasporti") draws up a report related to the infrastructures and transportation situation ("Conto Nazionale delle Infrastrutture e dei Trasporti") [1]. In 2009 the goods transit was equal to 197091 million tons and 62% of this quantity was transported on the Italian roadways. The scenario is not different considering the national passenger traffic. In fact during the same year, the Italian infrastructures supported 960573 million passing of passengers per km, but 92% was supported from road pavements.

These data highlight the importance to keep high quality level of the roadways, in order to provide a proper service to the road users. Moreover, an appropriate maintenance could extend the in-service life of the road pavements, taking into consideration the economic aspect. Usually, a high quality starts from an accurate design, which is the first and fundamental step. Sometime, projects can be supported by a preliminary study, in order to adopt the most suitable solution and get the best performance. Obviously, the investigations could be conducted in several ways, such as in a laboratory or testing real scale pavement in-situ or running simulations using specific software. On the other hand, the existing roadways could be rehabilitated adopting different strategies, according to the typology or the conditions of a specific road pavement and before a final reconstruction. The restoration of the superficial layers is a common technique to increase the serviceability of the roadways and it is often connected to the use of reinforcing systems, which eventually can help the lack of support of the existing base. However, both solutions could be considered a way to save money, since a correct design could guarantee a longer and better performance and a superficial maintenance could delay a total reconstruction.

This research work could be considered related to both the topics mentioned above. In fact, the

aim of this study was to set a new investigation method, as a proper support during the design of a project, although the whole work focused its attention on road pavements with reinforcing systems in a superficial position, which is a typical maintenance solution. There are several methods considered a worthy preliminary study before the finale project, such as a laboratory investigation or the analysis organized in-situ could provide useful information. However, in the last years the simulations are becoming a good technique to obtain reliable results investing less money and time. Discrete Element Analysis or Finite Element Analysis represent two examples of these new approaches. In particular, this study used this second typology of analyses making use of specific software, Abaqus. In fact, it was realized a model of a real scale sample which could reproduce a flexible pavement with a superficial reinforcing system. The multilayer model were simulated during the in-service conditions, reproducing for instance the passing of a vehicle with a fixed inflate pressure of the tyre and the stress/strain output were collected and analysed. This examination starting from a preliminary investigation related to the performance of the reinforced pavements, checking the differences between the pavements with certain kind of nets with the ones considered as a control sample. However, these simulations were compared with an analogous investigation carried out in the laboratory of the University of Parma. Here three typologies of samples were built (with steel net, with glass grid and without any kind of reinforcing system) following a strict procedure, which permitted to get real scale samples of a multilayer flexible pavement. Those slabs were tested in the laboratory carrying out the corresponding investigations simulated using the Finite Element software. The strain responses were collected in definite areas using electrical strain gauges, in order to study the distribution of the deformations. Obviously, a preliminary analysis of the information registered in the laboratory permitted to examine the diverse performance of the three typologies of slabs, likewise after the modelling studies. Finally, the data collected in the laboratory were compared with the ones got from the modelling outputs. These comparisons allowed to evaluate the reliability of the simulations and to validate the consistency of the results calculated by the software Abaqus. Therefore, this research work started with a proper laboratory investigation useful as a term of comparison for the Finite Element Analyses, which drew the attention on the multilayer flexible pavements with and without reinforcing systems in a superficial position. This object was jointed to a parallel evaluation of the reinforced infrastructures. However, this study would highlight the possibility to lay the bases for a new investigation method that could be related to any kind of road pavements and permit to reduce the laboratory or in-situ

investigations. In fact, as mentioned above, a suitable preliminary investigation during the design process would permit to avoid premature failures that could put an end to the in-service life of a road pavement.

This research work started with an introductory bibliography review, in order to evaluate the most relevant studies related to the investigations (simulations or in laboratory) of the reinforced road pavements. In the last ten years, the scientific publications put a lot of effort in the study of the reinforced pavements from different point of views. At the beginning of the XXI century Brown et al. [2] published a paper related to the reinforcing systems in the flexible pavements, which summarized the work developed at the University of Nottingham during the previous years. They collected data carrying out different tests in the laboratory, such as shear tests or flexure tests and investigating the benefits of the introduction of nets (steel, glass or polypropylene grids) in different positions of the superficial asphalt layers. This work was the basis of many studies until recently, such as the one developed by Rowe et al. [3] in 2009, which started from the results collected in the laboratories of Nottingham and highlighted one more time the advantage of the use of the reinforcing systems. In fact, they underlined that the presence of a net in the flexible pavements could help to prevent the reflective cracking phenomena. Moreover, the study related to the use of the reinforces were carried out in-situ, where it was possible to check the real effects of this interface systems. Al-Qadi et al. [4] started at the end of the last century to work on a proper validation of the data collected at the Virginia Tech laboratories (Virginia, USA). In fact, they performed experimental and analytical investigations to evaluate the performance of pavement sections with and without geotextile or geogrid between sub-grade and base course. Therefore, they monitored a road built in Bedford County (Virginia, USA) to quantify the benefits of the geosynthetics, as it was proved from the laboratory investigations. However, a full-scale accelerated performance test facility were studied in Alabama as well, by Powell [5], where 2.8 km of a multilayer flexible pavements were built and half of it were reinforced with a fibreglass geogrid positioned on the bottom of asphalt layers. After a preliminary analysis of the material quality control in laboratory, several million ESALs were applied on the surface of the experimental pavements in around 5 years and the benefits of the interface system were checked. In fact, in the test section, in which the geogrid was installed, rutting analyses were conducted, in order to draw conclusions related to the use of these reinforcing systems. More research studies were carried out using a full-scale

accelerated testing loading (ATLAS) machine at the University of Illinois (USA), where Al-Qadi et al. [6] tried to quantify the effectiveness of geogrids on low volume flexible pavement performance. The results collected in this study showed that the geogrid could reduce the horizontal shear deformations of the aggregate layer in the traffic direction. Additionally, it was possible to identify the optimal location of the geogrid, in order to obtain the best performance of the reinforcing system. In a further study, Perkins et al. [7] worked on a full-scale flexible pavement test sections, which was divided into four different area inserting three geosynthetic reinforcement products. Even though these sections were built in an indoor facility, they were loaded with a heavy vehicle simulator with a dual tire standard truck half axel, in order to simulate the real traffic conditions. The results showed the benefits of the reinforcing systems in terms of Traffic Benefit Ratio and the higher trend of the stress/strain responses on the control sections, the ones without any geosynthetics.

However, similar investigations could be carried out in the field, where it would be possible to monitor and examine a certain area of a real infrastructure with real traffic conditions. This can be considered the most realistic scenario, even if the cost in terms of time and money would be higher than analogous investigations in a laboratory. With this aim, Cox et al. [8] started to work a on a new field test section in Arkansas (USA) trying to understand the relative surface deformations due to dynamic loading. This study was conducted on sixteen sections (15 m long) reinforced with different geosynthetics and two base thickness, which were compared with a control section. The first results showed the effects of the geogrid with the difference thickness of base course. In fact, the contribution of the geosynthetics was observed in terms of a change in heave in those sections with a thinner base course. At the end of the last century, in Europe, the Portuguese Road Administration decided to study the performance of different anti-reflective cracking solutions placed on a damaged flexible pavement. Therefore, five experimental sections were built (using 4 different kinds of interlayer systems) and studied by Antunes et al. [9]. The effects of the different solutions adopted were monitored for few years, until 2005. The results showed the steel net had the best performance, followed by the section where a geotextile impregnated with bitumen was inserted.

These investigation methods are sometime compared to analogous simulations, which could model the laboratory tests or the analyses in-situ. In fact, the results collected at Virginia Smart Road, where combined by Al-Qadi et al. [10] with finite element modelling. This research work permitted to calibrate the simulations considering the instruments responses, which could

evaluate the effectiveness of the steel reinforcement in flexible pavements. At the same time, this study permitted to highlight the benefits of these interlayer systems inserted at the bottom of the base course. Further investigations were conducted by Tutumluer et al. [11, 12, 13], who combined tests in filed, discrete element modelling and finite element simulations. This work analysed the flexible pavements reinforced with geogrids inserted on the top of subgrade. Both investigation methods (real and modelling) demonstrated an improvement of the pavements responses and the performance, where an interlayer system was inserted.

The research works presented above were related to the performance of the flexible pavements with different kinds of reinforcing systems inserted at different depths. However, these investigations were also conducted on diverse typologies of roadways, such as rigid pavements where a jointed Portland Cement Concrete (PCC) layer is positioned on the bottom of an asphalt overlay. In fact, reinforcements could be inserted in the upper asphalt layers to rehabilitate an existing pavement or it could be considered an anti-reflective system. For instance, Doh et al. [14] carried out a laboratory investigation using multilayer beams composed by a jointed PCC layer, an asphalt concrete overlay and a geogrid in the middle. They testes four different kinds of grids and a significant retardation of the reflective cracking phenomena was observed in the reinforced samples, compared to the ones without any grid. Further studies on this kind of road pavements were run in-situ, where the responses of the reinforcements could be considered more realistic. In fact, Vervaecke et al. [15] reported the results collected in different sites in Belgium (Europe), where anti-cracking interface systems were used to rehabilitate existing road pavements consisting of concrete slabs. The different typologies of interface systems showed diverse trends. For instance, a steel reinforcement net or a geogrid were more efficient than SAMI or non-woven interface system delaying the reflective cracking phenomena. Moreover, there are research works which studied the same problems of this kind of pavements, but running simulations and avoiding any laboratory investigations as well, as tests in field. Kuo et al. [16] designed a Finite Element Model (FEM) of a cracked rigid pavement with a reinforced asphalt overlay. They simulated the three basic types of reflective cracking propagation, running eighteen FEM analysis cases. The results showed that the best positions for the geogrid was at the 1/3 depth of the overlay thickness, in order to obtain the maximum predicted service life. Similar studies were conducted at the University of Illinois (USA) by Baek et al. [17, 18, 19], who worked on the reflective cracking phenomena in the asphalt overlay, laid down on a jointed PCC base. This asphalt surface could be considered as a

rehabilitation method which is often reinforced with different kinds of interlayer systems, such as steel net or sand anti-fracture. This research worked on FEM analyses that tried to reproduce a real scale sample, in order to understand the behaviour of the pavements in the jointed area. These investigations permitted to highlight the benefits of the interlayer system to prevent reflective cracking phenomena.

The research works presented above showed different approaches to study reinforced road pavements and the versatility of the use of these interlayer systems. However, the bases of this research work could be considered the studies carried out at the University of Parma in the last year. In fact, Montepara et al. [20, 21, 22, 23, 24] organized a study related to the reinforcing systems inserted in flexible multilayer samples. The investigation was conducted in the laboratory and in field trying to examine the behaviour of the reinforce pavements compared to the unreinforced ones. In fact, the investigations conducted by Montepara et al. started collecting data in the field. They tried to laid the bases for a laboratory analysis, which could be defined a real scale study. Therefore, the research work presented in this thesis took advantage of these previous experiences and results, but tried to move forward with further investigations both in the laboratory and working on Finite Element Modelling.

CHAPTER 1

Laboratory.

The laboratory section was carried out on real scale samples of a multilayer road structure that would recreate a typical flexible pavement, in order to collect reliable data to validate the analogous Finite Element Analyses. Specimens were totally manufactured in the laboratory starting from the mixing of the asphalt concretes, passing through the characterization of the materials and concluding with the compaction phase. In fact, different kinds of samples were realized to reproduce road pavements with or without reinforcing systems. Moreover, this laboratory investigation, as well as FE Analyses, simulated the in-service life of road pavements, such as the passing of a wheel truck. This phase of the research work was set as a strict laboratory study. Moreover, several investigations were necessary to make sure that the collected results were trustworthy and comparable with the equivalent Finite Element Analyses.

1.1 Asphalt Materials.

The samples were manufactured using a typical Italian Hot Mix Asphalt, designed following Italian CIRS instructions [25], in order to recreate a 3-layers flexible pavement. Hence, three different asphalt mixtures were used to create the strata of the specimens, but using alike limestone aggregates from Northern Italy and the same natural bitumen (PG 64-28) shown in Table 1.1.

Table 1.1 Characteristics of natural bitumen.

Natural Bitumen 70/100	
Penetration index [dmm]	77.67
Softening-Point Ring&Ball [°C]	48.3
Breaking-Point Fraass [°C]	-14

The three asphalt concretes were a typical base (0÷30 mm), binder (0÷15 mm) and wearing (0÷10 mm). The particle-size curves of the wearing course, the binder layer and the base course are shown in Figures 1.1, where the amount of filler is different for base (5.7%) and the superficial layers (7.7%).

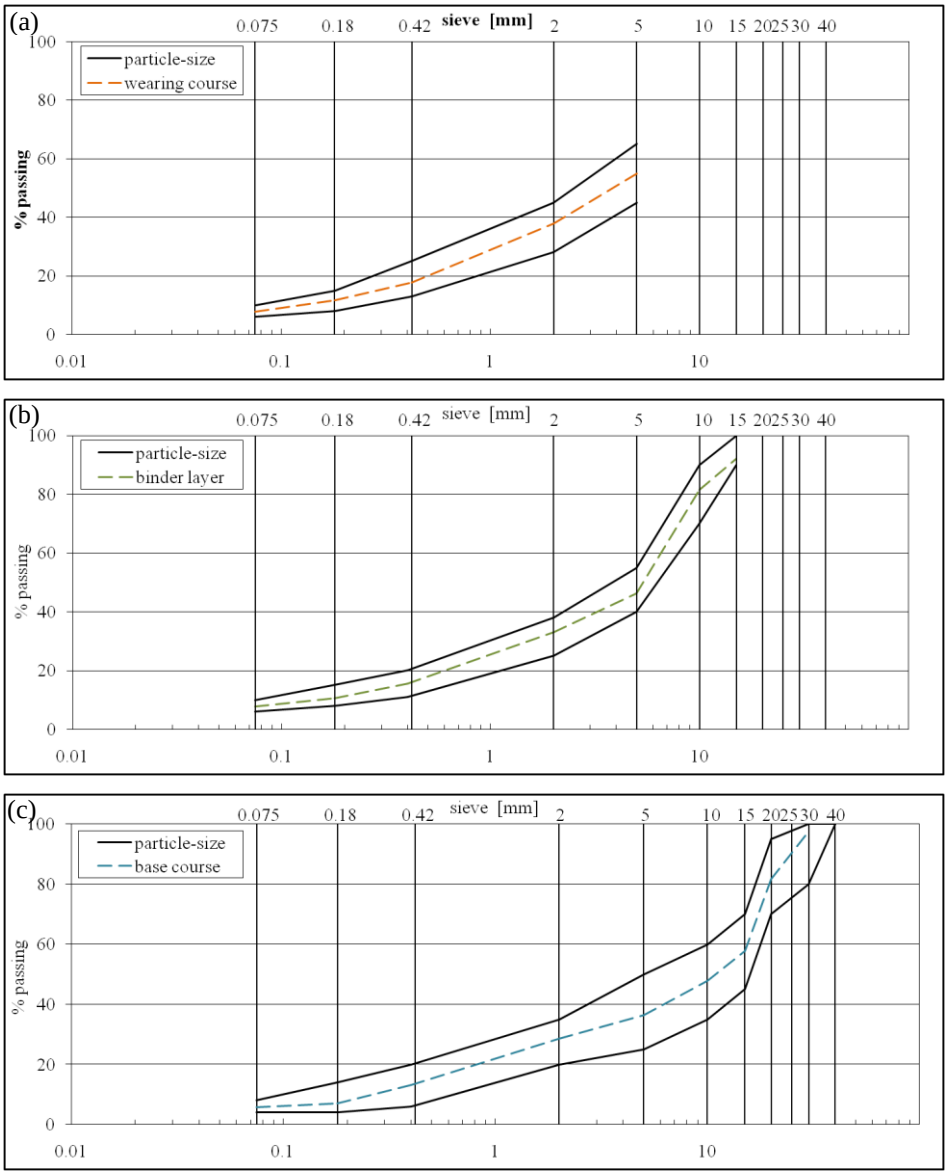

Figure 1.1 Particle-size curves of the wearing course (a), binder layer (b) and base course (c).

Moreover, the percentage of bitumen was chosen in the suggested range of the followed instructions and building density curves, in order to make the mixtures workable (Figures 1.2).

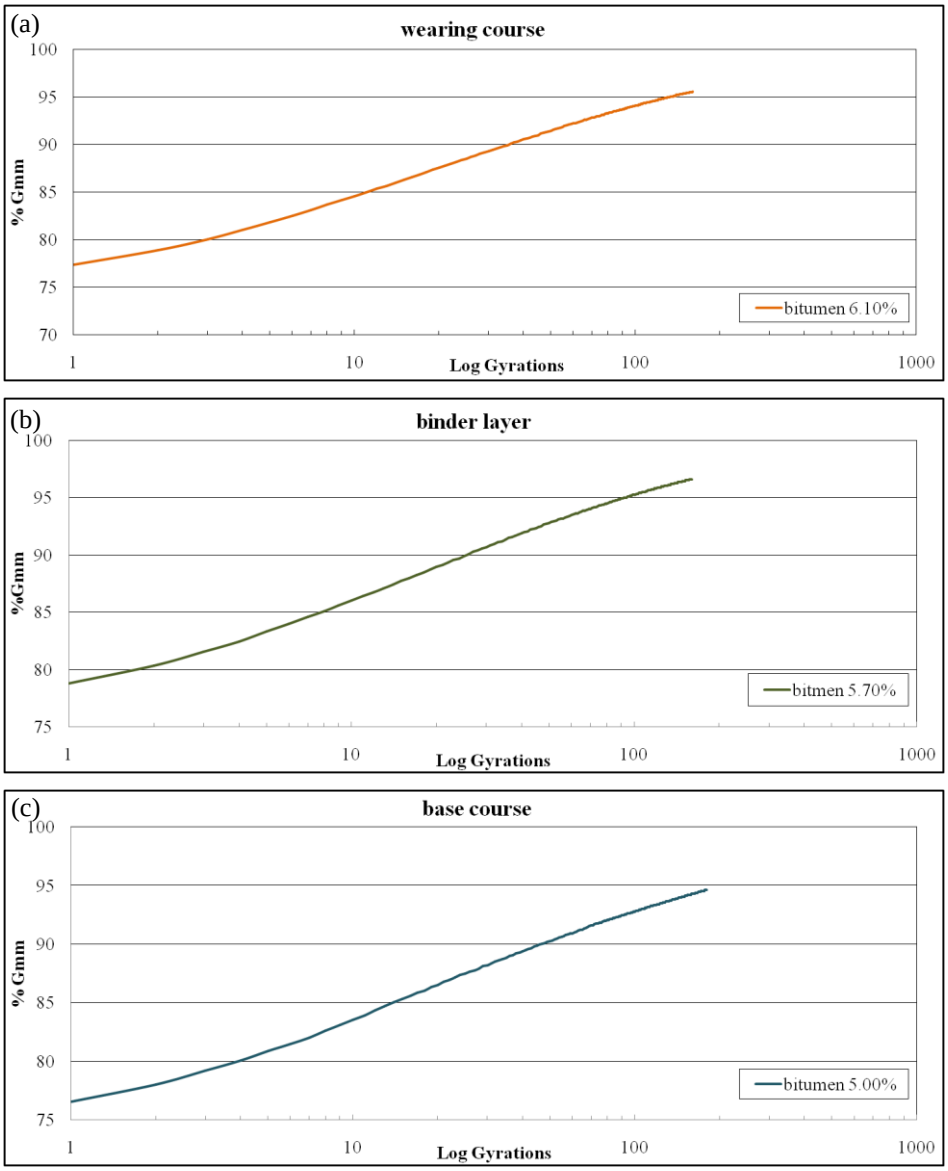

Figure 1.2 Density curves of wearing course (a), binder layer (b) and base course (c).

At this point, the asphalt materials were prepared using a proper asphalt mixer (Figure 1.3). In fact, the aggregates were heated in an oven at the temperature of 150°C and mixed with the asphalt binder at the same temperature. Once the mixture was homogeneous, the filler was

added in the mixer and the material was put again in an oven at 150°C to make the temperature uniform.

Figure 1.3 Asphalt Mixer available at the University of Parma.

In the following step, these asphalt mixtures were compacted using a heavy compactor specifically built up for the University of Parma. However, before the creation of the tested samples, it was necessary to set the compaction procedure to obtain the percentage voids suggested from the followed Italian instructions with these specific materials. For this reason, several slabs were manufactured changing the setting parameters of that heavy compactor, but using the same asphalt mixture. In fact, this equipment is composed by a cylindrical horizontally pivoted steel cap, placed under a hydraulic press that can give pressure until 35 bar. Below this press there is a mobile basement, where it is possible to situate a steel squared formwork (500 mm x 500 mm) with different depths. The compaction process takes place when the formwork moves back-and-forth on the mobile basement and the hydraulic press gives a certain pressure (Figure 1.4).

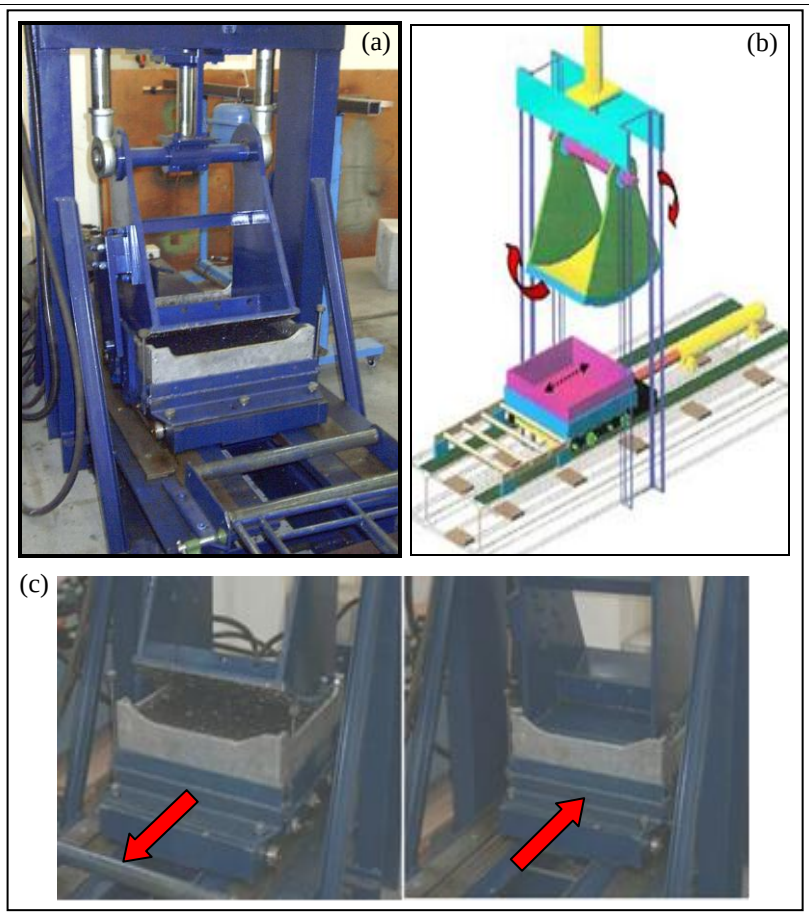

Figure 1.4 Heavy compactor (a), the relative scheme (b) and the same machine during the compaction process (c).

This movement reproduces the same conditions of a rolling compactor in the field. Moreover, setting the hydraulic press at 33 bar means that the compaction of the loose material is carried out with a peak pressure of 31 bar. Indeed, it is reasonable to take into account a 5-7% of loss during the compaction phase, caused by the shape of the hydraulic pressure pipes. Therefore, considering a real rolling compactor of steel with a mass of 12000 kg, its front module weights 6000 kg and it is 1950 mm long. So, in the field, this can be translated with a pressure of 31 bar applied on a strip about 10 mm large below the roller, which is exactly the same level of compaction of the heavy compactor used in this research work. Consequently, the equipment mentioned above, was used to prepare mono-material slabs where only the number of passing

of the press were different, and the applied pressure was the same. As a result, those different slabs were cut in several prismatic pieces, in order to check the distribution of the air voids in the whole sample (Figure 1.5).

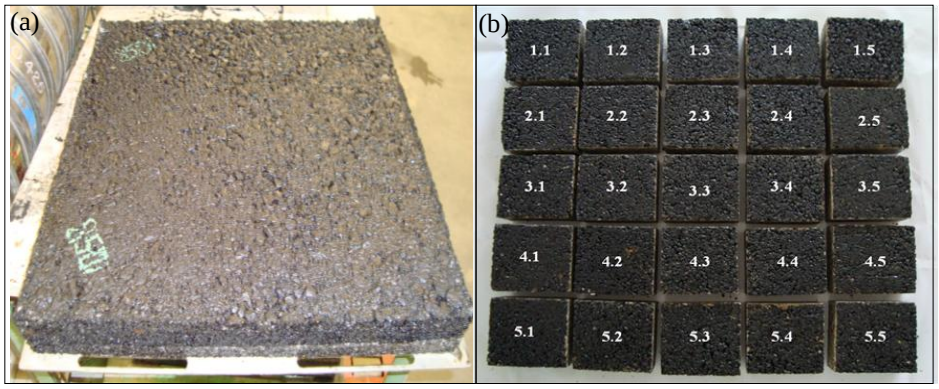

Figure 1.5 Mono-material slab (a) and the 25 prisms used for the volumetric analysis (b).

After several attempts, a homogeneous percentage of voids in the asphalt mixtures were defined and the range prescribed from the followed instructions was reached. In fact, it was possible to find a relation between the number of passing of the heavy compactor and the percentage of air voids [26]. Moreover, the volumetric properties were collected following the AASHTO or ASTM American guidelines, in order to characterize the three asphalt mixtures (Table 1.2).

Table 1.2 Volumetric properties of the three asphalt mixtures.

Volumetric Properties	**Wearing**	**Binder**	**Base**	**Regulation**
Asphalt Content P_b [%]	6.1	5.7	5.0	(fixed)
Percent Stone P_s [%]	88.65	90.45	92.26	(fixed)
Bulk Specific Gravity of Mix G_{mb} [g/cm^3]	2.3019	2.3530	2.3989	AASHTO T 166
Maximum Specific Gravity of Mix G_{mm} [g/cm^3]	2.4295	2.4473	2.4664	ASTM D 2041
Bulk Specific Gravity of Aggregates G_{sb} [g/cm^3]	2.4892	2.4935	2.4729	AASHTO T84 -T 85
Percent Voids Total Mix VTM [%]	5.25	3.85	2.74	-
Voids in Mineral Aggregates VMA [%]	18.02	14.65	10.50	-
Percent Voids Filled with Asphalt VFA [%]	70.95	73.73	74.09	-

After the volumetric characterization, new slabs mono-material were compacted following the same procedure explained above, but to collect Dynamic Complex Modulus (|E*|) and corresponding Phase Angles (ϕ) following AASHTO TP 62-03 guideline. In fact, from these new slabs were cored 5 cylinders 100 mm diameter and about 150 mm height in the central area of the samples (Figure 1.6) and the test was carried out on the 15 cores (three for each asphalt mixtures).

Figure 1.6 Slabs compacted (a) and cored (b) to obtain cylindrical samples.

In Figures 1.7 the mechanical characterization of each asphalt mixture is shown. In fact, from those tests three different Master Curves were designed with a sigmoidal shape (see the equations on the charts) and the corresponding Black Curves, where the phase angles were related to the Dynamic Complex Moduli.

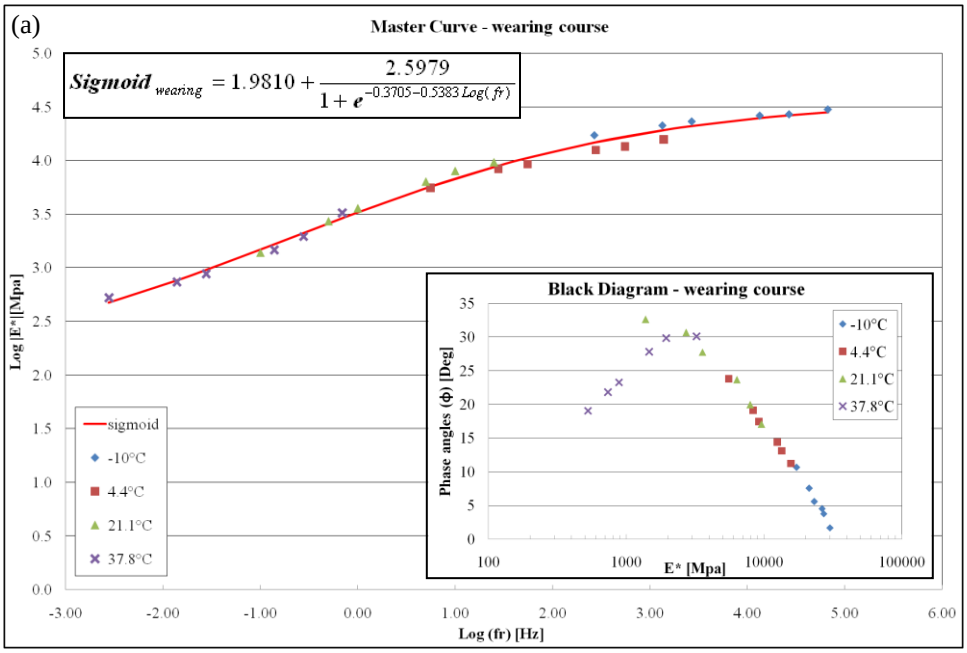

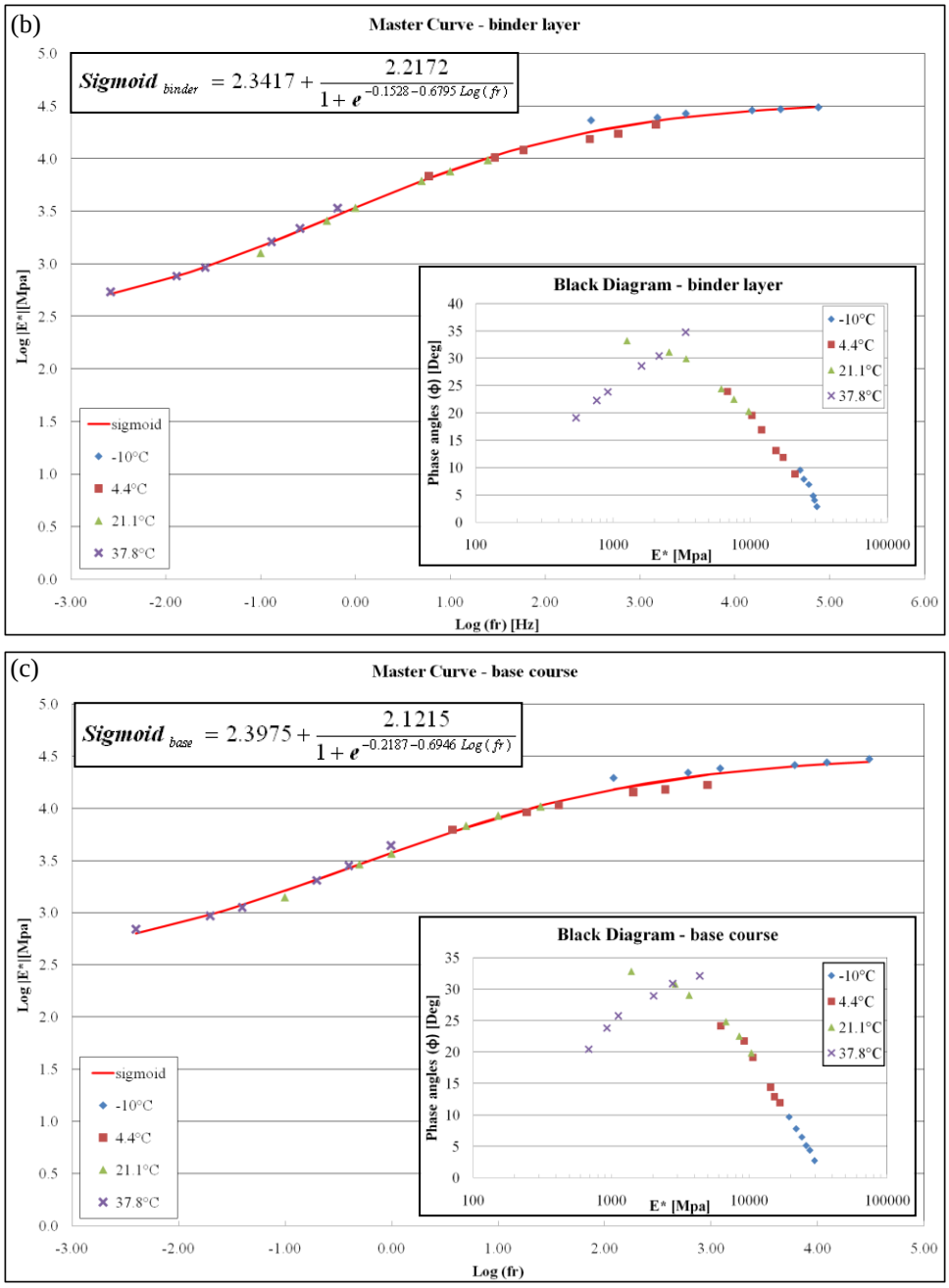

Figure 1.7 Dynamic Complex modulus master curves with relative equation and Black Diagram for wearing course (a), binder layer (b) and base course (c).

After these analyses, asphalt mixtures were described from volumetric and mechanical points of view and it was possible to state the reliability of the materials was totally guaranteed.

1.2 Samples.

The slabs tested in the laboratory were created using the same materials mentioned above as well as the same compactor and following the procedure explained in the previous paragraph. In that way, three different typologies of real scale samples were assembled as a square with 500mm size length, the same of the compactor formwork. However, in each specimen three asphalt strata with different thickness were created in order to recreate a real flexible pavement, as shown in Table 1.3.

Table 1.3 Features of multilayer flexible slabs from top to bottom.

MULTILAYER FLEXIBLE SLABS		
Stratum	**Thickness [mm]**	**Maximum aggregate size [mm]**
Wearing course	30	10
Binder layer	40	15
Base course	100	30

Therefore, the difference among the specimens consisted in inserting a reinforcing system positioned between the binder layer and the base course and totally embedded in the upper stratum. In one of the typology of slab a hexagonal steel net with transversal reinforcing bars was inserted (Figure 1.8) and the characteristics are explained in Table 1.4 (see in the Chapter 2 Figure 2.10 for the geometric characteristics).

Figure 1.8 Steel net reinforcing system (a) and a detail of the double twisted grid.

Table 1.4 Features of steel net reinforcing system.

STEEL NET	
Steel Net Diameter	2.4 mm
Reinforcing Bar Diameter	4.4 mm
Longitudinal Stiffness	22.7 MN/m
Transversal Stiffness	19.5 MN/m
Longitudinal Nominal Stiffness	35.00 MN/m
Transversal Nominal Stiffness	50.00 MN/m
Elastic Modulus (E)	200000 MPa

A second typology of slab was equipped with a different kind of reinforce: a glass grid composed by a squared mesh and with a thin bitumen film to guarantee a better adhesion with Hot Mix Asphalt (Figure 1.9). The characteristics are explained in Table 1.5 (Figure 2.11, Chapter 2 for the geometric characteristics).

Figure 1.9 Picture of the glass grid reinforcing system (a) and a detail of the squared net (b).

Table 1.5 Features of glass grid reinforcing system.

GLASS GRID	
Longitudinal Nominal Strength	100 KN/m
Typical Longitudinal Elongation (under max load)	<4%
Transversal Strength	100 KN/m
Typical Transversal Elongation (under max loading)	<4%
Elastic Modulus (E)	76 GPa

However, it was realized control samples, where there was not inserted any reinforcing system. That was necessary to make proper comparisons during this laboratory section, as well as in the Finite Element Analysis.

The procedure to assembly the multilayer slabs was divided into two steps. In the first one the upper layers (wearing and binder) were compacted one upon the other one. In the second step the base courses were created separately. In this way it was possible to monitor and record the deformations between the binder layer and the base course, where the reinforcement was

positioned applying strain gauges. Therefore, in the first step a certain amount of the binder mixture was prepared with the asphalt mixer and with this material at the uniform temperature of 150°C, a 40 mm thick slab was created using the heavy compactor. When this layer reached the room temperature, a wearing course layer 30 mm thick was compacted on the binder layer using the wearing mixture prepared with the same procedure mentioned above. In two typologies of slabs the reinforcing system were positioned at the bottom of the formwork of the compactor and so it was totally embedded into the asphalt mixture of the binder layer In particular, the steel net was placed with an entire hexagonal mesh without reinforcing bar in the centre area of the samples (Figure 1.10a). Since glass grid has a regular squared shape, it was simply positioned at the bottom of the formwork (Figure 1.10b). In the second step, slabs of 100 mm thick were created with the base mixture in a subsequent stage, but following the same procedure of compaction.

Figure 1.10 Reinforcing systems positioned in the formwork: steel net (a) and glass grid (b).

At the end of these two steps, a suitable procedure to assembly the surface layers and the base course was designed to guarantee proper adhesion and connection during the testing phase and in order to avoid any debonding phenomenon. It was important to assure the stress/strain responses of these real scale samples as an in continuum model. For this reason a shear test was design to set and control the interface characteristics.

1.3 Shear test.

The aim of this test was to define a straightforward methodology, in order to prepare real scale multilayer samples that could perform as an in-situ road flexible pavement of asphalt concrete mixtures during this laboratory section. A preliminary bibliography research showed that this is a widespread topic studied in several scientific investigations, to examine the crucial point of the interactions between layers in road infrastructures. A useful report created by the Illinois Center for Transportation in 2008 is an extensive survey of the most important studies focused on this topic [27] in these last years, besides being a reliable laboratory investigation. Therefore, a suitable shear test was set based on previous works and after several attempts. Cylinders with 150 mm diameter and around 60 mm height were manufactured with a Gyratory Compactor set at 600 kPa and 100 gyrations. Half of them were realized using the base mixture, but for the others binder asphalt concrete was used. In this case it was not important to take into consideration the volumetric properties of the samples, since during the shear test the interface behaviour was investigated and the most important aspect of the cylinder was the smoothness of the surface, the asphalt mixtures used and the aggregate sizes. Those specimens would have just recreated the surfaces to be put in contact in the real scale samples. Moreover, any reinforcing system was not inserted in the middle of the tested samples, since the presence of an interlocked net cannot compromise the effect of the interface shear strength [2]. The two kinds of cylinders were put inside the two halves of a non-deformable steel box, dipped in cement mortar, but with the interface area clear which was checkable while the tests were carried out. Natural binder (PG 64-28) was used to put the surfaces in contact with an amount rate of 0.92 l/m^2 and was spread at the temperature of 150°C on both surfaces in contact. Moreover, the tests were carried out using a Material Test System machine (MTS) setting the displacement rate at 0.042 mm/s [28] and the pressure normal to the interface shear zone at 0.002 MPa. This value was calculated considering the weight of the asphalt material that rested on the interface zone of the real scale samples, which is represented by the two surface layers (wearing and binder course). These two strata were 70 mm thick (Table 1.3) and the weight is around 4.2 kN, considering a slab of 500 mm x 500 mm. This meant that on the cylinders used for the shear tests, 0.35 kN were applied using loading cells (Figure 1.11).

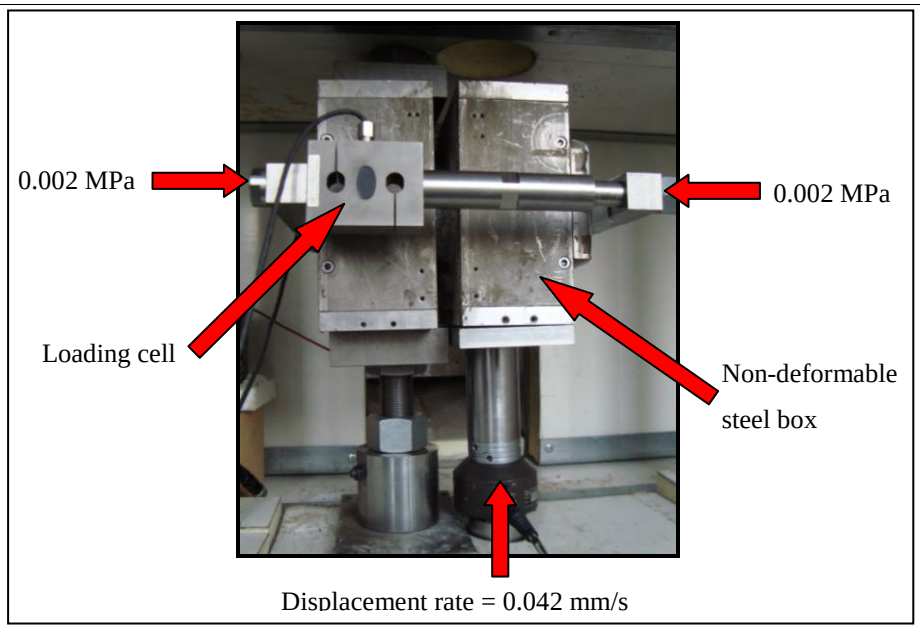

Figure 1.11 Set-up configuration of the shear test.

One more important aspect of the test set-up was related to the pressure applied to make perfectly in contact the two halves of the cylinder inserted into the steel box, besides the time of the application of this force before the execution of the shear tests. The pressure of 600 kPa of the Gyratory Compactor was assumed as a reference, which was the same applied during the creation of the cylinders for these shear tests. In summary, it means that the cylinders prepared with that Gyratory Compactor were dipped into the cement mortar inside the steel box, and then hot natural bitumen at 150°C was spread on the two surfaces which were put in contact. Finally the proper adhesion was recreated applying around 10÷11 kN with the two load cells. In few minutes (around 3) the load cells reached the maximum value of load and after half an hour the load cells were applying a load approximately equal to zero. The test was carried out when the bitumen reached the room temperature and the sample could be considered completely adherent (Figure 1.12). This "fixing procedure" was executed at room temperature (around 15÷20°C).

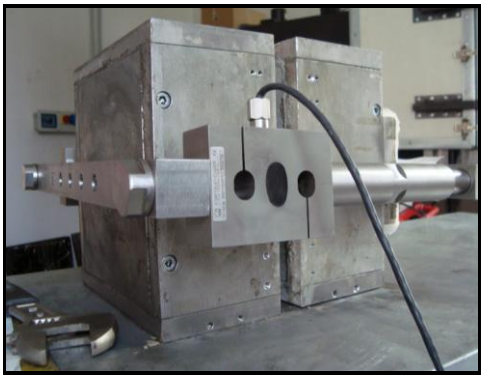

Figure 1.12 "Fixing procedure" for the preparation of the shear test samples.

Finally, it was fundamental to check if the load applied on the steel box with the two asphalt cylinders put inside would have caused permanent deformations. In that case the samples and the test itself would have been unreliable. Therefore, a new "test" was set to investigate the performance of the three different asphalt mixtures. Hence, on cylindrical samples a constant displacement rate was applied, in order to check the behaviour of the material before and post the failure range. For this purpose, cores 100 mm diameter taken from those mono-material slabs created to get samples to collect Dynamic Complex Moduli were used [see paragraph 1.1 "Asphalt Materials"]. Those cylindrical specimens could guarantee the same performance of the real scale slabs tested in this laboratory section, since they had equivalent features (composition of the mixtures and compaction method, as well as volumetric and mechanical characteristics). Hence, this test was again carried out using the MTS machine and with the displacement control set at 0.084 mm/s until the complete failure of the cylinders. This further investigation was carried out at the room temperature (around 15÷20°C), the same set during the "fixing procedure". Figure 1.13 shows few imagines during this investigation. Moreover, in Figure 1.14 the load-displacement curves are shown for each asphalt mixture (the wearing, binder and base respectively).

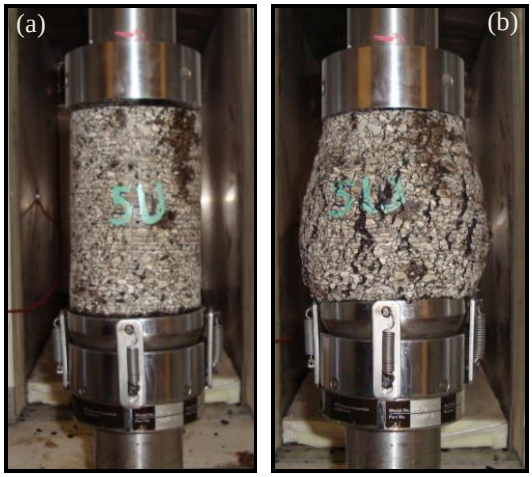

Figure 1.13 Cylindrical samples tested to investigate the elastic behaviour of the asphalt mixtures.

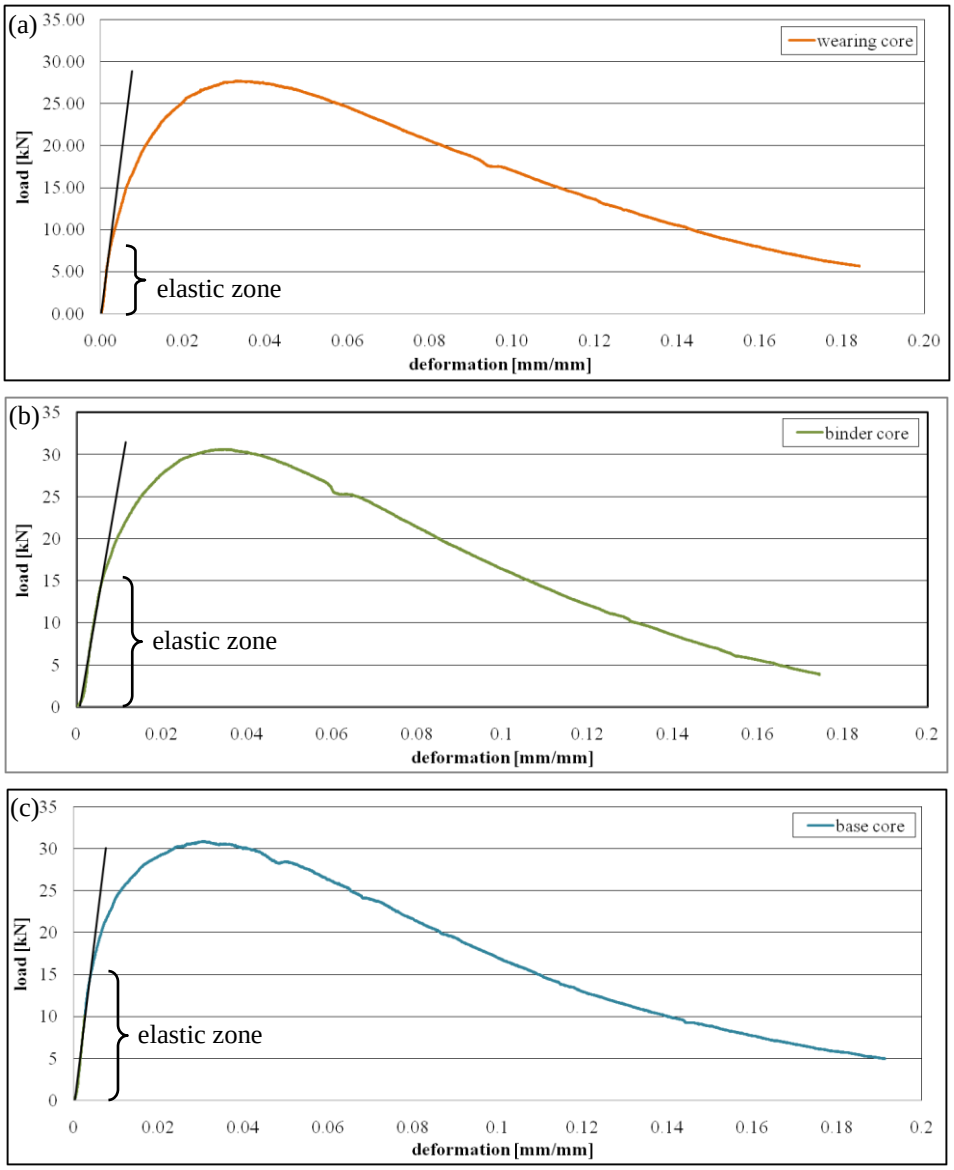

Figure 1.14 Elastic zone of the wearing course (a), binder layer (b) and base course (c) mixture.

The graphs in the last Figure show the range of the elastic zone in the three different mixtures. The analysis of those curves highlighted that the elastic range was minimum for the wearing asphalt mixture core, which was around 7÷8 kN. Applying this force on a 100 mm diameter cylinder, it can be transformed into a pressure of 900÷1000 kPa. Therefore, the asphalt mixtures

during the "fixing procedure" of the shear tests could be considered in a range of fully elasticity, since the load applied on the shear box (600 kPa) was 30÷40% less than the minimum value highlighted in the three previous Figures. After this last control, it was possible to state that the set-up of the shear test was trustworthy.

After these fundamental steps, several shear tests were carried out following the procedure explained above and at the temperature of 10°C, in order to keep the asphalt mixture in a visco-elastic domain [29] and avoid any plastic damage.
Figure 1.15 shows an average of the results collected during the shear tests: the interface shear strength versus displacement in mm and the peak value is around 0.60 MPa.

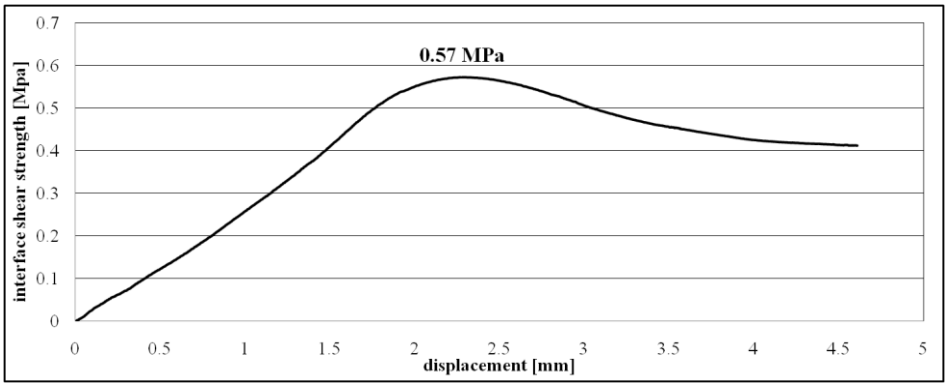

Figure 1.15 Results collected during shear test and the maximum interface shear strength.

Is it possible to state that this is a suitable interface shear strength according to the purpose of this work? In fact, the aim of this shear test was to guarantee a proper adhesion between the binder layer and the base course which was created separately and connected during the carrying out phase of the real scale slabs during the laboratory section. As mentioned in the introduction of this chapter, this consisted on applying a certain pressure which can reproduce the traffic load on a multilayer flexible pavement. Consequently, in order to answer to the question above, a further investigation became necessary. Therefore, the software BISAR was used to reproduce the same multilayer pavements created in the laboratory and simulating the passing of a truck wheel. In that way it was possible to check the horizontal stress level at the interface between the binder layer and the base course. This software considers a semi-

indefinite multilayer system, where the asphalt mixtures are isotropic linear elastic. In Figure 1.16 the Block Report is shown and it summarizes the results coming from the simulation with the software BISAR. The horizontal stress between the binder layer and the base course is around 16 times less than the peak interface shear strength collected with the shear tests in the laboratory. In fact, in Figure 1.16 it is possible to check the value of the horizontal shear stress between the binder layer and the base course calculated using BISAR (0.03495 MPa) and to compare it with the same datum get from the laboratory investigations (0.57 MPa). Therefore, even if BISAR makes a preliminary assumption of linear elasticity and the laboratory shear tests considered the material as a visco-elastic mixture, this considerable difference between the two values could make the interface shear strength reliable and the two upper surfaces could be considered an in-continuum system with the base layer.

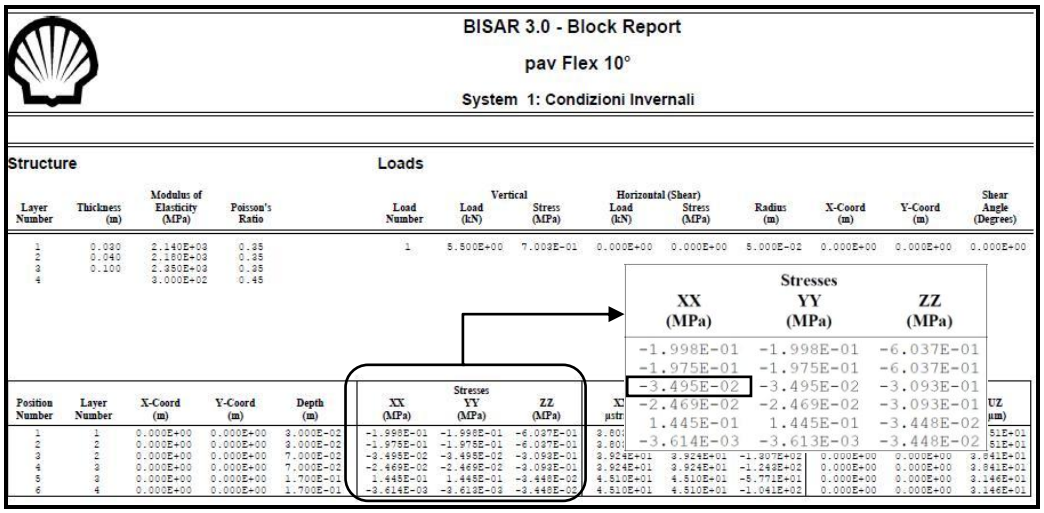

BISAR 3.0 - Block Report

pav Flex 10°

System 1: Condizioni Invernali

Structure

Layer Number	Thickness (m)	Modulus of Elasticity (MPa)	Poisson's Ratio
1	0.030	2.140E+03	0.35
2	0.040	2.160E+03	0.35
3	0.100	2.350E+03	0.35
4		3.000E+02	0.45

Loads

Load Number	Vertical Load (kN)	Vertical Stress (MPa)	Horizontal (Shear) Load (kN)	Horizontal (Shear) Stress (MPa)	Radius (m)	X-Coord (m)	Y-Coord (m)	Shear Angle (Degrees)
1	5.500E+00	7.003E-01	0.000E+00	0.000E+00	5.000E-02	0.000E+00	0.000E+00	0.000E+00

Position Number	Layer Number	X-Coord (m)	Y-Coord (m)	Depth (m)	Stresses XX (MPa)	Stresses YY (MPa)	Stresses ZZ (MPa)	XI µstr					UZ µm)
1	1	0.000E+00	0.000E+00	3.000E-02	-1.998E-01	-1.998E-01	-6.037E-01	3.80					51E+01
2	2	0.000E+00	0.000E+00	3.000E-02	-1.975E-01	-1.975E-01	-6.037E-01	3.80					51E+01
3	2	0.000E+00	0.000E+00	7.000E-02	-3.495E-02	-3.495E-02	-3.093E-01	3.924E+01	3.924E+01	-1.807E+02	0.000E+00	0.000E+00	3.841E+01
4	3	0.000E+00	0.000E+00	7.000E-02	-2.469E-02	-2.469E-02	-3.093E-01	3.924E+01	3.924E+01	-1.243E+02	0.000E+00	0.000E+00	3.841E+01
5	3	0.000E+00	0.000E+00	1.700E-01	1.445E-01	1.445E-01	-3.448E-02	4.510E+01	4.510E+01	-5.771E+01	0.000E+00	0.000E+00	3.146E+01
6	4	0.000E+00	0.000E+00	1.700E-01	-3.614E-03	-3.613E-03	-3.448E-02	4.510E+01	4.510E+01	-1.041E+02	0.000E+00	0.000E+00	3.146E+01

Stresses

XX (MPa)	YY (MPa)	ZZ (MPa)
-1.998E-01	-1.998E-01	-6.037E-01
-1.975E-01	-1.975E-01	-6.037E-01
-3.495E-02	-3.495E-02	-3.093E-01
-2.469E-02	-2.469E-02	-3.093E-01
1.445E-01	1.445E-01	-3.448E-02
-3.614E-03	-3.613E-03	-3.448E-02

Figure 1.16 Bisar report with the horizontal stress between base and binder layer highlighted.

Consequently, it was possible to state the method set to assembly the slabs for this laboratory section was consistent and it permitted to say the multilayer samples could work in continuum.

1.4 Test set-up.

The aim of this work was to analyse the responses of a reinforced flexible pavement during the in-service life. So, the laboratory investigations were carried out using the MTS machine and setting the temperature at 10°C, in order to maintain the material in a visco-elastic domain. Therefore, on the top of the specimens, on the central zone of the wearing course, a circular loading mark with 100 mm diameter was set with the purpose of simulating the wheel of a truck. Obviously, the dimension of the samples as well as the loading mark could be considered on a smaller scale compared with the in-situ situation. However, the set-up of this configuration was studied during previous research works at the University of Parma, as regard the real conditions [21]. The load matched the inflate pressure of a truck wheel, that normally is set around 7 bar. Considering an equivalent axel load in Italy, that is usually 6000 kg, it means a load of 5.5 kN applied on the wearing surface of the multilayer laboratory slabs (Figure 1.17).

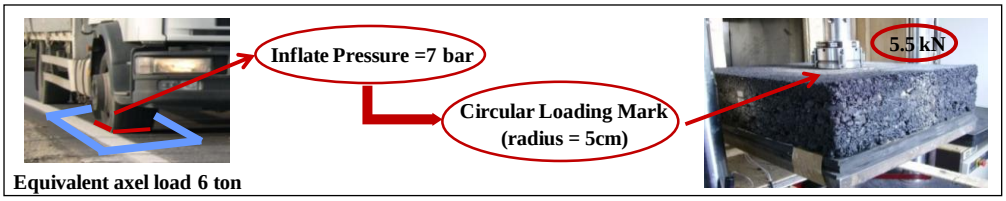

Figure 1.17 The correlation between the equivalent axel load and the equivalent laboratory investigation.

Moreover, the multilayer slabs were tested positioning the specimens on a neoprene stratum 40 mm thick, in order to recreate a sub-base layer [20]. In fact, this polymeric material can simulate 150 mm of sub-base layer with a Deformation Modulus (M_d) of 500 kN/mm^2 and the whole tested slab is shown in Figure 1.18.

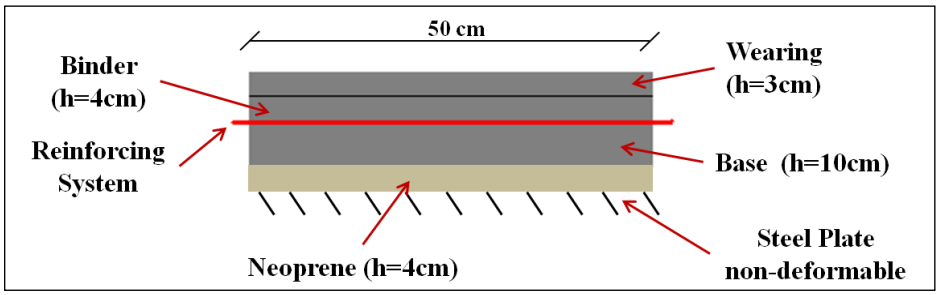

Figure 1.18 The strata of the asphalt multilayer slabs.

In order to record the performance of tested slabs, several strain gauges were positioned around the load mark and at the interface of the binder and base layers (see paragraph 1.2 "Samples"). This equipment consisted of electrical gauges that could register the deformations in one direction and they were connected to a National Instrument control unit system. This tool was set inserting proper parameters, such as gauge factors, and the calibration was automatic, in order to collect reliable results. Moreover, these strain gauges were positioned where the highest deformations would have expected. Figure 1.19 shows a scheme of the multilayer slabs with strain gauges on the top of the wearing course and on the upper surface of the base stratum. These acquisition devices were placed around the load mark and perpendicularly, in order to investigate the growth of the deformations on the surface of the slabs in both directions. In Figure 1.19 the strain gauges I and L were 60 mm long instead of the ones coloured in red, which were 100 mm long.

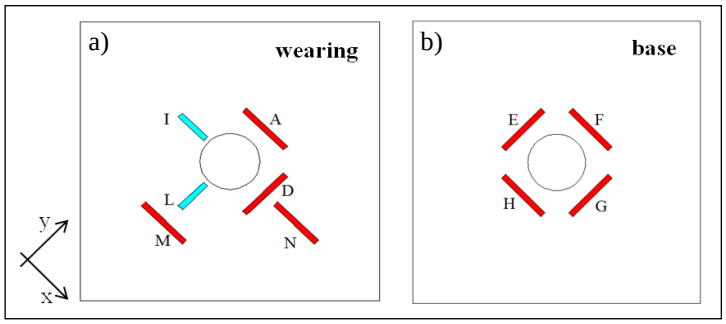

Figure 1.19 Position of the strain gauges on the wearing course (a) and on the base course (b).

Following this set-up, diverse tests were carried out: static and dynamic. The first one was a classic creep test, in which the load of 5.5 kN was statically applied for 1000 seconds. At the end of this initial loading phase, the load was quickly removed. However, the deformations were recorded for further 1000 seconds (Figure 1.20). Consequently, this kind of investigation could provide information related to the stress/strain behaviour of these multilayer slabs and the respective asphalt mixtures responses during loading phase besides the following recovery step. Therefore, this static test could inform about the effects of a heavy vehicle stop on a flexible pavement and its consequent effects after its removal.

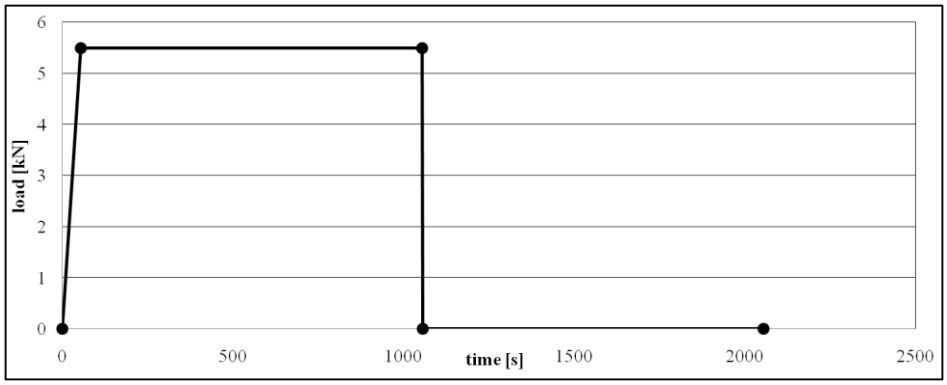

Figure 1.20 Creep test carried out on multilayer slabs.

The dynamic tests consisted in applying a sinusoidal load, in order to simulate the repeating passing of vehicles. The tests were carried out at two different frequencies: 0.5 Hz and 2 Hz. These values are set using the Klomp equation (1), which is an empirical formula. It established a relation between frequency and velocity [30].

$$Frequency = 0.4 \cdot V \tag{1}$$

In this equation, frequency is expressed in Hz and velocity (V) in km/h. The highest frequency selected meant a vehicle speed of 5km/h. While 0.5 Hz corresponded to a vehicle in a manoeuvre stage that meant a velocity lower than 5 km per hour. This choice permitted to investigate the behaviour of the road pavements under a cyclic passing of vehicles with low

speed that is when traffic loads are more important. Using these two load waves, two different tests were carried out. In the first one 100 load cycles were applying on the slabs at the two different frequencies. However, the second typology was analogous to the first phase of the creep mentioned above, even if the loading procedure consisted of a sinusoidal wave instead of a constant load. Figure 1.21 shows the load trend at the two frequencies during the dynamic tests.

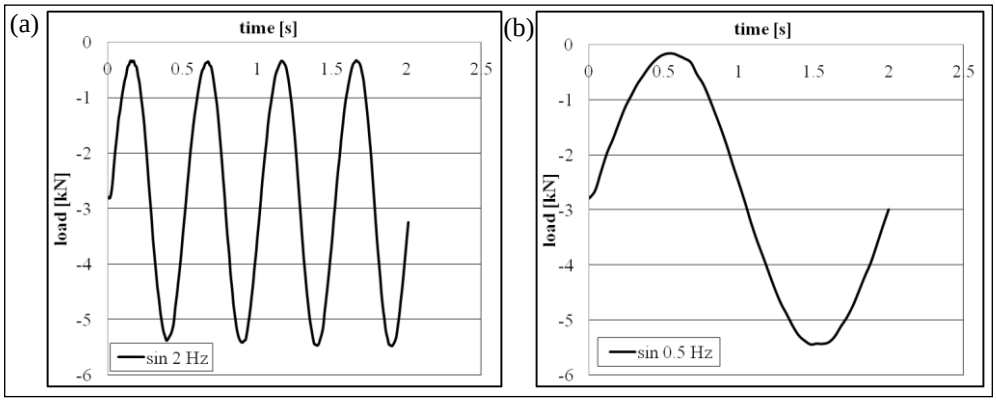

Figure 1.21 Sinusoidal test carried out on multilayer slabs at 2 Hz (a) and 0.5 Hz (b).

These two different approaches were designed to highlight different aspects of the stress/strain responses of the multilayer flexible pavements with and without two different reinforce systems and during the in-service life. Moreover, this laboratory investigation could collect reliable data, in order to validate the Finite Element Analyses, since it was conducted followed a strict procedure. However, before running the tests explained in this paragraph, a further analysis was conducted in the laboratory using samples with different shapes. This choice permitted to collect information related to the same multilayer flexible pavements with different reinforcement studied in this work, but when the structure is at the end of the in-service life. In fact, the bibliography research clearly showed that a fair method to emphasize the effects of any kind of reinforcing system could be carrying out of those "destroying" tests, which forced road pavements to the extreme limits [2, 31, 32]. Moreover, it is a fair starting point to initiate an analysis where reinforcing systems are involved. A widespread example could be recognized in bending tests because of its easiness of execution. That is the reason why a new laboratory investigation was set, before running the tests mentioned above.

1.5 Three-point Bending Test.

As explained above, the aim of these kinds of tests was to lay the basis of this research work related to reinforced flexible pavements. Therefore, this investigation could study the macroscopic effects of the grids inserted between the binder layer and the base course. This step was absolutely necessary before the beginning of a research that can be considered more refined, since it pretended to simulate the in-situ condition of a real road pavement.

Two different shapes of samples were created to carry out three-point bending tests: one was a typical beam [33] and the second one was a bi-layer slab more similar to the ones tested over this research work. It is important to underline that, in order to guarantee a complete repeatability and coherence, both typologies of specimens were created using the same asphalt mixtures and following the same compaction procedure explained in paragraph 1.1 and 1.2. Keeping this in mind, multilayer beams were suitably built. The samples had the geometry showed in Figure 1.22 where it is possible to notice that the thickness of the three asphalt layers was equal to the ones picked for the slabs created for this research work: 30 mm of the wearing course, 40 mm of the binder layer and 100 mm of the base course (Table 1.3).

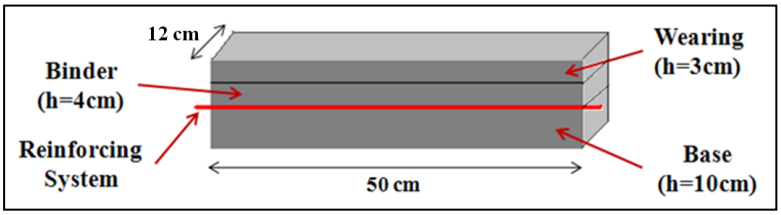

Figure 1.22 The geometric features of the multilayer beams used for 3-point bending tests.

Obviously, three typologies of beams were constructed: one with the steel net, one with the glass grid and the last one without any kind of reinforce, as control sample. The specimens reinforced with the steel net were divided into two more typologies. In fact, the dimensions of the beams could not allow the insert of a whole mesh including the reinforcing bar. Therefore, there were beams with steel mesh and others with steel mesh plus bars (Figure 1.23).

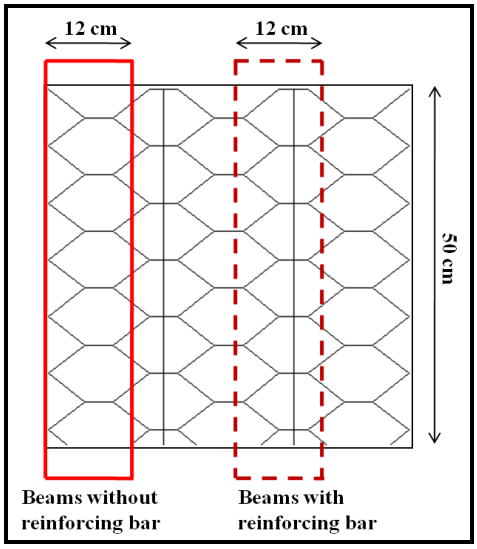

Figure 1.23 The two typologies of multilayer beams reinforced with steel net: on the left the ones without bar and on the right with bar.

This issue was totally meaningless for those beams reinforced with glass grid. In fact, the smaller dimensions of this kind of mesh permitted to insert the whole geometry in each sample.
The second typology of samples used to carry out three-point bending tests was the same squared slabs 500 mm x 500 mm, but thinner. In fact, these were composed by 2 layers: 30 mm of the wearing course and 40 mm of the binder layer. Once more, these specimens were divided into three types: one was the control specimens without any kind of reinforce and the others two with the net (steel or glass) totally embedded at the bottom of the binder layer. In this case, the dimensions of these samples could include the whole geometry of the steel net, such as the entire mesh as well as the reinforcing bars. Hence, this second typology of specimens could be only divided into three categories. The test set-up was the same in both cases and the data were collected using the MTS machine. The tests were run following the regular three-point bending configuration and fixing a displacement rate of 0.084 mm/s (Figure 1.24). The investigation was totally conducted at 10°C.

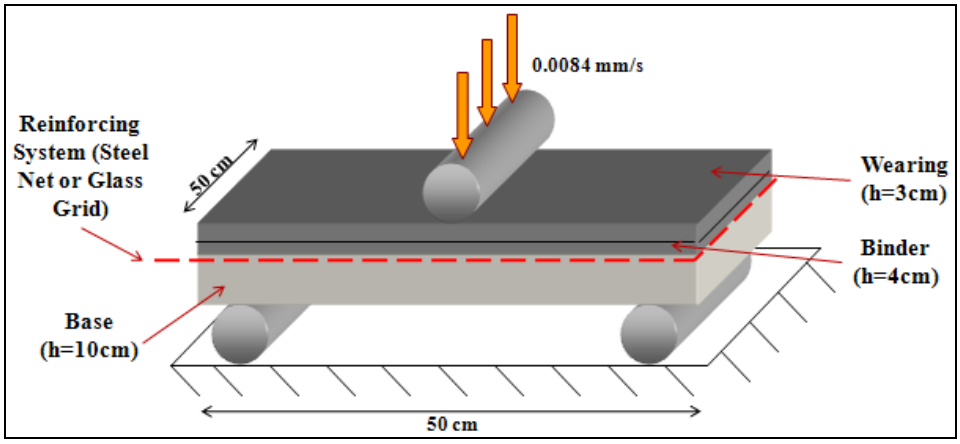

Figure 1.24 The geometric features of the bi-layer slabs used for three-point bending tests and the test set-up.

The graph in Figure 1.25 shows the results collected during the carrying out of the three-point bending tests and using the samples with beam shape. Four curves represent the different typologies of specimens. Furthermore, the investigation was implemented with an energetic analysis, in order to study the different levels of the stores of energy for each type of specimens (Figure 1.26).

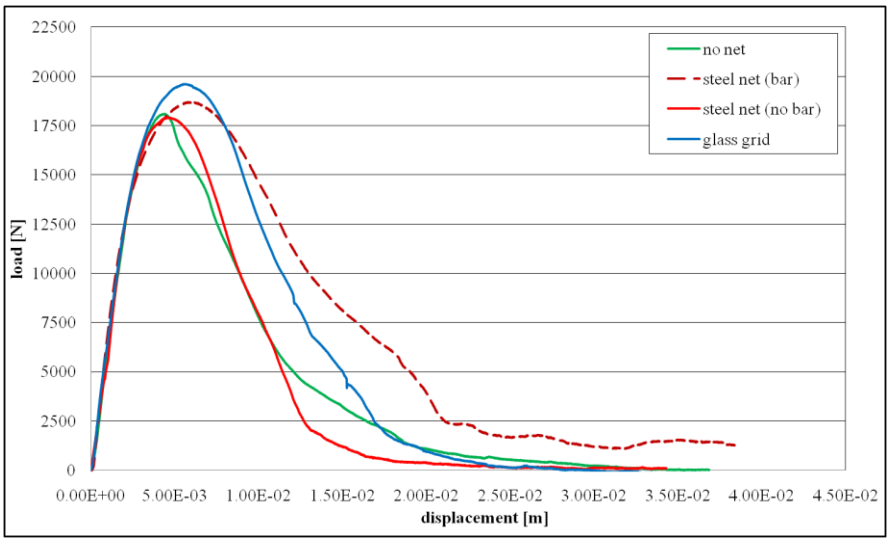

Figure 1.25 The results collected running three-point bending tests on the four typologies of the multilayer beams.

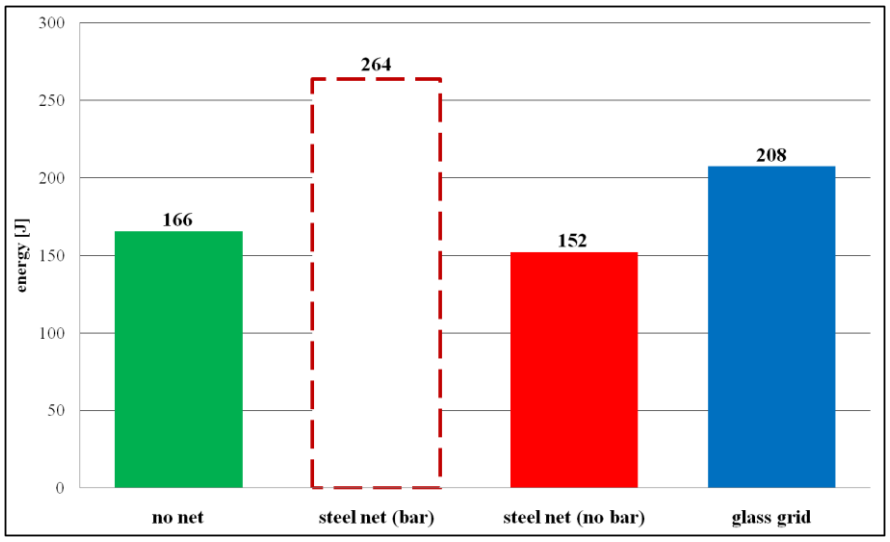

Figure 1.26 The energetic analysis of the four typologies of the multilayer beams running three-point bending tests.

However, the Figure 1.27 shows the output data collected during the analogous tests, but carried out using bi-layer slabs. Here there were only three curves: one for each sample. Moreover, in

Figure 1.28 it is possible to observe the corresponding store of energy in this second kind of samples.

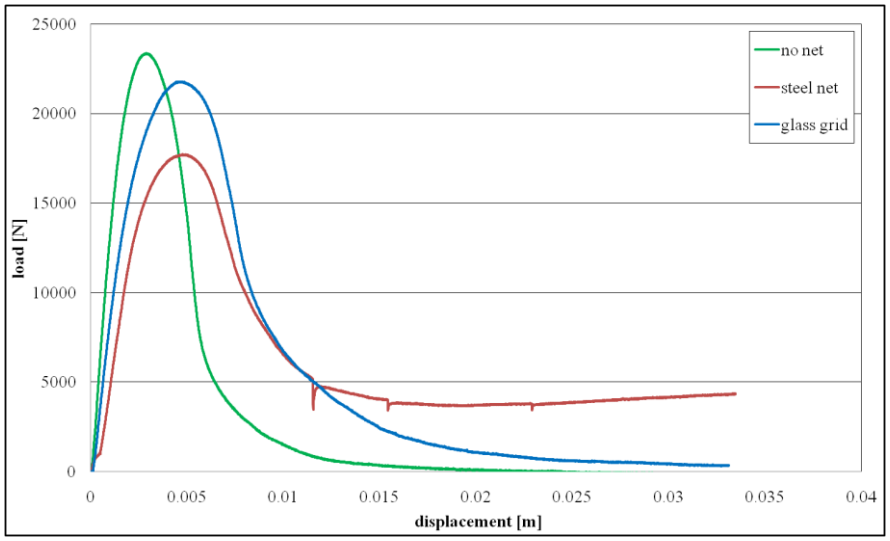

Figure 1.27 The results collected running three-point bending tests on the three typologies of the bi-layer slabs.

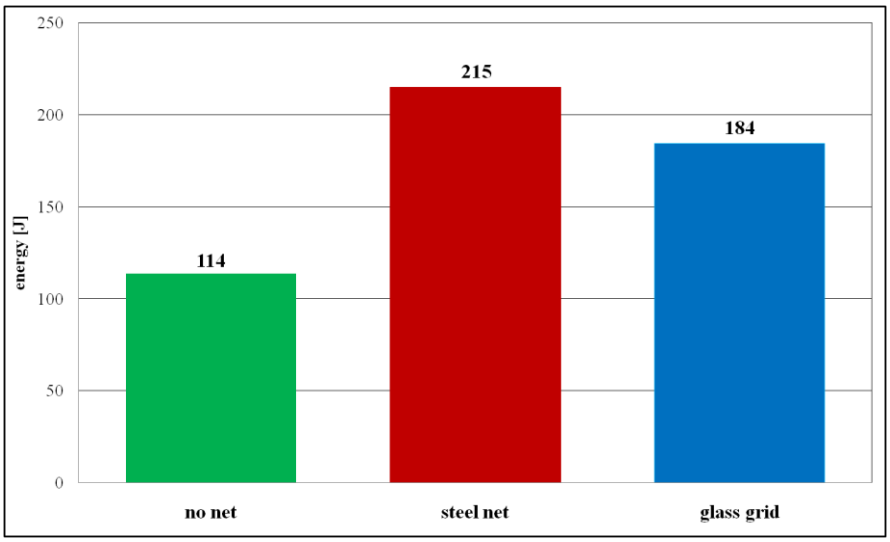

Figure 1.28 The energetic analysis of the four typologies of the bi-layer slabs running three-point bending tests.

The results presented in the Figures above show the different behaviour of the two typologies of samples. In fact the peak values of stress or the store of energy is not only different between reinforced and unreinforced specimens. But also slabs and multilayer beams provided with the same kind of reinforcing system exhibit different behaviours. This is not a brand-new discovery [33] and in fact this investigation does not pretend to make any conclusions about the performance of reinforcing nets inserted in flexible pavements. It was only a preliminary analysis of this research work, in order to demonstrate the macroscopic effects of these grids. Moreover, in this laboratory section the reinforcing systems are positioned between the binder layer and the base course, which is considered a superficial position and using a precise configuration of in-layer flexible infrastructures. Additionally, the asphalt concretes were totally mixed in the laboratory and compacted with a heavy compactor that is not a standardized equipment. Because of all these reasons, these three-point bending tests could be considered a fair starting point for the following analyses executed on the multilayer slabs. This prospective permitted to evaluate the data collected and make proper conclusions, useful for this work. Three point bending tests permitted to state that both kinds of samples highlight the effects of reinforcing systems. Obviously, the study of the graphs in Figure 1.25, 1.26, 1.27 and 1.28 has to consider the shape of the curves and not only the peak values of the stress. In fact, the area under those curves represented the energy. Table 1.6 shows that the beams with steel net plus bars or the bi-layer slabs with the same grid can store more energy than the other specimens. In fact, the unreinforced samples (both typologies) could store around 40÷50% more energy than the ones with a reinforcing system.

Table 1.6 Energy stored by multilayer beams and bi-layer slabs during 3-point bending tests.

Samples	***Multilayer beams*** ***Energy stored [J]***	***Bi-layer slabs*** ***Energy stored [J]***
No Net	166	114
Steel Net (with bar)	264	215
Steel Net (no bar)	152	-
Glass Grid	208	184

On the other hand, control samples are the ones that could reach the highest stress values. However, when the failure started they immediately collapsed and the specimens with

reinforcing systems showed a better post-failure resistance. This behaviour is evident in both typologies of samples: in the multilayer beams (Figure 1.29) the crack arrived straight to the top of the samples and the bi-layer slabs (Figure 1.30) broke completely into two parts.

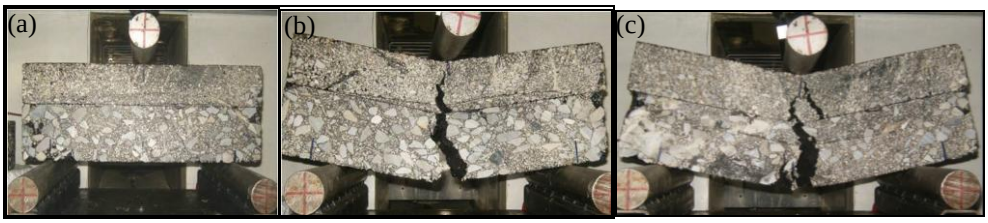

Figure 1.29 Three-point bending test carried out of the multilayer beams at the beginning of the analysis (a) and the different failure of unreinforced samples (b) and the reinforced ones (c).

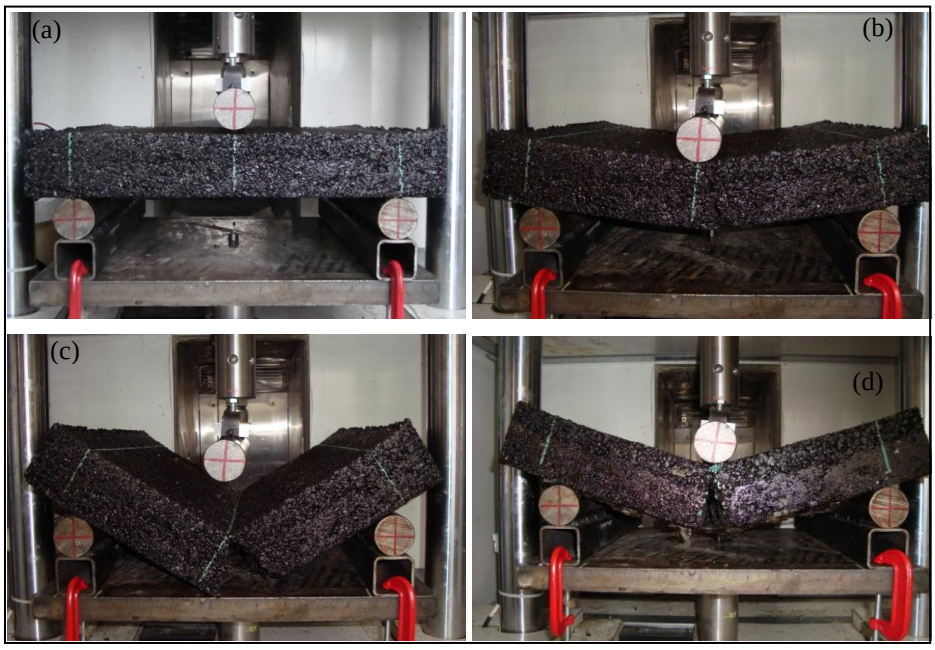

Figure 1.30 Three-point bending test carried out of the bi-layer slabs at the beginning of the analysis (a) (b) and the different failure of unreinforced samples (c) and the reinforced ones (d).

Consequently, it is reasonable to think that it would be possible to see the effects of the reinforcement during the in-service life, which is the analysis planned for this research work.

1.6 Results.

Previous paragraphs explained step by step how data were collected and the procedure to get reliable and testable samples. In this section of the Chapter, the results are exposed starting from the tests carried out on control slabs (without any kind of reinforce) and going through the reinforced samples. Moreover, the static tests were divided from the dynamic ones, but the positions monitored are the ones showed in Figure 1.19. In addition, conclusions were drawn considering each typology of specimens, but also making proper comparisons among the analogous investigations carried out on the different kind of slabs. Finally, it is important to underline that all the data presented below are an average of several investigations run on different specimens (with and without reinforcing systems).

Control slabs (without any reinforcing system)

Figure 1.31 shows the data collected by strain gauges placed in two different areas close to the loading mark while a creep test was run on the control slabs.

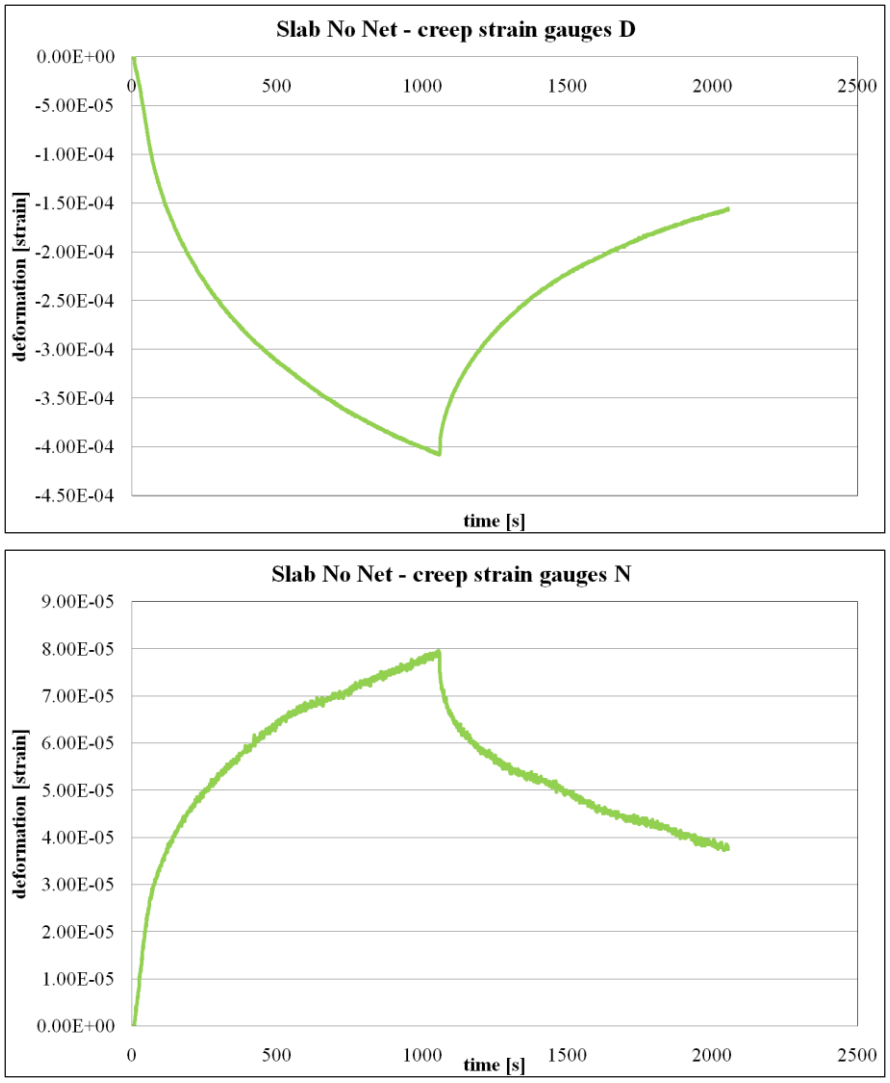

Figure 1.31 Creep test on control slab - strain gauges D and N.

Table 1.7 highlights the strain peak values and the percentages of the recovered strain collected by the strain gauges in position D and N.

Table 1.7 Peak value and recovery of control slab during creep test.

CREEP – CONTROL SLAB		
Strain Gauges Position	***D***	***N***
Peak value [μstrain]	-408	79
Recovery [%]	60	50

Figure 1.32 shows the data collected by strain gauges placed in different areas close to the loading mark of the control slabs and applying 100 cycles of a sinusoidal load at 0.5 Hz.

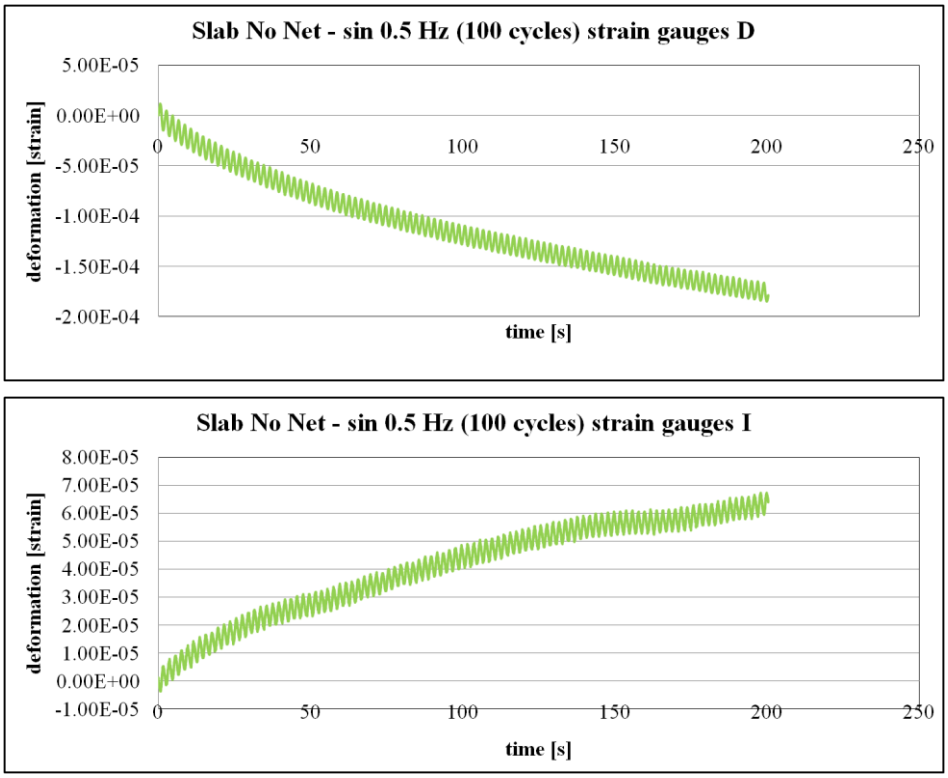

Figure 1.32 Sinusoidal test (100 cycles, 0.5 Hz) on control slab - strain gauges D and I.

Table 1.8 highlights the strain peak values and the wave amplitude of the strain collected by the strain gauges in position D and I.

Table 1.8 Peak value and wave amplitude of control slab (sinusoidal test 100 cycles, 0.5 Hz).

SIN 0.5Hz (100 Cycles) – CONTROL SLAB		
Strain Gauges Position	***D***	***I***
Peak value [μstrain]	-173	62
Wave amplitude [μstrain]	18.6	8.2

Figure 1.33 shows the data collected by strain gauges placed in different areas close to the loading mark of the control slabs and applying a sinusoidal load at 0.5 Hz for 1000 seconds.

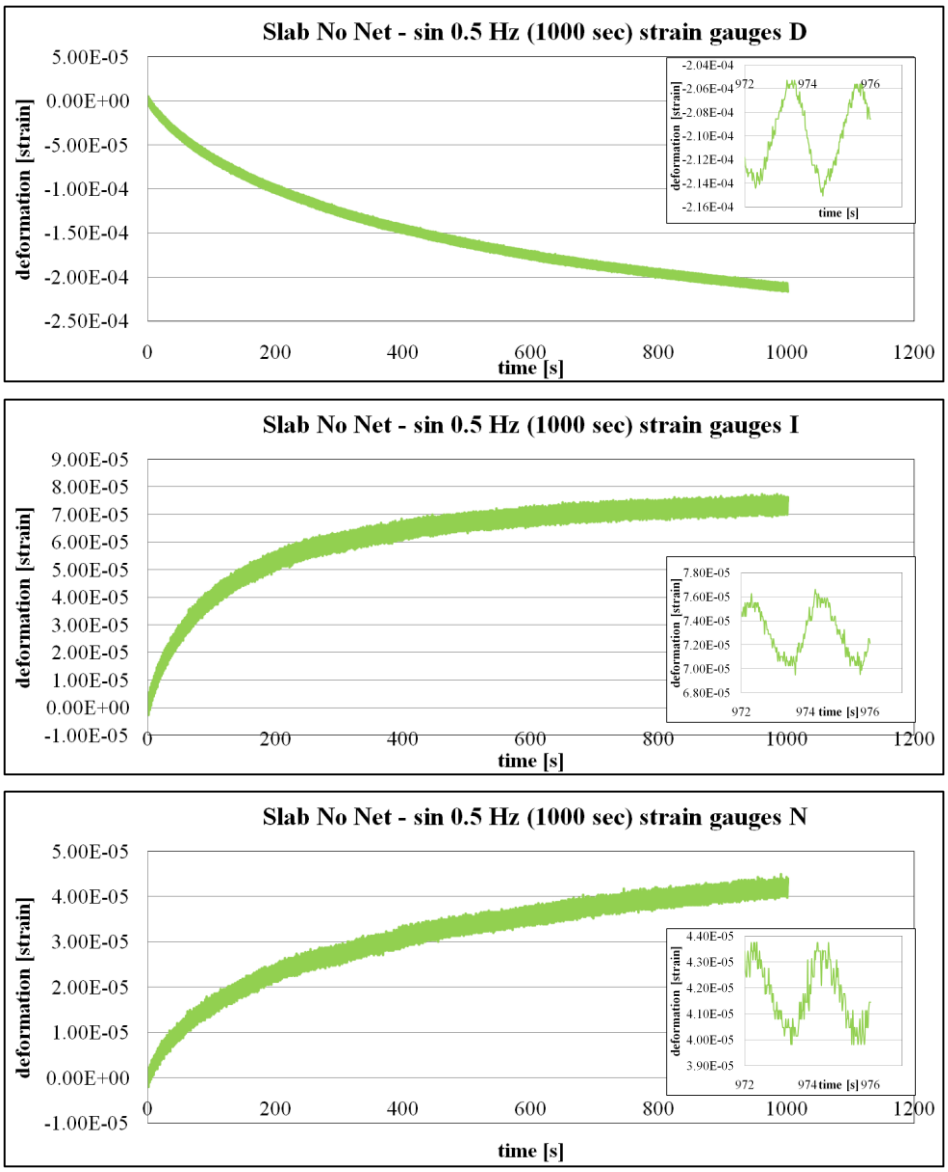

Figure 1.33 Sinusoidal test (1000s, 0.5 Hz) on control slab - strain gauges D, I and N.

Table 1.9 highlights the strain peak values and the wave amplitude of the strain collected by the strain gauges in position D, I and N.

Table 1.9 Peak value and wave amplitude of control slab (sinusoidal test 1000s, 0.5 Hz).

SIN 0.5Hz (1000 seconds) – CONTROL SLAB			
Strain Gauges Position	***D***	***I***	***N***
Peak value [μstrain]	-214	73	42
Wave amplitude [μstrain]	9.8	7.1	3.9

Figure 1.34 shows the data collected by strain gauges placed in different areas close to the loading mark of the control slabs and applying 100 cycles of a sinusoidal load at 2 Hz.

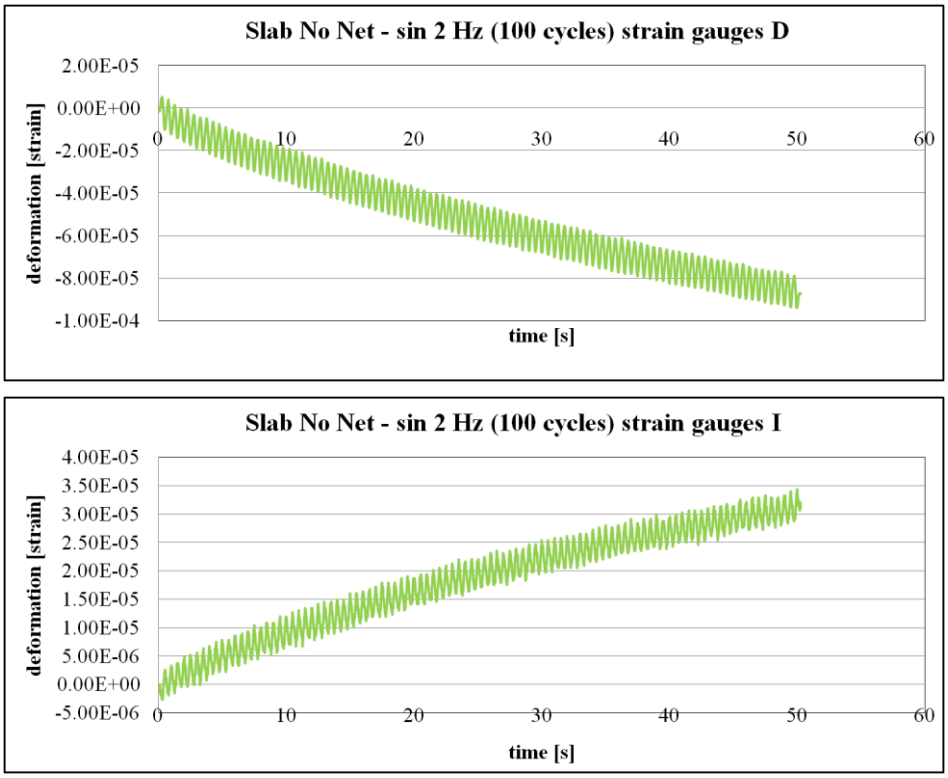

Figure 1.34 Sinusoidal test (100 cycles, 2 Hz) on control slab - strain gauges D and I.

Table 1.10 highlights the strain peak values and the wave amplitude of the strain collected by the strain gauges in position D and I.

Table 1.10 Peak value and wave amplitude of control slab (sinusoidal test 100 cycles, 2 Hz).

SIN 2Hz (100 Cycles) – CONTROL SLAB		
Strain Gauges Position	***D***	***I***
Peak value [µstrain]	-82	31
Wave amplitude [µstrain]	15.3	6

Figure 1.35 shows the data collected by strain gauges placed in different areas close to the loading mark of the control slabs and applying a sinusoidal load at 2 Hz for 1000 seconds.

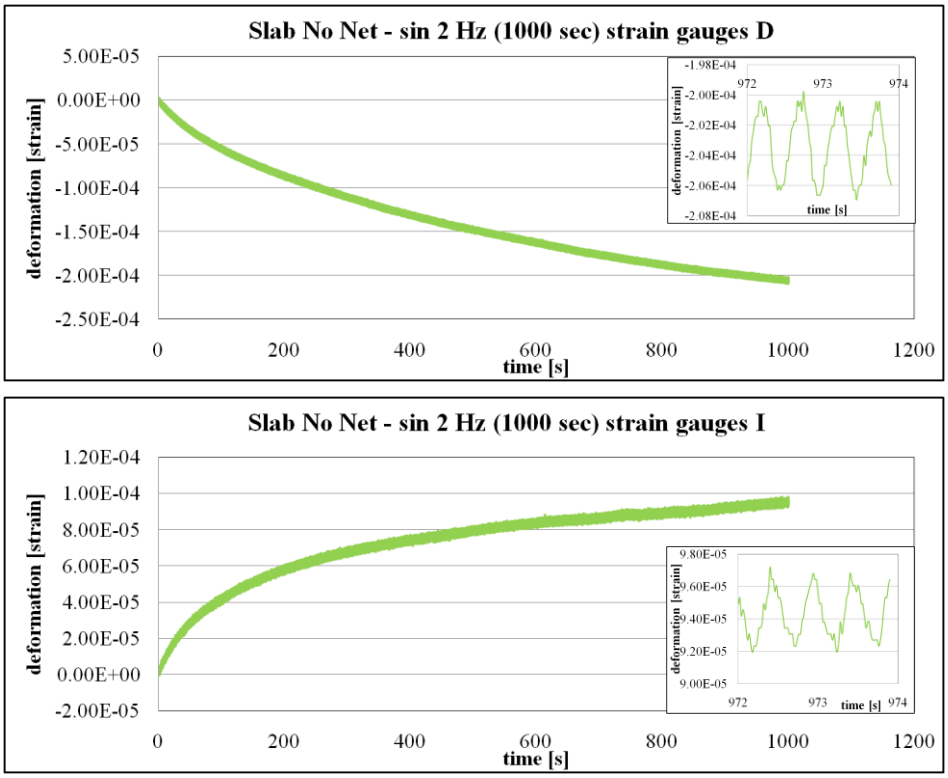

Figure 1.35 Sinusoidal test (1000s, 2 Hz) on control slab - strain gauges D and I.

Table 1.11 highlights the strain peak values and the wave amplitude of the strain collected by the strain gauges in position D and I.

Table 1.11 Peak value and wave amplitude of control slab (sinusoidal test 1000s, 2 Hz).

SIN 2Hz (1000 seconds) – CONTROL SLAB		
Strain Gauges Position	***D***	***I***
Peak value [μstrain]	-204	93
Wave amplitude [μstrain]	7.5	4.9

- ***Slabs reinforced with Steel Net***

Figure 1.36 shows the data collected by strain gauges placed in three different areas close to the loading mark while a creep test was run on the slabs reinforced with a steel net between binder layer and base course.

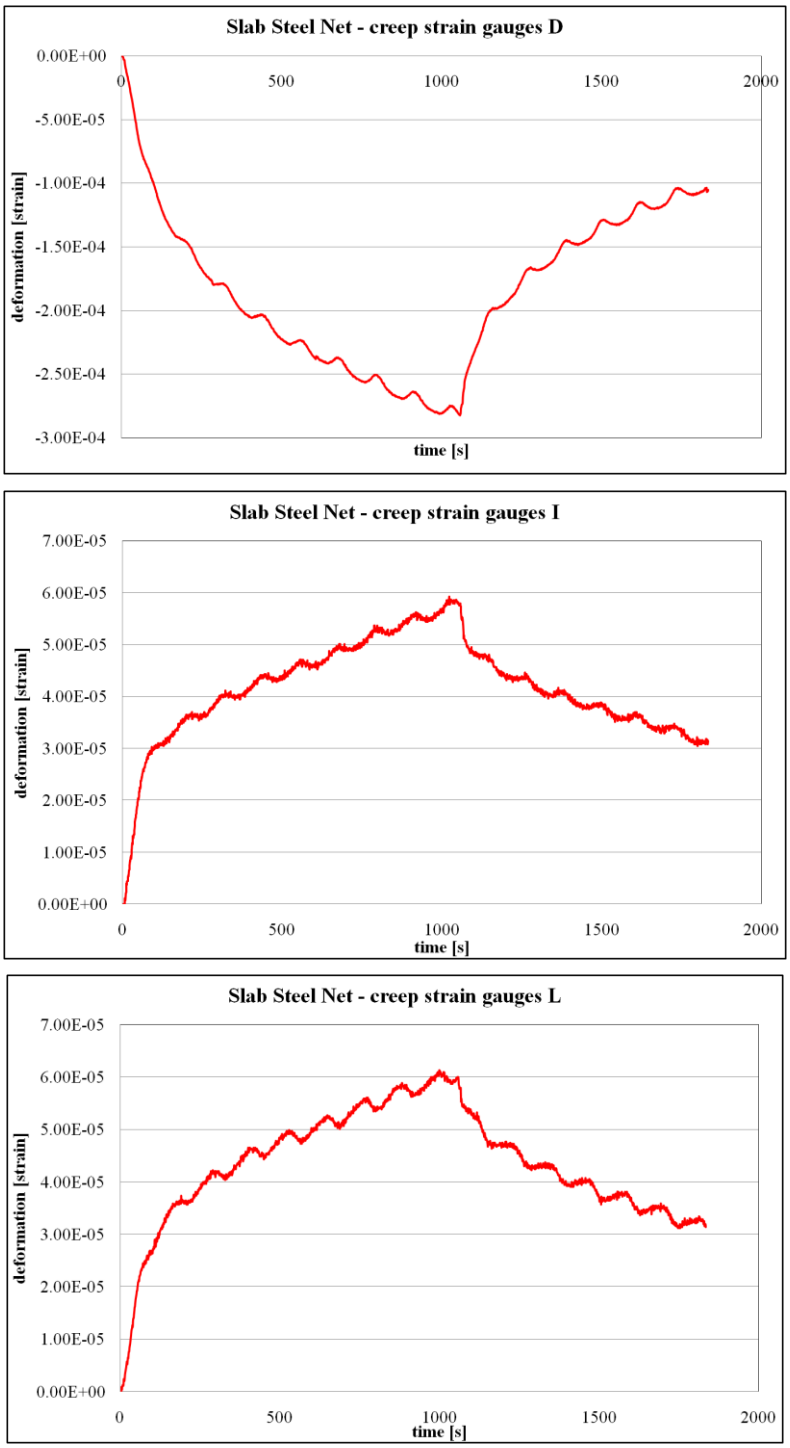

Figure 1.36 Creep test on slab with steel net - strain gauges D, I and L.

Table 1.12 highlights the strain peak values and the percentages of the recovered strain collected by the strain gauges in position D, I and L.

Table 1.12 Peak value and recovery of slab with steel net during creep test.

CREEP – SLAB WITH STEEL NET			
Strain Gauges Position	***D***	***I***	***L***
Peak value [μstrain]	-283	59	61
Recovery [%]	63	47	49

Figure 1.37 shows the data collected by strain gauges placed in different areas close to the loading mark of the slabs reinforced with steel net and applying 100 cycles of a sinusoidal load at 0.5 Hz.

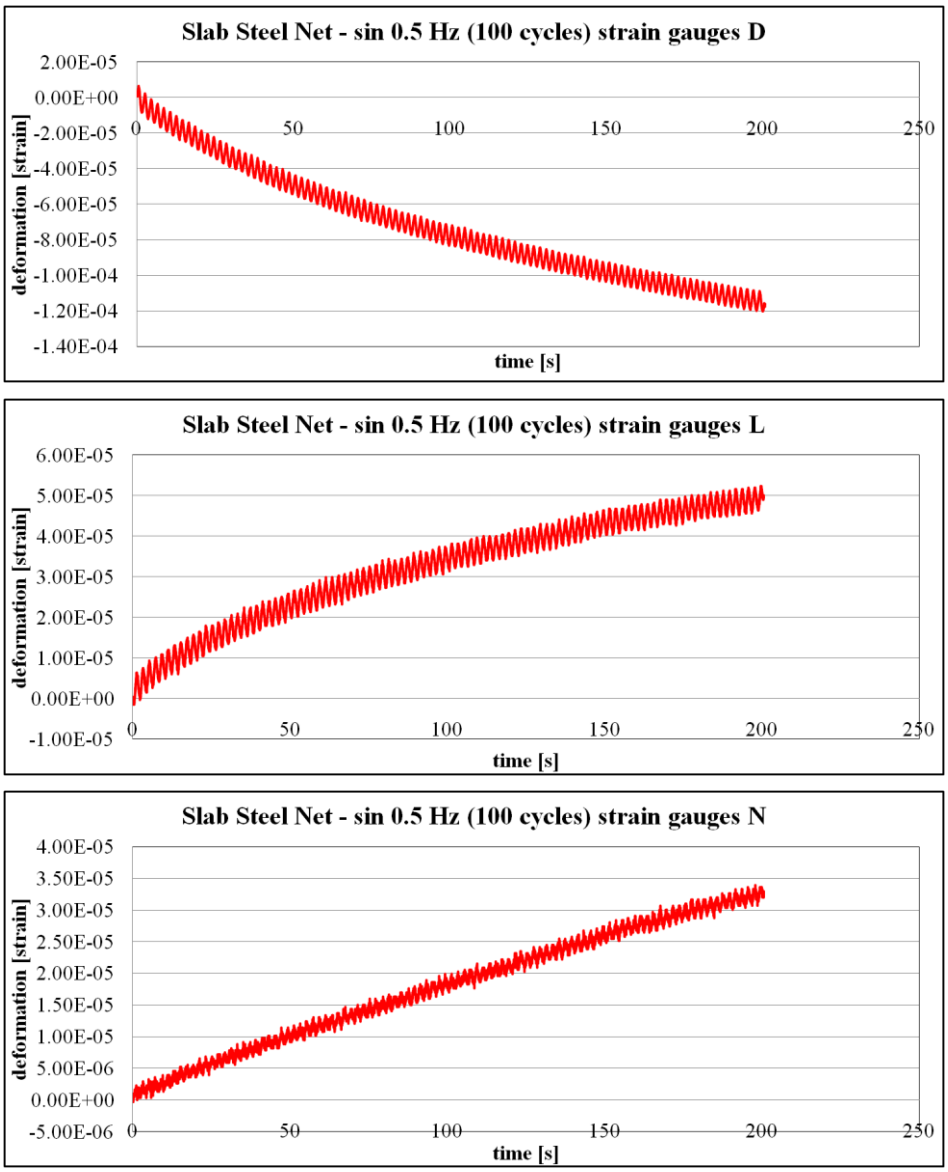

Figure 1.37 Sinusoidal test (100cycles, 0.5Hz) on slab with steel net - strain gauges D, L and N.

Table 1.13 highlights the strain peak values and the wave amplitude of the strain collected by the strain gauges in position D, L and N.

Table 1.13 Peak value and wave amplitude of slab steel net (sinusoidal test 100 cycles, 0.5 Hz).

SIN 0.5Hz (100 Cycles) – SLAB WITH STEEL NET			
Strain Gauges Position	***D***	***L***	***N***
Peak value [μstrain]	-115	48	31
Wave amplitude [μstrain]	11.7	6.7	2.9

Figure 1.38 shows the data collected by strain gauges placed in different areas close to the loading mark of the slabs reinforced with steel net and applying 100 cycles of a sinusoidal load at 2 Hz.

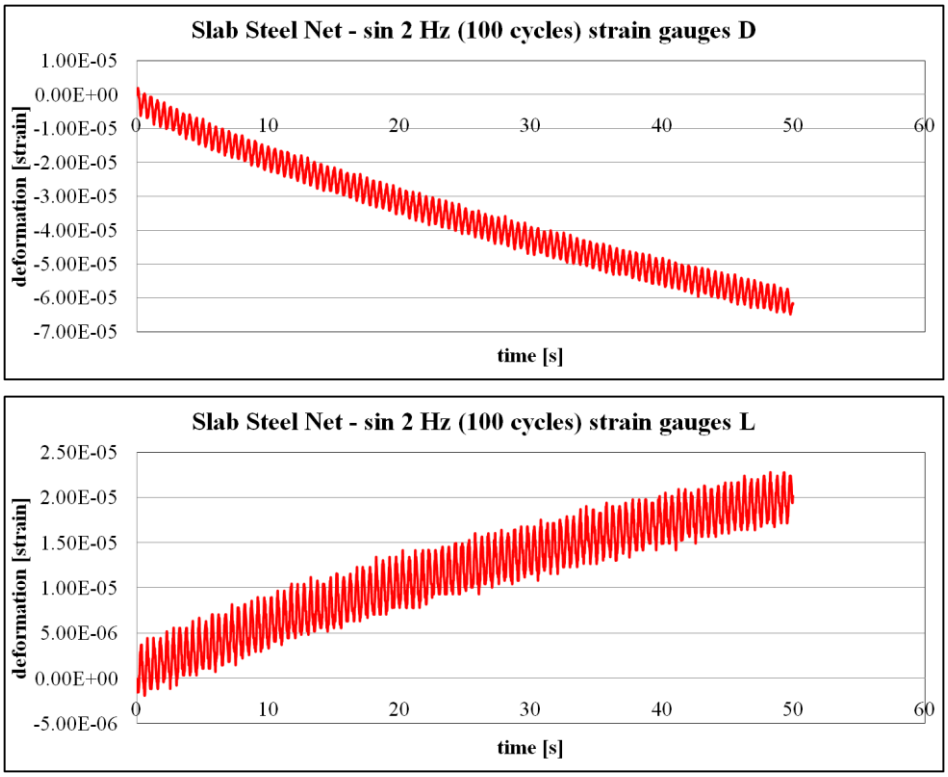

Figure 1.38 Sinusoidal test (100 cycles, 2 Hz) on slab with steel net - strain gauges D and L.

Table 1.14 highlights the strain peak values and the wave amplitude of the strain collected by the strain gauges in position D and L.

Table 1.14 Peak value and wave amplitude of slab steel net (sinusoidal test 100 cycles, 2 Hz).

SIN 2Hz (100 cycles) – SLAB WITH STEEL NET		
Strain Gauges Position	***D***	***L***
Peak value [μstrain]	-56	17
Wave amplitude [μstrain]	8.8	5.6

Figure 1.39 shows the data collected by strain gauges placed in different areas close to the loading mark of the slabs reinforced with steel net and applying a sinusoidal load at 2 Hz for 1000 seconds.

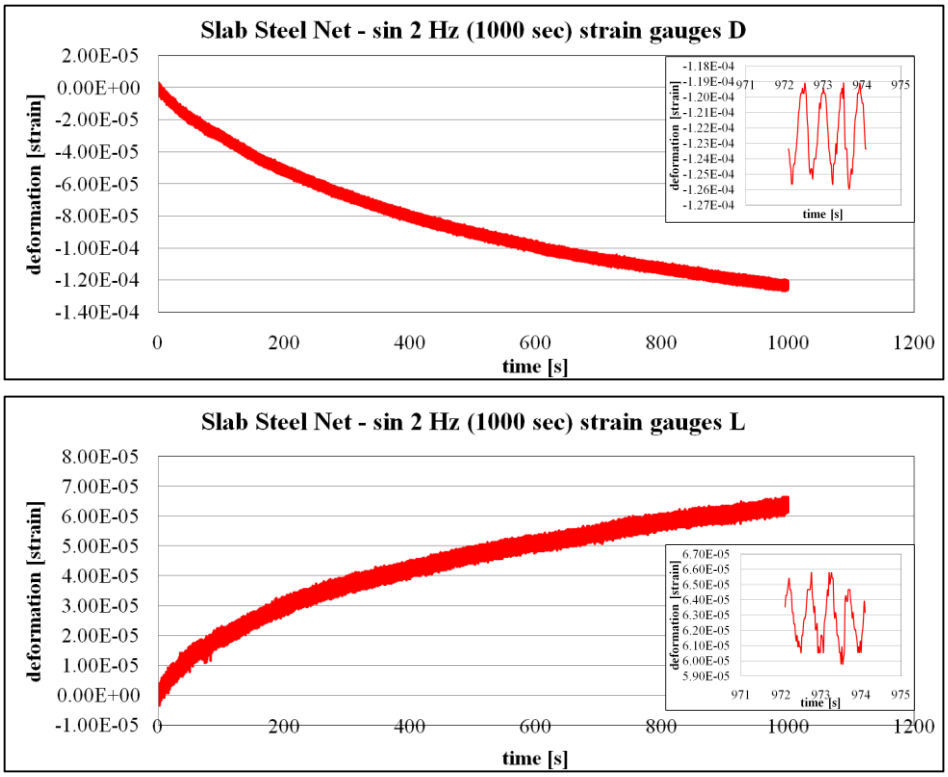

Figure 1.39 Sinusoidal test (1000s, 2 Hz) on slab with steel net - strain gauges D and L.

Table 1.15 highlights the strain peak values and the wave amplitude of the strain collected by the strain gauges in position D and L.

Table 1.15 Peak value and wave amplitude of slab steel net (sinusoidal test 1000s, 2 Hz).

SIN 2Hz (1000 seconds) – SLAB WITH STEEL NET		
Strain Gauges Position	***D***	***L***
Peak value [μstrain]	-123	65
Wave amplitude [μstrain]	6.0	6.2

- ***Slabs reinforced with Glass Grid***

Figure 1.40 shows the data collected by strain gauges placed in two different areas close to the loading mark while a creep test was run on the slabs reinforced with a glass grid positioned between binder layer and base course.

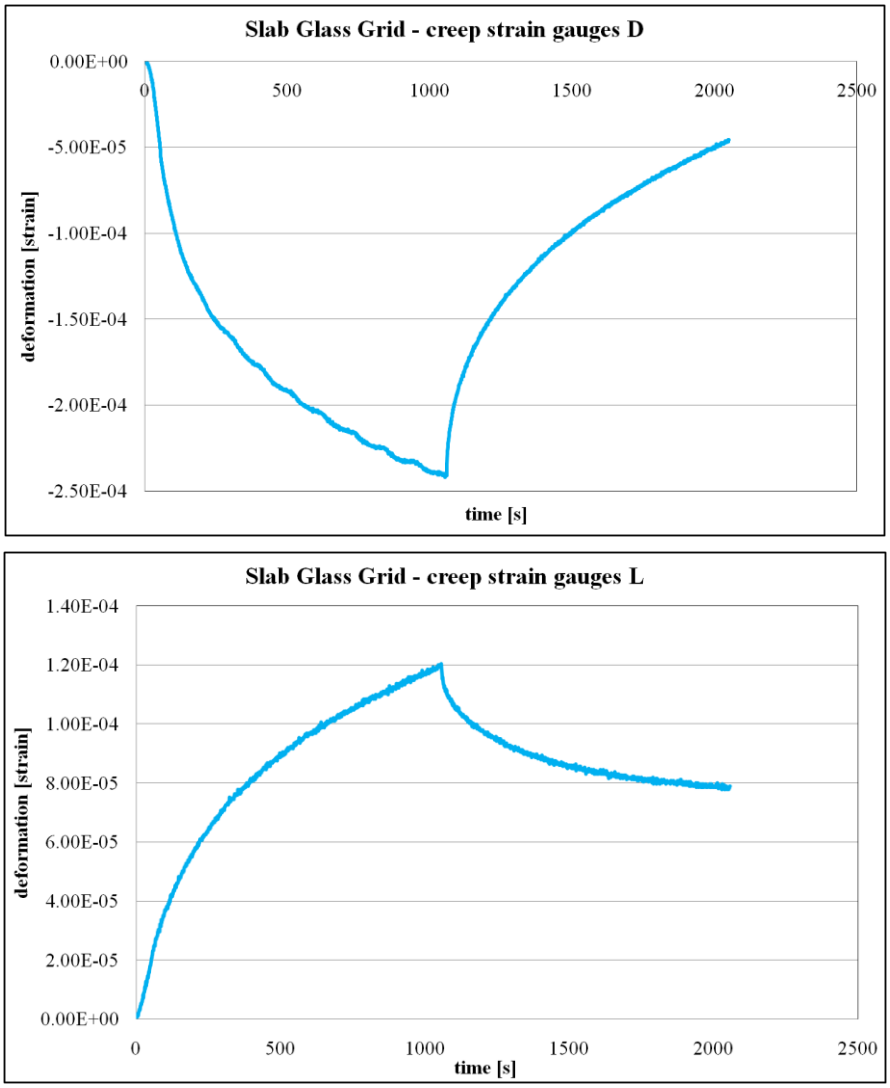

Figure 1.40 Creep test on slab with glass grid - strain gauges D and L.

Table 1.16 highlights the strain peak values and the percentages of the recovered strain collected by the strain gauges in position D and L.

Table 1.16 Peak value and recovery of slab with glass grid during creep test.

CREEP – SLAB WITH GLASS GRID		
Strain Gauges Position	***D***	***L***
Peak value [µstrain]	-242	120
Recovery [%]	84	35

Figure 1.41 shows the data collected by strain gauges placed in different areas close to the loading mark of the slabs reinforced with glass grid and applying 100 cycles of a sinusoidal load at 2 Hz.

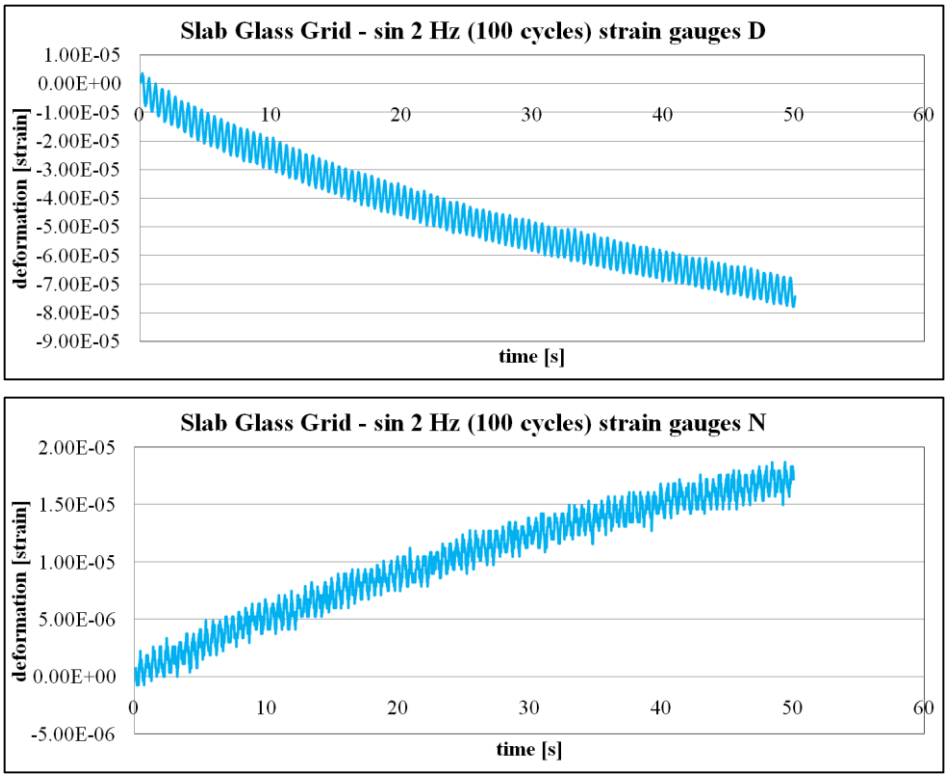

Figure 1.41 Sinusoidal test (100 cycles, 2 Hz) on slab with glass grid - strain gauges D and N.

Table 1.17 highlights the strain peak values and the wave amplitude of the strain collected by the strain gauges in position D and N.

Table 1.17 Peak value and wave amplitude of slab glass grid (sinusoidal test 100 cycles, 2 Hz).

SIN 2Hz (100cycles) – SLAB WITH GLASS GRID		
Strain Gauges Position	***D***	***N***
Peak value [µstrain]	-68	16
Wave amplitude [µstrain]	10.0	3.5

Figure 1.42 shows the data collected by strain gauges placed in different areas close to the loading mark of the slabs reinforced with steel net and applying a sinusoidal load at 2 Hz for 1000 seconds.

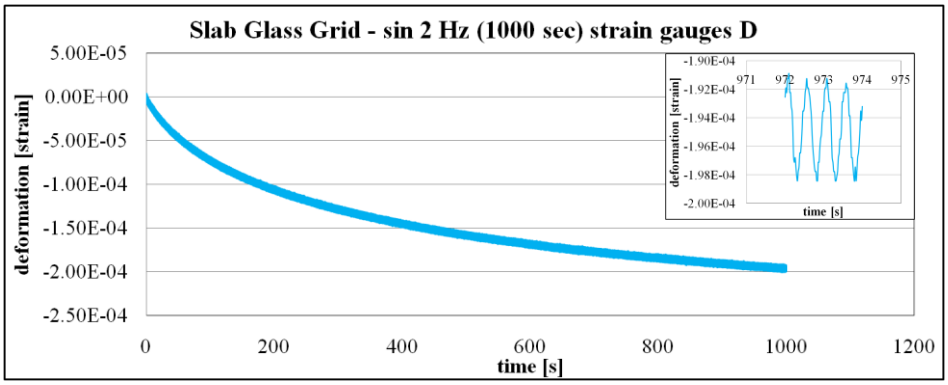

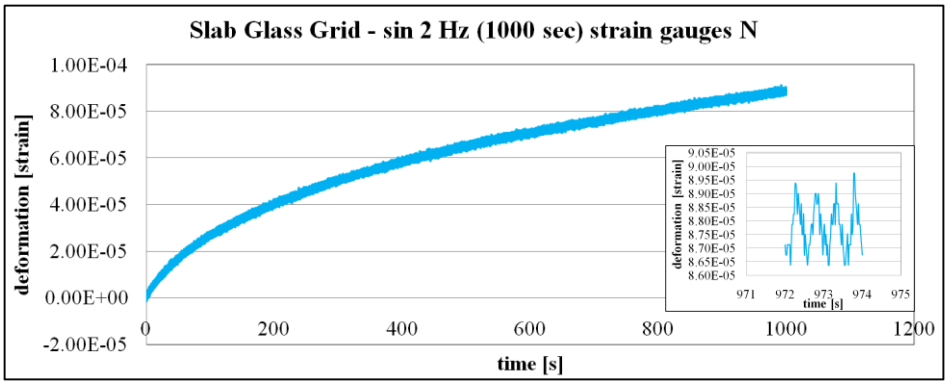

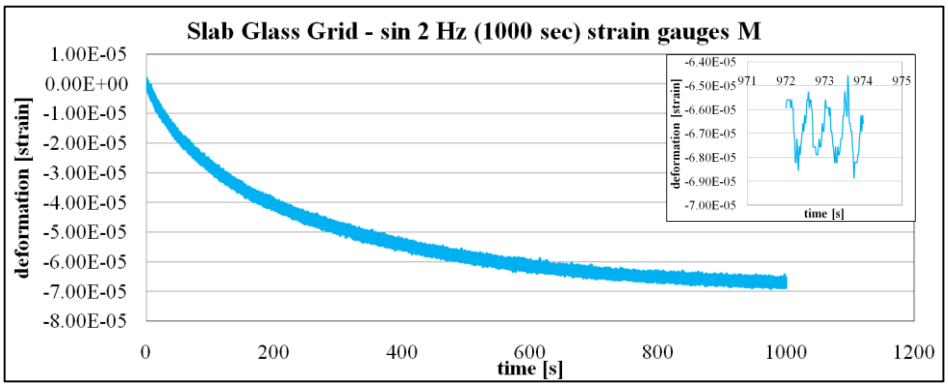

Figure 1.42 Sinusoidal test (1000s, 2 Hz) on slab with glass grid - strain gauges D, N and M.

Table 1.18 highlights the strain peak values and the wave amplitude of the strain collected by the strain gauges in position D, N and M.

Table 1.18 Peak value and wave amplitude of slab glass grid (sinusoidal test 1000s, 2 Hz).

SIN 2Hz (1000 seconds) – SLAB WITH GLASS GRID			
Strain Gauges Position	***D***	***N***	***M***
Peak value [μstrain]	-195	88	-67
Wave amplitude [μstrain]	7.1	2.6	2.6

The results presented above could be analysed following a common scheme and finding a trend which could make a connection between the three typologies of slabs. The creep tests highlighted the tendency to accumulate more strains than the dynamic tests. The results collected during the sinusoidal cyclic tests at different frequencies highlighted that the tendency of each typology of samples was to store more deformations when the frequency of the load was lower and this could be considered a reasonable behaviour. In fact, the stress on a road pavement is usually higher when a vehicle has a lower speed (which corresponded to a lower frequency). Moreover, the sinusoidal tests (1000 seconds long) meant different number of the load cycles according to the frequency: 2 Hz meant 2000 cycles and 0.5 Hz meant a quarter of

cycles (500). Therefore, the amplitude of the waves was bigger in the "slower" investigations (0.5 Hz) compared to the analogous tests at 2 Hz. Obviously, these considerations made the results reliable, since usually a static load or a lower load frequency are reasonably the cause of a higher level of stresses and strains. A further consideration could take into consideration the results presented for the slabs reinforced with steel net related to the creep tests. The data collected from strain gauges I and L were very similar and with a common trend (Figure 1.36). In fact, those monitored positions could be considered analogous (see Figure 1.19) and the results met the expectations highlighting a comparable behaviour.

After these preliminary considerations, the data collected permitted to compare the different behaviours of the three typologies of slabs, checking the dissimilarities between the reinforced and unreinforced samples through the analysis of the carried out tests. The following Figures show the data collected from strain gauges positioned in the same area close to the loading mark (position D), but placed on the three different kinds of specimens.

Figure 1.43 shows the data collected by strain gauges placed in position D running a creep test on the three kinds of slabs.

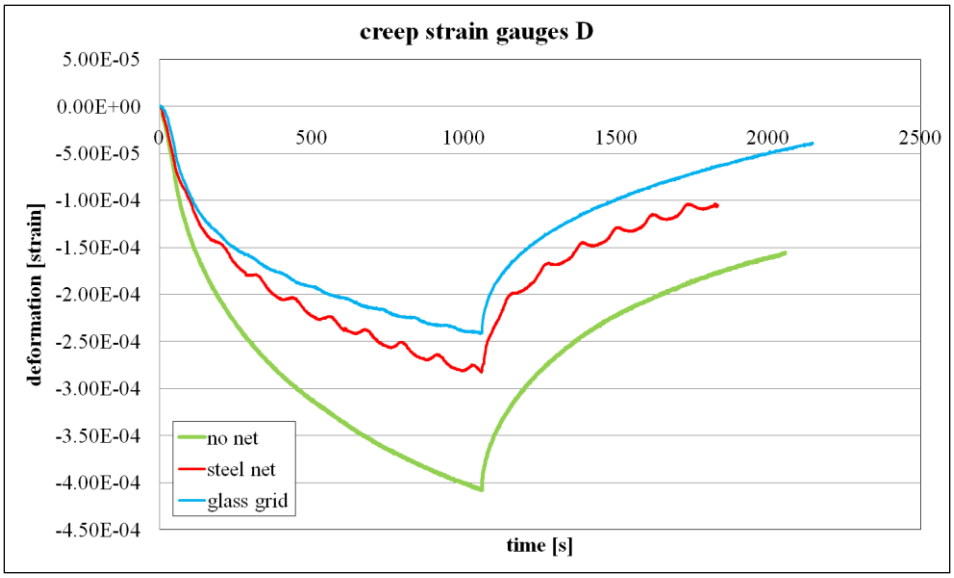

Figure 1.43 Comparison of the creep test carried out on the three typologies of slabs (with no net, steel net and glass grid - strain gauges D.

Table 1.19 highlights the strain peak values and the percentages of the recovered strain collected by the strain gauges in position D on the three different kinds of slabs.

Table 1.19 Peak values and recovery of the three typologies of slabs during creep test.

CREEP – STRAIN GAUGES D			
Typology of Slab	***No Net***	***Steel Net***	***Glass Grid***
Peak value [μstrain]	-408	-283	-242
Recovery [%]	60	63	84

Figure 1.44 shows the data collected by strain gauges placed in the same area close to the loading mark (position D) on the three kinds of slabs and applying 100 cycles of a sinusoidal load at 2 Hz.

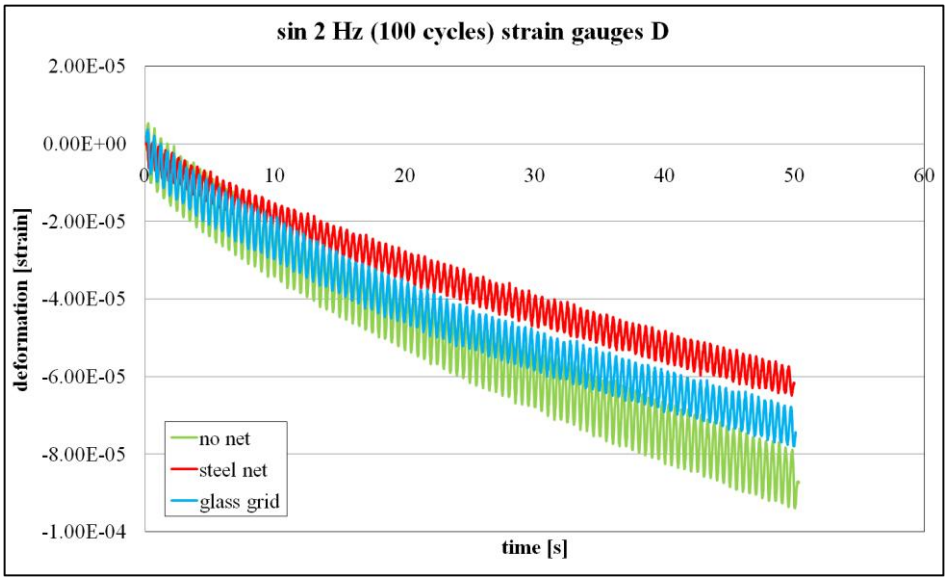

Figure 1.44 Comparison of the sinusoidal test (100 cycles, 2 Hz) carried out on the three typologies of slabs (with no net, steel net and glass grid - strain gauges D.

Table 1.20 highlights the strain peak values and the wave amplitude of the strain collected by the strain gauges in position D on the three kinds of slabs.

Table 1.20 Peak value and wave amplitude of the three kinds of slabs (sin. test 100cycles, 2Hz).

SIN 2Hz (100 cycles) – STRAIN GAUGES D			
Typology of Slab	***No Net***	***Steel Net***	***Glass Grid***
Peak value [μstrain]	-82	-56	-68
Wave amplitude [μstrain]	15.3	8.8	10.0

Figure 1.45 shows the data collected by strain gauges placed in the same areas close to the loading mark (position D) of the three kinds of slabs and applying a sinusoidal load at 2 Hz for 1000 seconds.

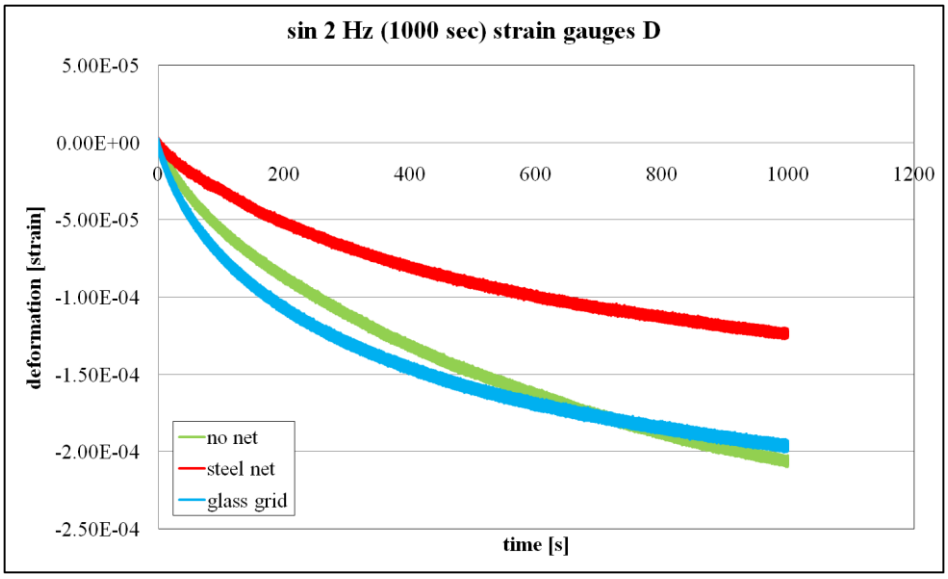

Figure 1.45 Comparison of the sinusoidal test (1000 s, 2 Hz) carried out on the three typologies of slabs (with no net, steel net and glass grid - strain gauges D.

Table 1.21 highlights the strain peak values and the wave amplitude of the strain collected by the strain gauges in position D on the three kinds of slabs.

Table 1.21 Peak value and wave amplitude of the three kinds of slabs (sin. test 1000s, 2 Hz).

SIN 2Hz (1000 seconds) – STRAIN GAUGES D			
Typology of Slab	***No Net***	***Steel Net***	***Glass Grid***
Peak value [μstrain]	-204	-123	-195
Wave amplitude [μstrain]	7.5	6.0	7.1

The analysis of the results presented in the graphs and tables above highlighted that the reinforced samples showed better performance than the unreinforced ones. The trend was to accumulate fewer amounts of deformations when reinforcing systems were placed at the interface of binder layer and base course. Moreover, the amplitude of the waves of the dynamic tests run at 2 Hz (both 100 cycles and 1000 seconds) was smaller for reinforced samples that the control slabs.

The strain gauges positioned on the top of the base course did not collect any reliable information, even though the equipments were set trying to follow a strict procedure. The few data collected showed a trend not consistent; therefore any analyses or comparisons were completely trustworthy.

Hence, this phase of this research work can be considered a preliminary validation step for the Finite Element Modelling. However, the investigations conducted on the different slabs permitted to make some conclusions about the behaviours of the road pavements with nets inserted below the superficial layers. Obviously, this is an additional remark that can be included in the final results of this research work, even if it is not the main purpose of this study.

CHAPTER 2

Finite Element Analysis.

Finite Element Analyses simulated a real scale sample of a multilayer flexible road pavement with or without a reinforcing system and it was possible using specific software, Abaqus 6.9 [34]. As mentioned in the previous Chapter the aim of this research work was to investigate the behaviours of road pavements in real conditions. The creation of a real scale model could simulate these conditions. Therefore, these analyses were conducted recreating a 500 mm squared samples, composed by three asphalt concrete layers with a circular loading mark on the top of the upper stratum. This simulation was analogous to the laboratory investigations explained in the previous chapter. In fact, that study could be considered a proper way to validate the results collected with these Finite Element Models. Firstly, these simulations started with an accurate study of the suitable mechanical and mathematical models, which could reproduce the materials behaviours. However, the interactions between the asphalt layers were investigated as well as the reinforce interfaces.

1.1 Material Properties.

The most important aspect of Finite Element Analyses was the simulation of the material characteristics, since their behaviours could really influence the responses of the modelling. In this research study several materials were involved with different properties, but basically

divided into two categories: visco-elastic such as the asphalt mixtures and linear elastic, such as the neoprene and the reinforcing systems.

One of the reinforcing is made of steel and it behaves as the typical isotropic linear elastic material. It was simulated inserting in Abaqus the Young modulus (E = 200000 MPa) and the Poisson's ratio (ν = 0.28). Analogously, the glass that composed the glass grid was simply reproduced inserting the same parameters: the Young Modulus of 76000 MPa and the Poisson's ratio of 0.22. Finally, the neoprene is a material which behaves again as an isotropic linear elastic object. Therefore it was characterized in Abaqus inserting the Young Modulus value (E = 400 MPa) and the Poisson's ratio (ν = 0.40). In fact, these are the typical parameters of a sub-base layer of a flexible road pavement. In Table 2.1 the linear elastic parameters of each material are summarized.

Table 2.1 Elastic parameters of reinforcing systems and neoprene.

	Steel Net	***Glass Grid***	***Neoprene***
Young Modulus [MPa]	200000	76000	400
Poisson's ratio	0.28	0.22	0.40

On the contrary, Hot-Mix Asphalt is a heterogeneous material and its behaviours are strictly related to the temperature, time and load application rate. In fact, it should be described using a visco-elasto-plastic theory model. However, at medium/low temperatures and short periods of loading, it could be simply assumed as a linear visco-elastic material [35]. There are several mathematical models to describe this behaviour that is typical of polymeric materials. Fractional Derivative Models or Modified Power Laws or Standard Mechanical Models [36] are just some examples of these mathematical theories, which obviously describe corresponding mechanical models of viscoelasticity, such as the Maxwell model or the Kelvin-Voigt model. Figure 2.1 shows the schemes of these two models composed by springs and dashpots connected in series or parallel. These elements represent respectively the elastic and the viscous aspect of the material.

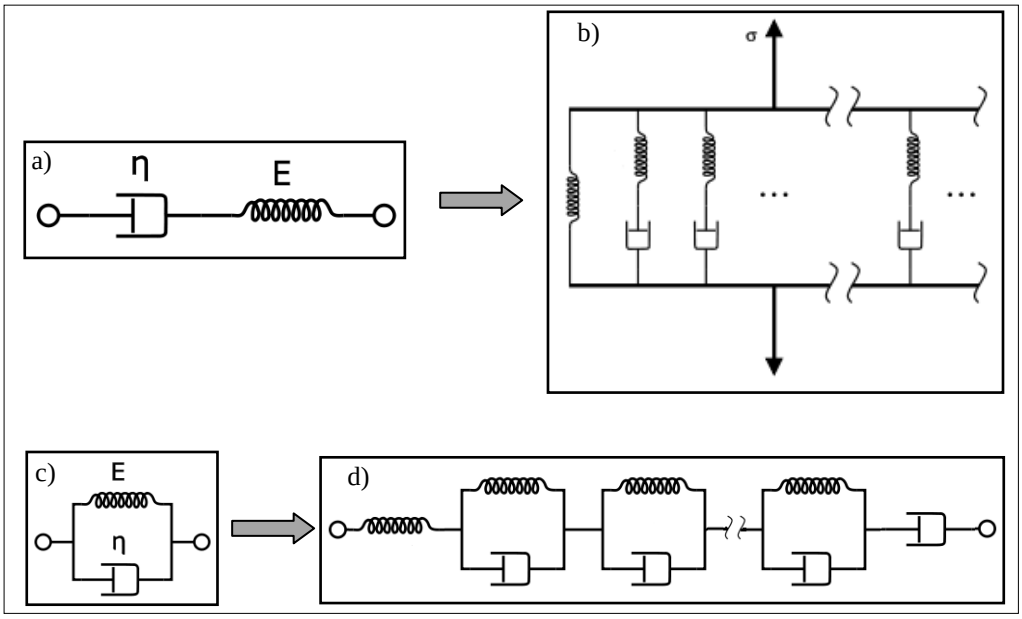

Figure 2.1 Maxwell model: single unit (a) and the generalized model (b) - Kelvin-Voigt model: single unit(c) and the generalized model (d).

The single unit Maxwell model shown in Figure 2.1(a) is composed by a spring and a dashpot in series and its constitutive relation can be represented by the equation (1):

$$\dot{\varepsilon} = \frac{1}{E} \cdot \dot{\sigma} + \frac{1}{\eta} \cdot \sigma \tag{1}$$

where:

σ is the stress;

ε the deformation;

E is the elastic modulus of the spring and

η the viscosity of the dashpot.

In constant stress condition ($\sigma = \sigma_0$), the Maxwell model shows that the strains linearly increase with respect to time (2):

$$\varepsilon = \varepsilon(0) + \frac{1}{\eta} \cdot \sigma_0 \cdot t \tag{2}$$

However, if a constant strain occurs ($\varepsilon = \varepsilon_0$), the stress gradually decline (3) showing a simplification from the polymeric behaviour.

$$\sigma(t) = \sigma(0) \cdot e^{-\frac{E}{\eta} \cdot t} \tag{3}$$

On the other hand, the single unit Kelvin-Voigt model shown in Figure 2.1(c) has a different governing equation (4), since it is composed by a spring and a dashpot in parallel.

$$\sigma(t) = E\varepsilon(t) + \eta \cdot \dot{\varepsilon} \tag{4}$$

Applying a constant stress ($\sigma = \sigma_0$), the model shows a material that asymptotically decreases the rate deformations until a steady-state, but during the recovery it can recuperate this rate completely (5).

$$\varepsilon(t) = \varepsilon_0 \cdot e^{-\frac{E}{\eta} t} + \frac{\sigma_0}{E} \cdot (1 - e^{-\frac{E}{\eta} t}) \tag{5}$$

However, when a constant strain is applied ($\varepsilon = \varepsilon_0$) it tends to a certain value at infinitive time (6) and the model shows a less accuracy in describing a viscoelastic material.

$$\sigma(t) = E \cdot \varepsilon_0 \tag{6}$$

It is evident that the two mechanical models represent better the viscoelastic behaviour when the stress is constant (Kelvin-Voigt) or when the strain is constant (Maxwell). However, this research work adopted a generalized Maxwell model to simulate viscoelastic behaviour, which is composed by single units of the Maxwell model in parallel and an additional spring (Figure 2.1(b)). Obviously, the mathematical expression of this model (7) is a summation of the

equation (3), which can describe the single units of the Maxwell model in strain constant domain.

$$\sigma(t) = \varepsilon_0 (E_{eq} + \sum_{i=1}^{N} C \cdot e^{-\frac{E_i}{\eta_i} \cdot t}) \tag{7}$$

This expression belongs to the Prony series family (8):

$$PRONY = (\sum_{i=1}^{N} \alpha_i \cdot e^{-t/\tau_i}) \tag{8}$$

There are numerous methods for determining the N Prony series parameters (α_i and τ_i) either from relaxation or creep data. These data could be collected carrying out suitable tests, or they could be obtained starting from the volumetric properties of the asphalt materials and using the Hirsh Model [37]. In this work it was adopted a generalized Maxwell mechanical model starting from the relative relaxation moduli that were got from the appropriate laboratory investigations, in order to create a proper simulation of the asphalt mixtures in the software Abaqus.

In Chapter 1, the three asphalt concretes were analyzed from a mechanical point of view, collecting Dynamic Complex Moduli (|E*|) and corresponding phase angles (φ) following AASHTO TP 62-03. The tests were running at four different temperatures (-10°C, 4.4°C, 21.1°C and 37.8°C), as well as five diverse frequencies (25 Hz, 10 Hz, 5 Hz, 1 Hz, 0.5 Hz and 0.1 Hz) and using mono-material cores, got from specific slabs compacted in the laboratory (see Chapter 1). The information collected for each asphalt mixture is summarized in Table 2.2. Obviously, the source data contained scatters and were pre-smoothed using the Chauvenet's criterion.

Table 2.2 Dynamic Complex moduli for asphalt mixtures at each temperature and frequency.

Temperature = -10°C							
Frequency		***25 Hz***	***10 Hz***	***5 Hz***	***1 Hz***	***0.5 Hz***	***0.1 Hz***
WEARING	***|E*| [MPa]***	30126	27111	26361	23237	21297	17254
	Φ [deg]	1.68	3.77	4.48	5.58	7.56	10.63
BINDER	***|E*| [MPa]***	30715	29473	28795	26840	24588	23189
	Φ [deg]	2.85	4.05	4.82	6.93	7.86	9.53
BASE	***|E*| [MPa]***	29683	27526	25934	24093	21926	19501
	Φ [deg]	2.75	4.39	5.13	6.50	7.80	9.70

Temperature = +4.4°C							
Frequency		***25 Hz***	***10 Hz***	***5 Hz***	***1 Hz***	***0.5 Hz***	***0.1 Hz***
WEARING	***|E*| [MPa]***	15761	13493	12511	9213	8369	5533
	Φ [deg]	11.24	13.12	14.37	17.40	19.09	23.78
BINDER	***|E*| [MPa]***	21313	17337	15451	12121	10330	6845
	Φ [deg]	8.81	11.88	13.08	16.88	19.47	23.93
BASE	***|E*| [MPa]***	16749	15200	14352	10683	9213	6235
	Φ [deg]	11.93	12.86	14.36	19.14	21.74	24.14

Temperature = +21.1°C (reference temperature)							
Frequency		***25 Hz***	***10 Hz***	***5 Hz***	***1 Hz***	***0.5 Hz***	***0.1 Hz***
WEARING	***|E*| [MPa]***	9602	7962	6343	3587	2717	1386
	Φ [deg]	17.06	19.94	23.65	27.75	30.68	32.58
BINDER	***|E*| [MPa]***	9743	7603	6157	3414	2566	1262
	Φ [deg]	20.27	22.49	24.42	29.93	31.10	33.19
BASE	***|E*| [MPa]***	10398	8491	6788	3675	2903	1402
	Φ [deg]	19.87	22.54	24.82	29.04	30.82	32.82

Temperature = +37.8°C							
Frequency		***25 Hz***	***10 Hz***	***5 Hz***	***1 Hz***	***0.5 Hz***	***0.1 Hz***
WEARING	***|E*| [MPa]***	3255	1956	1475	884	740	527
	Φ [deg]	30.04	29.79	27.77	23.28	21.78	19.06
BINDER	***|E*| [MPa]***	3389	2161	1619	918	762	539
	Φ [deg]	34.73	30.37	28.57	23.87	22.27	19.07
BASE	***|E*| [MPa]***	4400	2799	2036	1125	931	692
	Φ [deg]	32.07	30.85	28.96	25.72	23.84	20.48

These data were shifted following the time-temperature superposition principle [38, 39] which permits to investigate either the instantaneous or long-term behaviour of visco-elastic materials, changing the setting of the temperature and/or frequency. In this way it was possible to design a sigmoidal master curve selecting a reference temperature of 21.1°C [40, 41]. The formula of the curve is shown in the following equation (9).

$$Log\,|\,E^*\,| = \delta + \frac{\alpha}{1 + e^{\beta - \gamma \cdot Logf_r}} \tag{9}$$

Where:

|E*| is the Dynamic Complex Modulus;

δ is the lower asymptote of the curve;

(δ + α) is the upper asymptote of the curve;

β and γ are shape parameters and

f_r is the reduced frequency.

Reduced frequencies were calculated using the Arrhenius shift factor α_t (10).

$$Log(f_r) = Log(f) + Log(\alpha_t) \tag{10}$$

The Arrhenius factor (α_t) is shown in the following expression (11) which is typical for asphalt mixtures:

$$Log(\alpha_t) = Log(e) \cdot \frac{\Delta H}{R} \cdot \left(\frac{1}{T} - \frac{1}{T_s} \right) \tag{11}$$

where:

ΔH is the activation energy;

R is the universal gas constant, 8.314 J/(°K mol);

T and T_s are the target temperature and the reference temperature respectively expressed in °K.

In order to calculate a proper Arrhenius shift factor, it was selected the appropriate value of ΔH in a proper range for asphalt concretes, which could be considered equal to 147÷272 kJ/mol [42]. Among these values, the ones which could minimize the error between data from the laboratory (|E*|) and the sigmoidal curve mentioned above were picked using a Simplex Method, which is an option available in Office Excel. Moreover, these fittings permitted to determine the parameters necessary to draw the sigmoidal curves, as well as the long term moduli (E_∞) and the instantaneous moduli (E_0) for each asphalt mixture (Figure 2.2). As it was explained at the beginning of the chapter, these simulations were conducted assuming the same set-up mentioned in the chapter related to the analogous laboratory investigations (Chapter 1). Therefore, both analyses were run at 10°C in order to keep the material in a visco-elastic domain and it was necessary to obtain the characteristics of the asphalt mixtures at that specific temperature. For this reason, |E*| values were calculated at 10°C using the master curves showed in Figures 2.2. In fact, using the equation of the sigmoidal function it was possible to calculate Dynamic Complex Moduli suitable for the wearing course, the binder layer and the base course asphalt mixtures at 10°C (Figure 2.3). Analogously, a proper fitting of the phase angle data provided these values at 10°C (Figure 2.4).

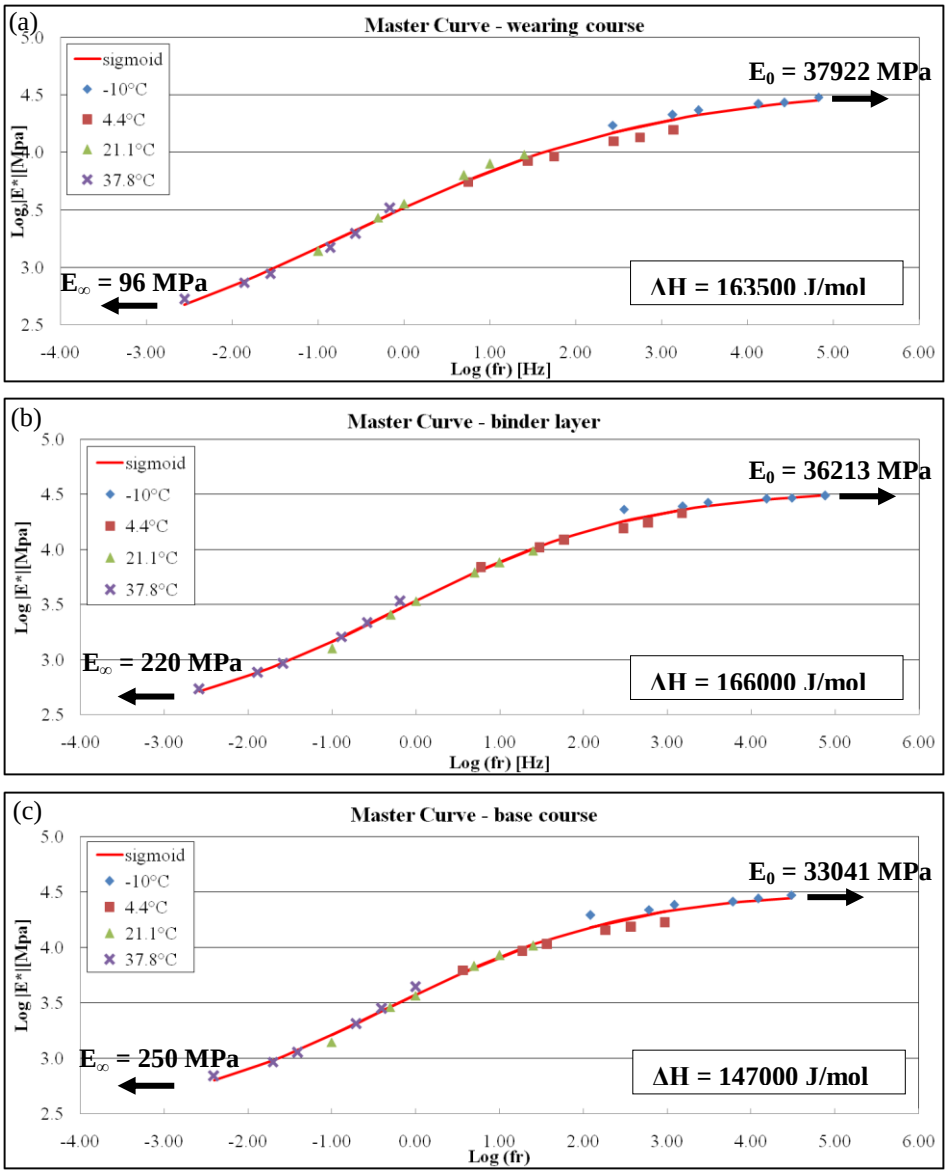

Figure 2.2 Dynamic Complex modulus master curve with relative activation energy, the long-term and instantaneous moduli for wearing course (a), binder layer (b) and base course (c).

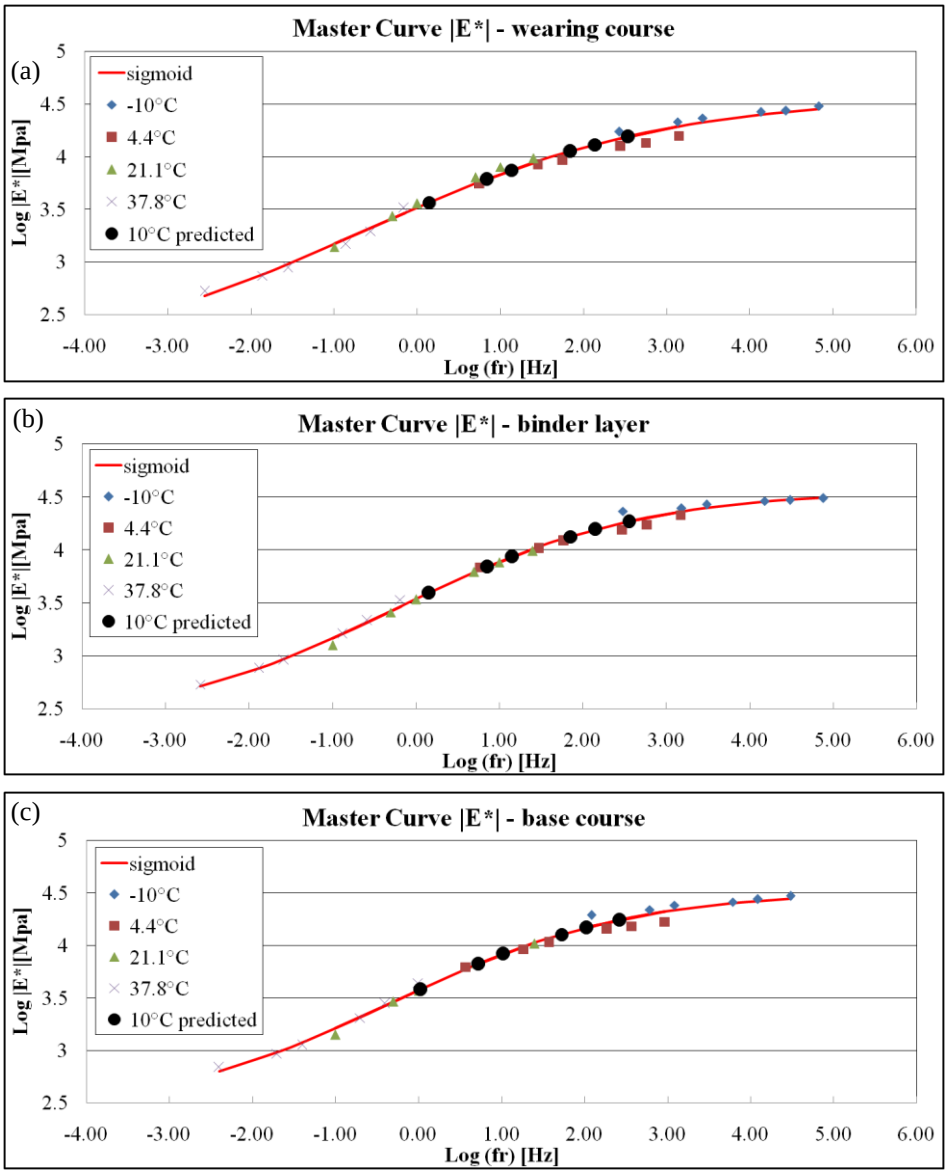

Figure 2.3 Dynamic Complex modulus master curve with the predicted value at 10°C for the wearing course (a), binder layer (b) and base course (c).

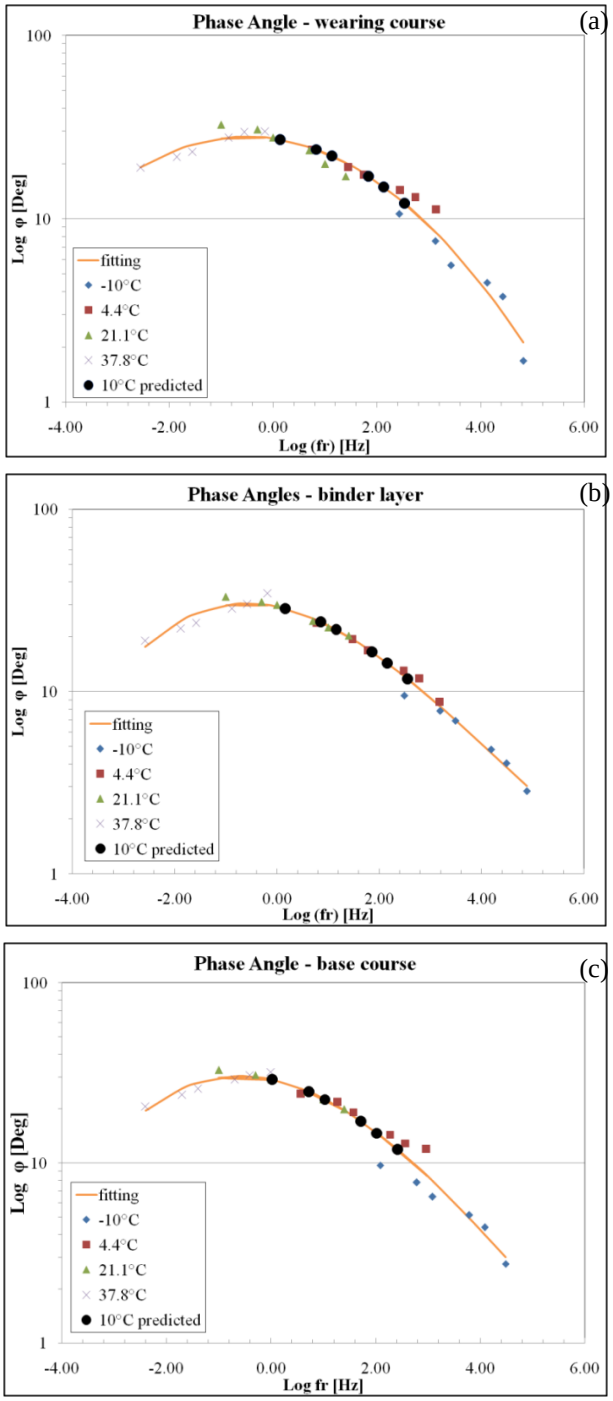

Figure 2.4 Fitting of phase angle data with the predicted value at 10°C for the wearing course (a), binder layer (b) and base course (c).

These data were useful to represent the behaviours of asphalt concretes at that temperature and to characterize the asphalt mixtures behaviour in Abaqus. At this point, it is important to highlight that these data were collected assigning a sinusoidal load and monitoring the consequent strains. So the collected data could be considered as stress constant values. However, as it was explained above, in this work a generalized Maxwell model was adopted, since it describes better the viscoelastic behaviour under a strain constant domain. In fact, relaxation data were inserted into the software used for the Finite Element Analyses (Abaqus) as the corresponding Prony parameters. Consequently, |E*| data shifted on sigmoidal curves were transformed into Shear Complex Moduli (|G*|) assuming asphalt mixtures as an isotropic material and using the following relation (12), even if these data are usually collected in a strain constant domain.

$$|G^*| = \frac{|E^*|}{2 \cdot (\nu + 1)} \tag{12}$$

where:
|G*| is the Shear Complex Modulus;
|E*| is the Dynamic Complex Modulus and
ν is the Poisson's ratio.

At the same time Dynamic Complex Moduli could be transformed into Complex Bulk Moduli making the same isotropic hypothesis for the material and using the following relation (13) [43]:

$$|K^*| = \frac{|E^*|}{3 \cdot (1 - 2\nu)} \tag{13}$$

Moreover, Poisson's ratio is time/temperature dependent. Hence, it was preliminarily set equal to 0.30 for temperatures equal or lower than 4.4°C and 0.35 with temperatures higher than 4.4°C [16], since this parameter was not directly measured in this research work. Therefore, Shear Complex Moduli were arranged on new master curves with the same sigmoidal shape with respect to the reduced time (τ) on a logarithmic scale. Analogously to the Dynamic

Complex Moduli (|E*|), Shear Complex Moduli (|G*|) were calculated at 10°C using the equation of the sigmoidal curve. Moreover, in Figure 2.5 the long term values (G_∞) as well as the instantaneous moduli (G_0) were highlighted.

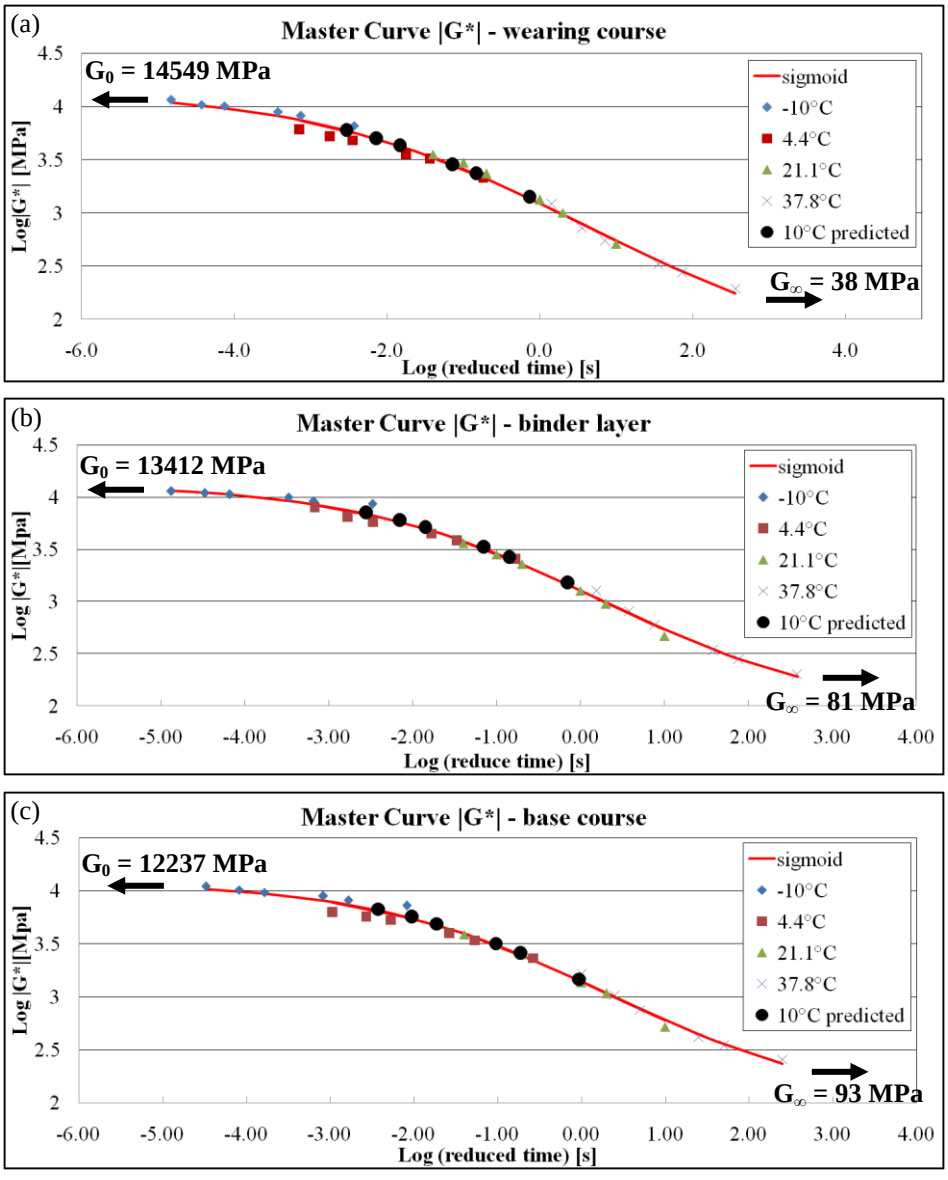

Figure 2.5 Shear Complex modulus curves with the predicted values at 10°C, the instantaneous and long-term moduli for the wearing course (a), binder layer (b) and base course (c).

The Shear Complex Moduli were divided into the real and imaginary part, which respectively represent the storage (G') and the loss (G'') parts using the corresponding phase angles (14) collected in the laboratory:

$$|G^*| = G' + iG'' = |G^*| \cdot \cos\phi + i\,|G^*|\, sen\phi \tag{14}$$

At the same time it was possible to calculate the same real and imaginary values (G' and G'') using the Fourier transformation with the Prony parameters in a time domain (15) (16) [36, 44]:

$$G'(\omega) = G_0\left[1 - \sum_{i=1}^{N} g_i\right] + G_0 \sum_{i=1}^{N} \frac{g_i \tau_i^2 \omega^2}{1 + \tau_i^2 \omega^2} \tag{15}$$

$$G''(\omega) = G_0 \sum_{i=1}^{N} \frac{g_i \tau_i \omega}{1 + \tau_i^2 \omega^2} \tag{16}$$

where:

G'(ω) is the storage modulus [MPa];

G''(ω) is the loss modulus [MPa];

G_0 instantaneous modulus [MPa];

ω is the angular frequency [Hz];

g_i and τ_i are the Prony parameters [dimensionless] and

N is the number or the Prony series parameters.

At this point it was calculated those Prony parameters which could minimize the difference between the experimental dynamic moduli got from the laboratory investigations and the ones calculated with the Prony mathematical series. A minimization algorithm (Simplex Method) was used to optimize the fitting. However, some of these variables were fixed a priori. In fact, N was fixed equal to 3, since the relaxation time (τ_i) was assumed equal to three decades (0.1 – 1 – 10 sec.) [45]. However, the angular frequencies were the six ones adopted during the Dynamic Complex Modulus |E*| and mentioned above. Obviously, this fitting permitted to obtain the Prony parameters for each asphalt mixture as summarized in Table 2.3. Moreover, in

the same Table the density values are added, as well as the elastic properties for each asphalt concrete, in order to explain the complete characterization of these materials.

Table 2.3 Visco-elastic characteristics of each asphalt mixtures to insert in Abaqus.

WEARING COURSE			
g_i	0.398763	0.322762	0.267828
τ_i	0.1	1	10
Instantaneous Elastic Modulus (E_0) [MPa]	15125		
Poisson's ratio (v)	0.35		
Density [g/cm^3]	2.30		

BINDER LAYER			
g_i	0.407292	0.347813	0.233963
τ_i	0.1	1	10
Instantaneous Elastic Modulus (E_0) [MPa]	18120		
Poisson's ratio (v)	0.35		
Density [g/cm^3]	2.35		

BASE COURSE			
g_i	0.396557	0.350615	0.241885
τ_i	0.1	1	10
Instantaneous Elastic Modulus (E_0) [MPa]	17130		
Poisson's ratio (v)	0.35		
Density [g/cm^3]	2.40		

The good agreement between the dynamic moduli predicted from the laboratory data and the ones calculated with the Prony parameters is showed in Figure 2.6 where the curves represent the behaviours (predicted and calculated) of the three asphalt mixtures at 10°C.

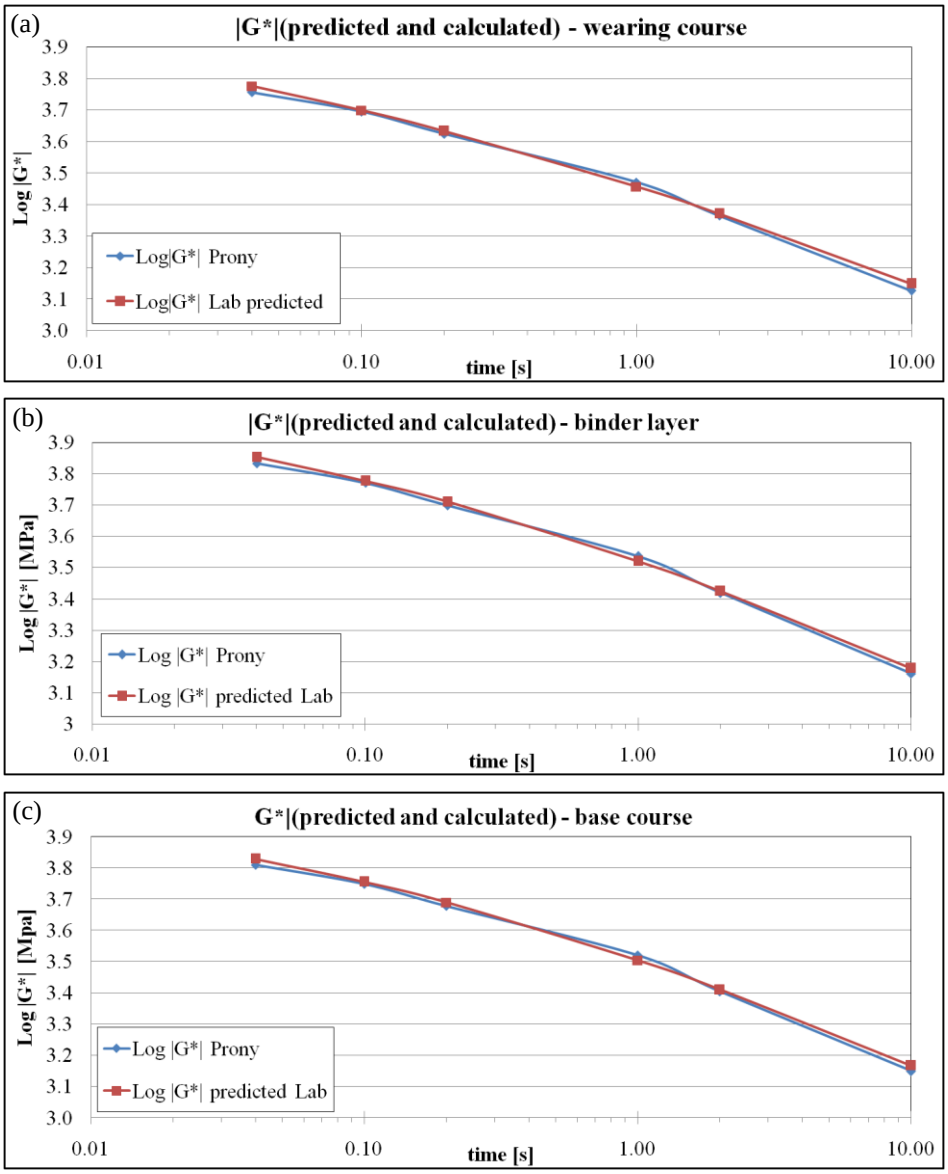

Figure 2.6 Comparison between the Shear Complex modulus predicted with laboratory investigations and calculated with Prony series for each asphalt mixtures (a) (b) (c).

The following step was fundamental and permitted to validate these parameters, in order to check the reliability of these data which had to reproduce the asphalt mixture behaviours.

1.1.1 *Validation.*

The data calculated above were validated carrying out a specific test that took AASHTO TP 62-03 as a reference. In fact, the specimens tested for this validation were those cylindrical cores (100 mm diameter) used for that AASHTO TP 62-03 test to collect Dynamic Complex Moduli and prepared with the three asphalt mixtures created during this research work (see paragraph 1.1 Chapter 1). In this way, the connection between the laboratory section and the Finite Element Analyses was perfectly guaranteed. The test set-up chose one frequency (0.1 Hz and 100 cycles) and only one temperature, which was the one fixed during the whole study: 10°C. The loading rate was set interpolating linearly the amount of load set in AASHTO TP 62-03 test at 4.4°C and 21.1°C. Hence, the three kinds of cylindrical cores were subjected to these investigations, monitoring the vertical displacements with proper extensimeter. At the same time, in Abaqus analogous models were created and they could reproduce the same laboratory tests. Cylinders with corresponding geometry were simulated and the same load rate was applied, in order to check the vertical deformations of the samples (Figure 2.7). Obviously, the asphalt mixtures were simulated as a visco-elastic material inserting those parameters summarized in Table 2.3.

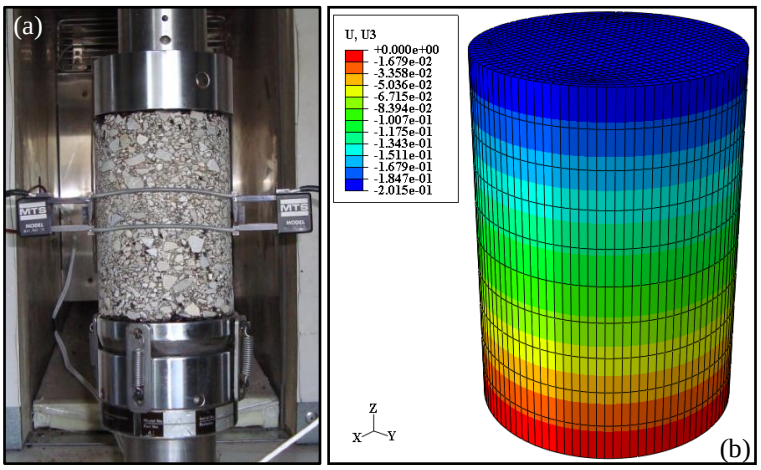

Figure 2.7 Laboratory investigation (a) and the corresponding simulation in Abaqus (b).

In Figure 2.8 the vertical deformations of the cylinders in the laboratory were compared to those got from the simulations.

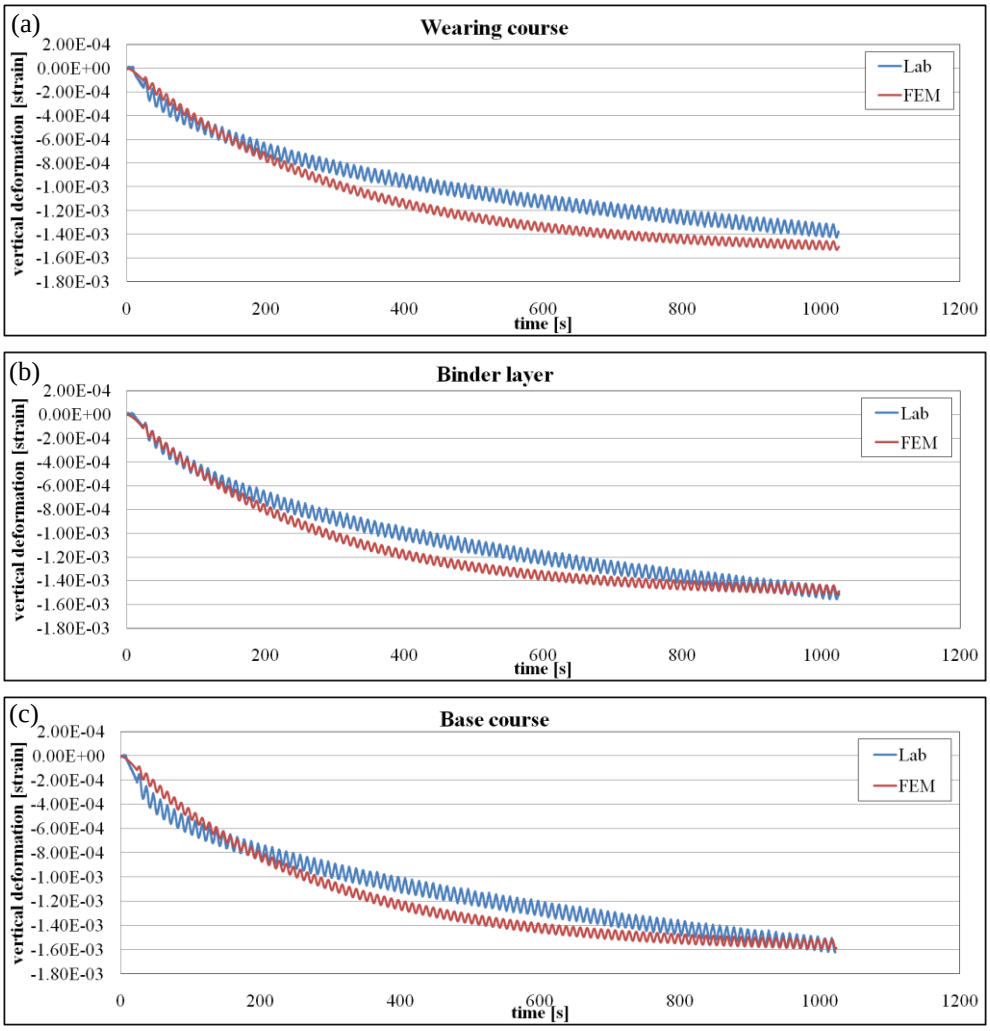

Figure 2.8 Laboratory vertical deformations and the corresponding simulated for wearing course (a), binder layer (b) and base course (c).

Results showed a good agreement between the vertical displacements collected in the laboratory and the simulated ones (FEM). Hence, it was possible to simulate asphalt mixtures using the parameters in Table 2.3 and analyse their behaviours as reliable results.

1.2 Three-Dimensional Modelling.

The 3-Dimensional Finite Element modelling recreated a typical flexible pavement composed by a three-layer asphalt concrete with different thickness: 30 mm of the wearing course, 40 mm of the binder layer and 100 mm of the base course. Moreover, the sub-base stratum was simulated with a 40 mm thick neoprene layer. Finally the whole model was a square with a 500 mm side length and it was reproduced using 3-Dimensional eight-node brick elements with a reduced integration (C3D8R) available in Abaqus. The analogy between the geometry of the laboratory samples and the corresponding 3-Dimensional models could be verified comparing Figure 2.9 with Figure 1.18 (Chapter 1).

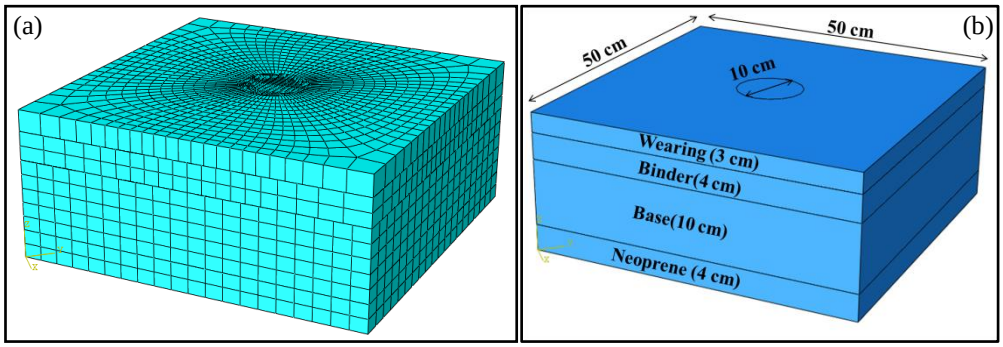

Figure 2.9 Model with squared meshes (a) and geometry of the modelled sample (b).

This analysis simulated a flexible road pavement with a steel reinforcing system or a glass grid positioned between the binder layer and the base course. Obviously, a control model without any kind of interlayer system was added, in order to make proper comparisons. The steel net was simulated as a wire with three different diameter dimensions: the reinforcing bars, the double twisted wire and the single wire. The Figure 2.10 shows the shape of this reinforcing system and the different dimensions. On the other hand, the glass grid was simulated as 3-Dimensional elements, 1 mm thick, with a regular squared shape (Figure 2.11).

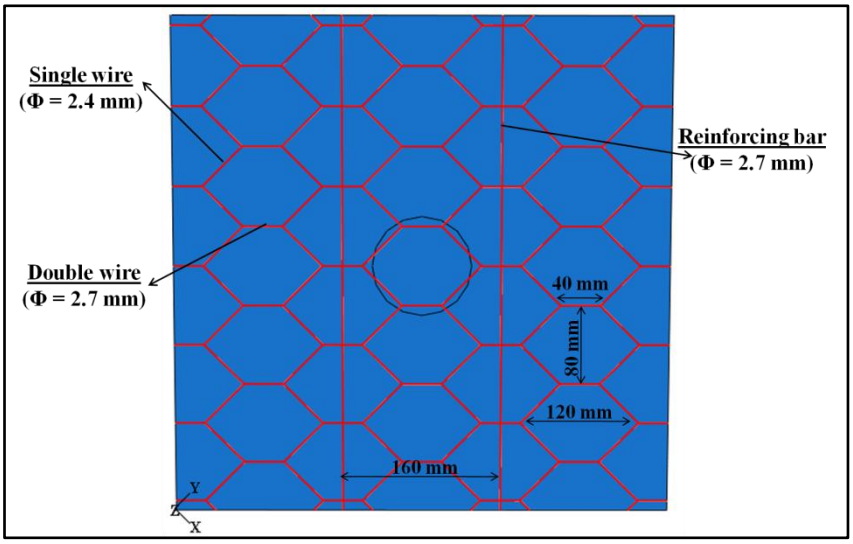

Figure 2.10 The model of the steel net reinforcing system on the bottom of the binder layer.

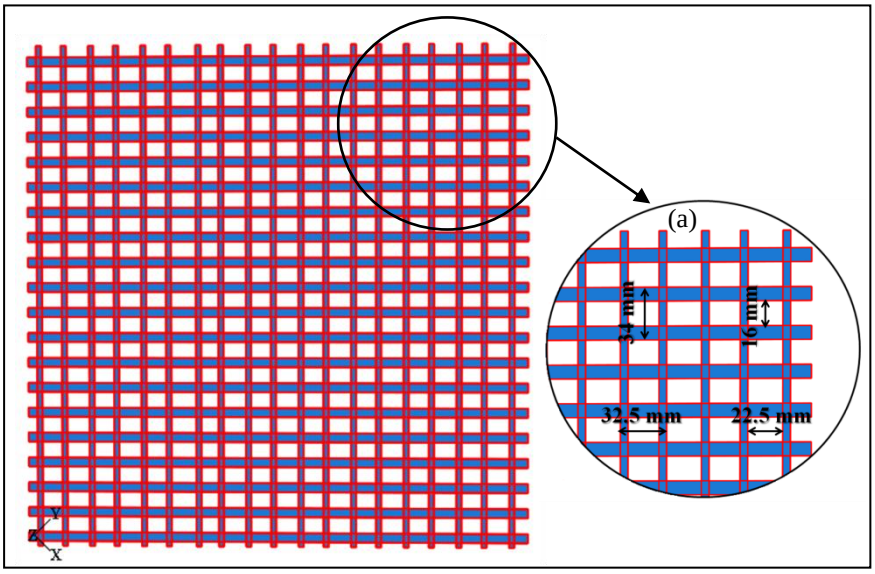

Figure 2.11 The model of the glass grid reinforcing system and a detail (a).

In the whole model the mesh sizes were different according to the zone of the specimen. In fact,

on the top of the upper layer the area close to the loading mark highlights a more refined mesh, since it was the target area. However, the dimension of the mesh becomes coarser at the edges of the model and outside the zone where strains were monitored (Figure 2.12). This choice could save computational time, since a reduced amount of brick elements were used.

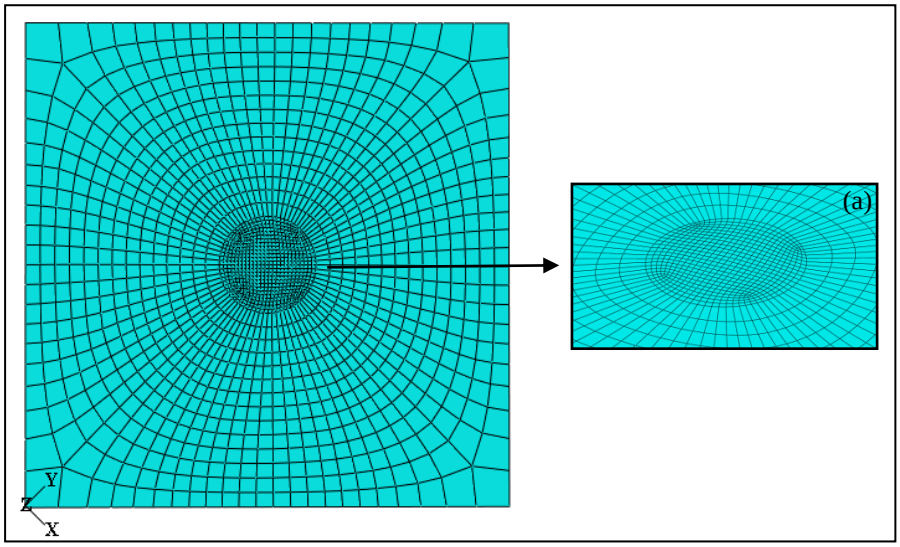

Figure 2.12 The mesh on the top of the wearing course and a detail of the loading mark (a).

An important aspect was related to the boundary conditions and interactions. The bottom part of the neoprene layer was fixed, even if it could not be considered as an in-situ condition. In fact, the sub-base (simulated using the neoprene layer) in real flexible pavements is laid down on a semi-infinite region, which cannot completely block the vertical movements. However, it was not possible to recreate this condition during the validation phase of this study in the laboratory, therefore this assumption was made. As regarding the interfaces, the tangential behaviours were managed by the Coulomb law, which could control the level of the adhesion between the layers in contact. In fact, the friction coefficient between the asphalt layers was set equal to 0.7 [46], since the three layers of the model could not be considered fully bonded. In fact, in-situ they are compacted one upon the other, as well as during the validation investigations in the laboratory. Moreover, in the normal direction the interfaces did not allow any separation, when the two surfaces were in contact. However, in those models where a reinforcing system was inserted,

the grids were totally embedded at the bottom of the binder layers and behaved as a unique part. On the wearing surface the passing of a vehicular loading, with a tire inflation pressure of 7 bars was simulated. It was applied on a circular loading mark of a 100 mm diameter (corresponding to 5.5 kN) creating a partition on the upper part of the model with this shape (Figure 2.9 and 2.12).

The simulations reproduced the in-service life of a flexible road pavement. A typical creep test was run, in order to check the behaviours of the material under a static load. Moreover, sinusoidal cycles (100 cycles or 1000 seconds) were simulated using the Fourier equation available in Abaqus, in order to reproduce the passing of the above mentioned tire at different velocities, which corresponded to different values of frequency. In Figure 2.13 the scenarios simulated during these analyses are shown, which are analogous to the laboratory investigations (Figure 1.20 – 1.21, Chapter 1).

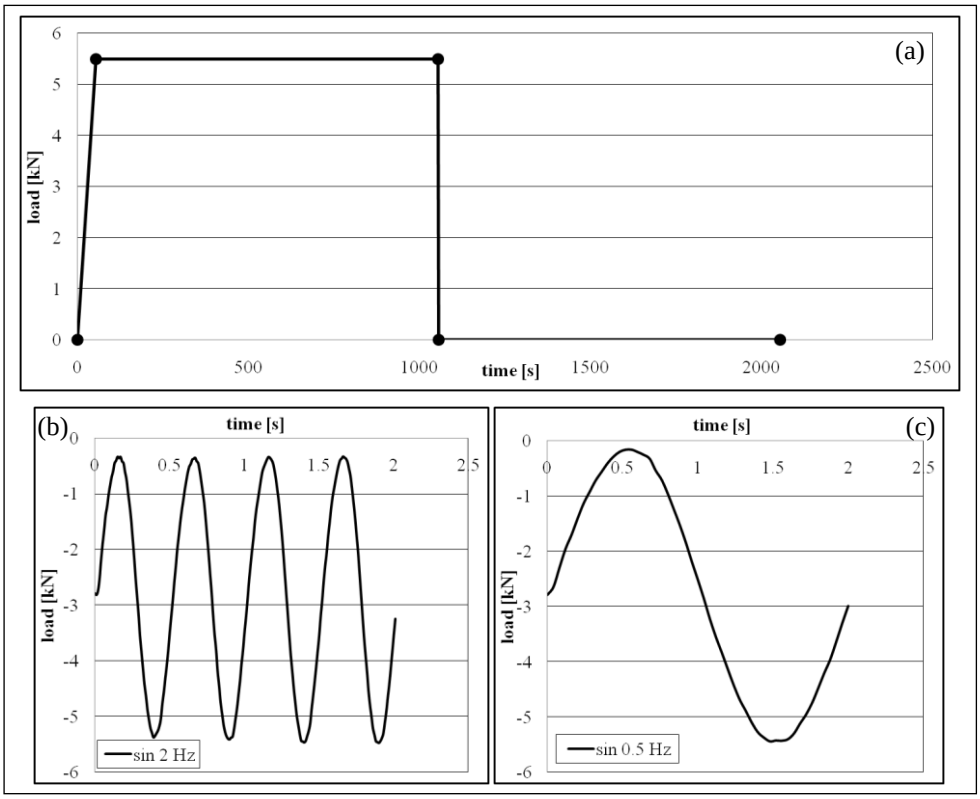

Figure 2.13 Creep (a) and sinusoidal test at 2 Hz (b) and 0.5 Hz (c) simulated in Abaqus.

In the previous paragraphs the configuration of the three modelling analyses was explained and it pretends to reproduce the real scale samples of a multilayer flexible pavement with or without reinforcing systems, in order to investigate the in-service behaviours.

1.3 Results.

The previous paragraph explained the creation of a Finite Element Model using the software Abaqus. In this section, the results are presented showing the deformations close to the loading mark. The output results of the control samples without any kind of reinforce are firstly analyzed and the data related to the reinforced slabs follow in the subsequent paragraphs. The results are presented dividing static tests (creep tests), from the dynamic ones (sinusoidal tests). Figure 2.14 shows an example of the output results obtained in Abaqus on the top of the wearing course in both directions, x and y. Therefore the subsequent analyses were organized following the same approach of the Chapter 1.

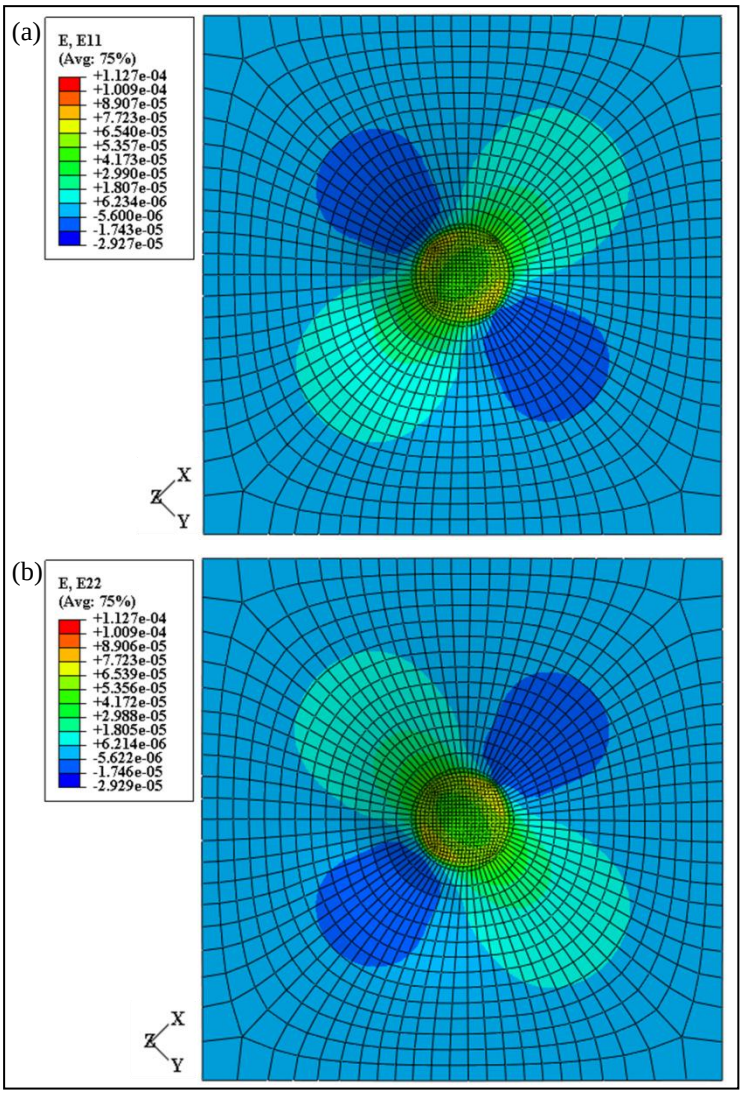

Figure 2.14 Strain distribution around the loading mark, direction X (a) and Y (b).

The strain distributions were checked in the same area investigated in the laboratory using strain gauges close to the loading mark on the surface of the slabs (Figure 2.15). Following the same criteria, proper comparisons among the three typologies of simulations were made, in order to check to different behaviours of the slabs.

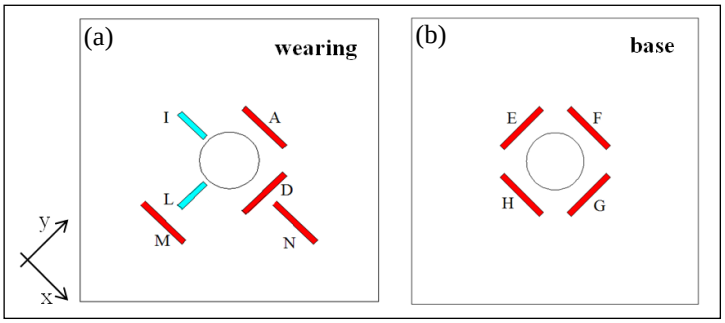

Figure 2.15 Position of the strain gauges on the wearing course (a) and on the base course (b).

- ***Control slabs (without any reinforcing system)***

Figure 2.16 shows the strain response of the control slab modelling in two different areas close to the loading mark while a creep test was simulated.

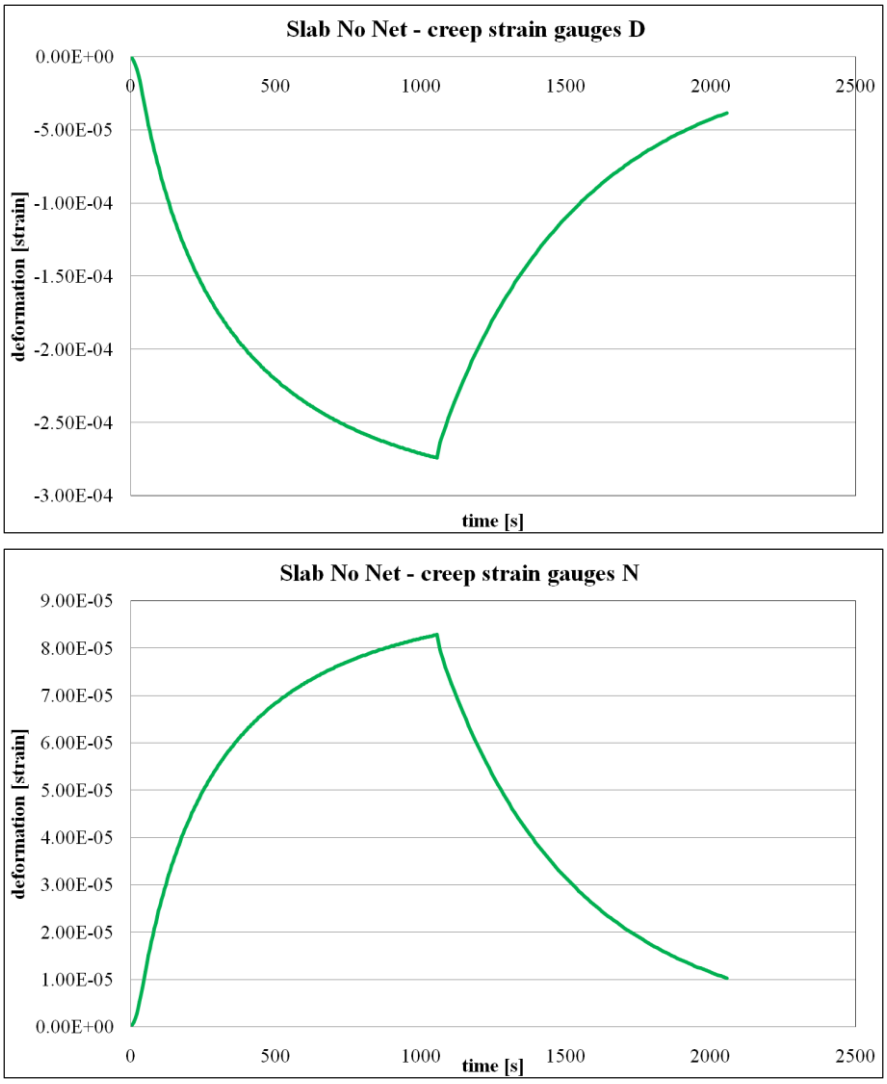

Figure 2.16 Creep test on control slab - strain gauges D and N.

Table 2.4 highlights the strain peak values and the percentages of the recovered strain that were the output of Abaqus during the modelling investigations in those areas which corresponded to the laboratory strain gauges in position D and N.

Table 2.4 Peak value and recovery of control slab during the simulation of the creep test.

CREEP – CONTROL SLAB		
Area corresponding to the Laboratory Strain Gauges Position	***D***	***N***
Peak value [μstrain]	-274	83
Recovery [%]	86	88

Figure 2.17 shows the strain response in different areas close to the loading mark of the control slabs and applying 100 cycles of a sinusoidal load at 0.5 Hz.

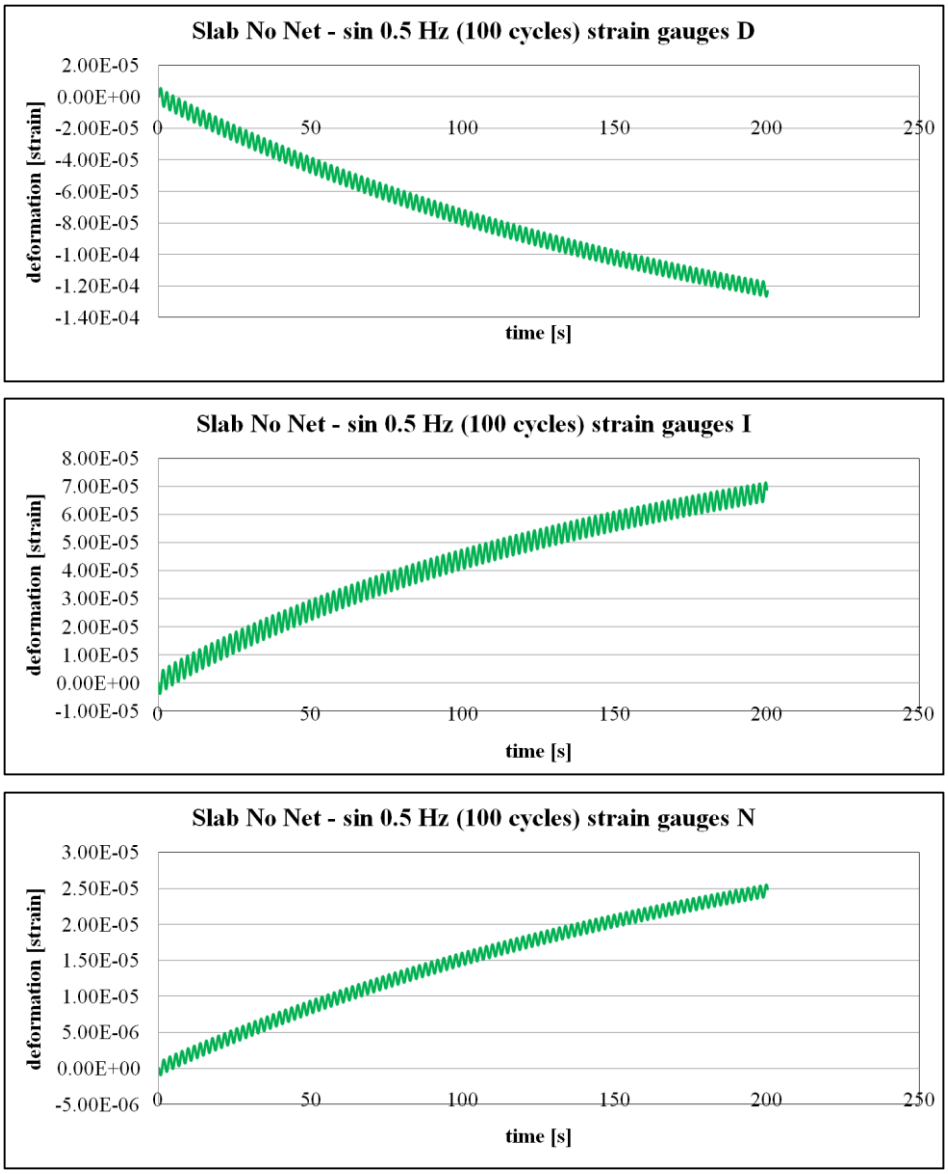

Figure 2.17 Sinusoidal test (100 cycles, 0.5 Hz) on control slab - strain gauges D, I and N.

Table 2.5 highlights the strain peak values and the wave amplitude of the strain that were the output of Abaqus during the modelling investigations in those areas which corresponded to the laboratory strain gauges in position D, I and N.

Table 2.5 Peak value and wave amplitude of control slab (sinusoidal test 100 cycles, 0.5 Hz).

SIN 0.5Hz (100 cycles) – CONTROL SLAB			
Area corresponding to the Laboratory Strain Gauges Position	***D***	***I***	***N***
Peak value [μstrain]	-122	68	25
Wave amplitude [μstrain]	9.7	7.0	1.8

Figure 2.18 shows the strain response in different areas close to the loading mark of the control slabs and applying a sinusoidal load at 0.5 Hz for 1000 seconds.

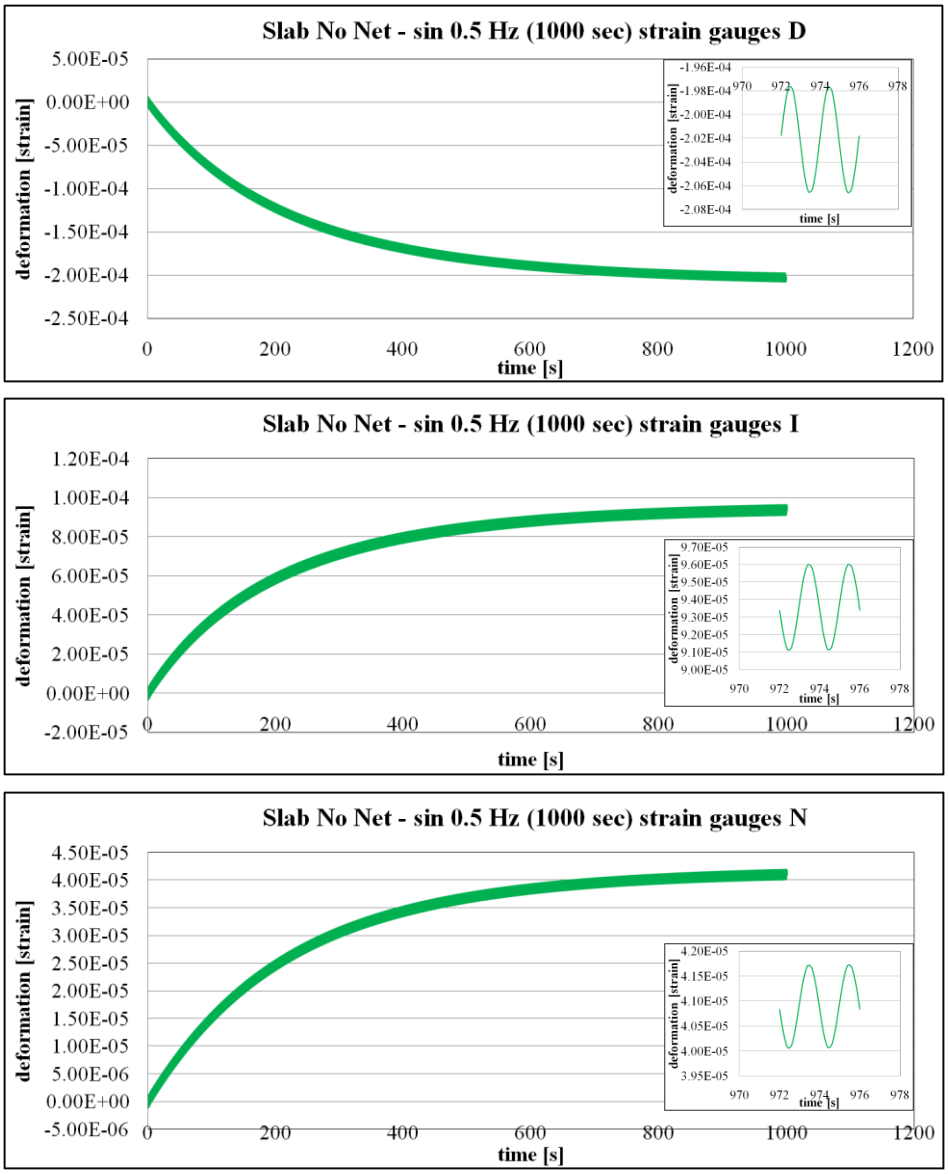

Figure 2.18 Sinusoidal test (1000 s, 0.5 Hz) on control slab - strain gauges D, I and N.

Table 2.6 highlights the strain peak values and the wave amplitude of the strain that were the output of Abaqus during the modelling investigations in those areas which corresponded to the laboratory strain gauges in position D, I and N.

Table 2.6 Peak value and wave amplitude of control slab (sinusoidal test 1000 s, 0.5 Hz).

SIN 0.5Hz (1000 seconds) – CONTROL SLAB			
Area corresponding to the Laboratory Strain Gauges Position	***D***	***I***	***N***
Peak value [μstrain]	-203	94	41
Wave amplitude [μstrain]	8.9	4.8	1.6

Figure 2.19 shows the strain response in different areas close to the loading mark of the control slabs and applying 100 cycles of a sinusoidal load at 2 Hz.

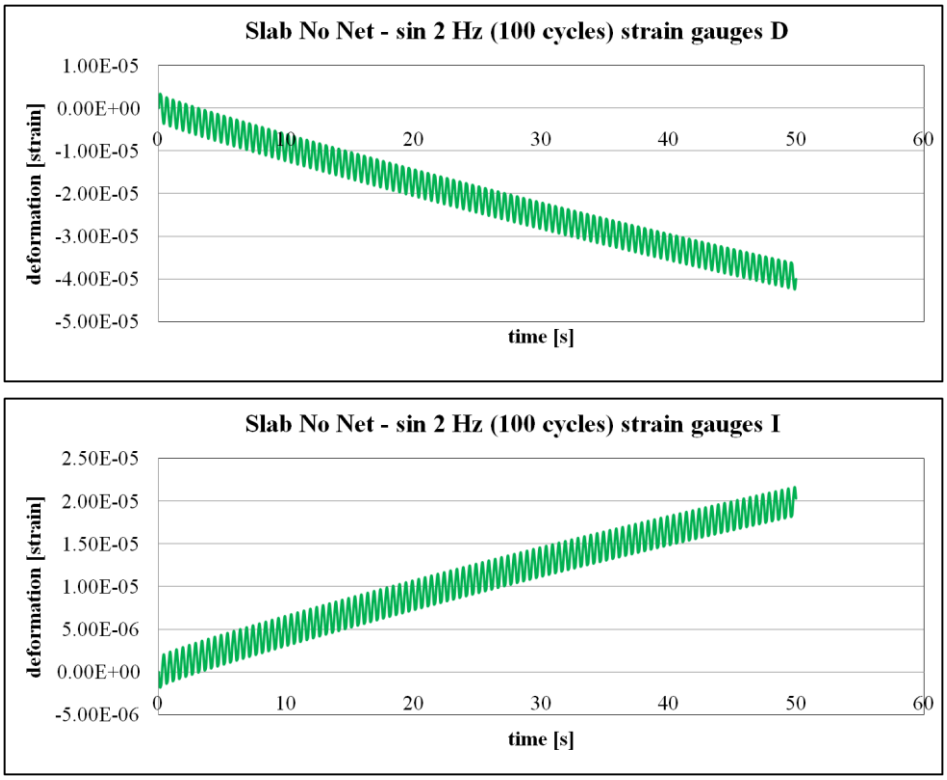

Figure 2.19 Sinusoidal test (100 cycles, 2 Hz) on control slab - strain gauges D and I.

Table 2.7 highlights the strain peak values and the wave amplitude of the strain that were the output of Abaqus during the modelling investigations in those areas which corresponded to the laboratory strain gauges in position D and I.

Table 2.7 Peak value and wave amplitude of control slab (sinusoidal test 100 cycles, 2 Hz).

SIN 2Hz (100 cycles) – CONTROL SLAB		
Area corresponding to the Laboratory Strain Gauges Position	***D***	***I***
Peak value [μstrain]	40	20
Wave amplitude [μstrain]	6.3	3.5

Figure 2.20 shows the strain response in different areas close to the loading mark of the control slabs and applying a sinusoidal load at 2 Hz for 1000 seconds.

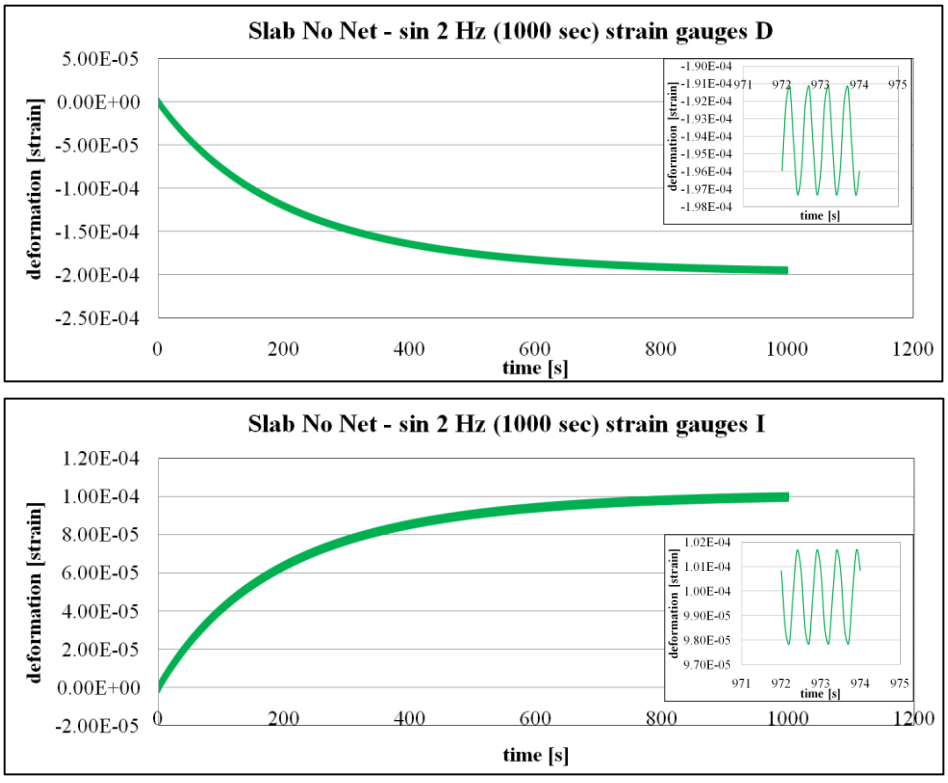

Figure 2.20 Sinusoidal test (1000 s, 2 Hz) on control slab - strain gauges D and I.

Table 2.8 highlights the strain peak values and the wave amplitude of the strain that were the output of Abaqus during the modelling investigations in those areas which corresponded to the laboratory strain gauges in position D and I.

Table 2.8 Peak value and wave amplitude of control slab (sinusoidal test 1000 s, 2 Hz).

SIN 2Hz (1000 seconds) – CONTROL SLAB		
Area corresponding to the Laboratory Strain Gauges Position	***D***	***I***
Peak value [μstrain]	-195	100
Wave amplitude [μstrain]	6.2	3.8

- ***Slabs reinforced with Steel Net***

Figure 2.21 shows the strain response of the slab modelled with a steel reinforcing net between binder layer and base course in three different areas close to the loading mark while a creep test was simulated.

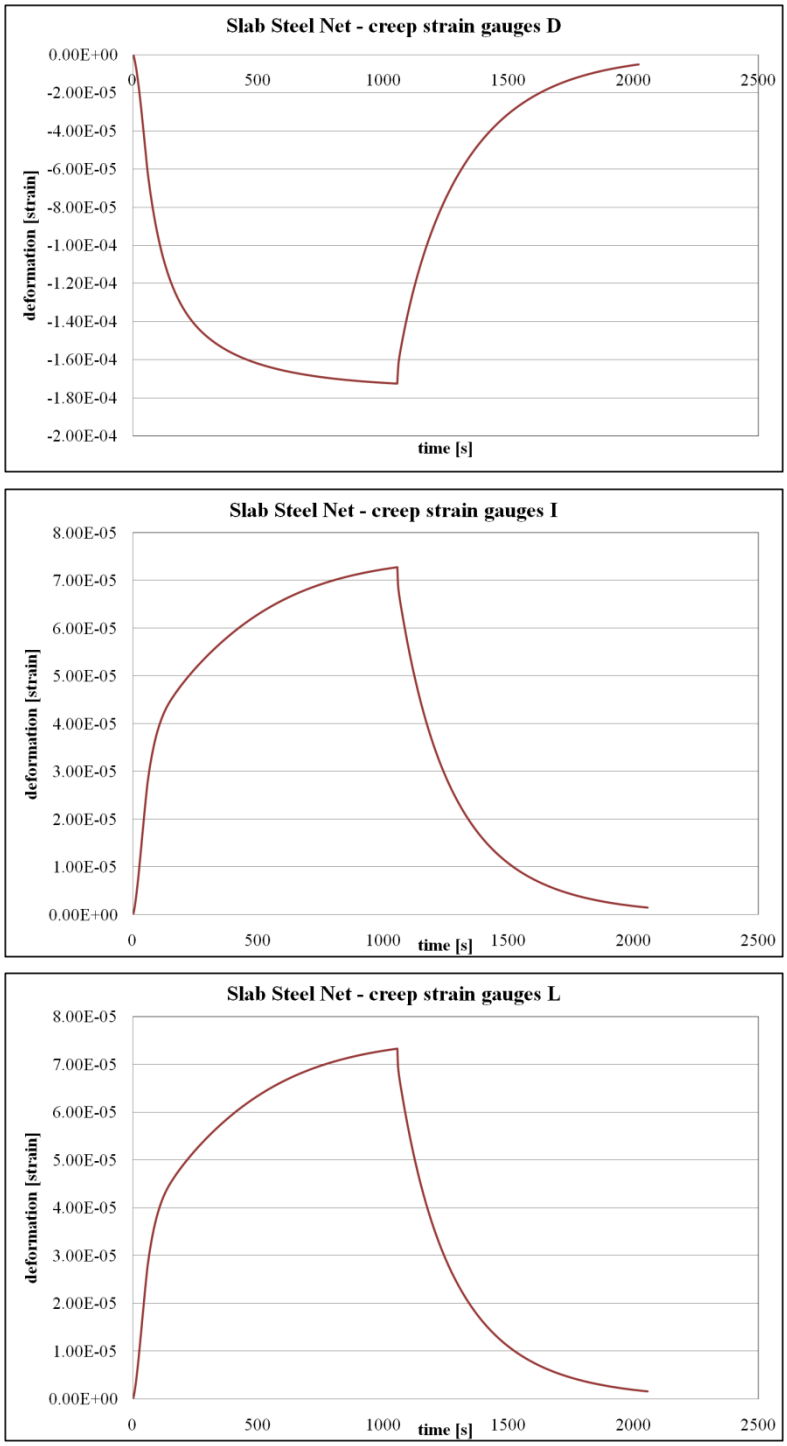

Figure 2.21 Creep test on slab with steel net - strain gauges D, I and L.

Table 2.9 highlights the strain peak values and the percentages of the recovered strain that were the output of Abaqus during the modelling investigations in those areas which corresponded to the laboratory strain gauges in position D, I and L.

Table 2.9 Peak value and recovery of slab with steel net during the simulation of the creep test.

CREEP – SLAB WITH STEEL NET			
Area corresponding to the Laboratory Strain Gauges Position	***D***	***I***	***L***
Peak value [μstrain]	-173	73	73
Recovery [%]	97	98	98

Figure 2.22 shows the strain response in different areas close to the loading mark of the control slabs and applying 100 cycles of a sinusoidal load at 0.5 Hz.

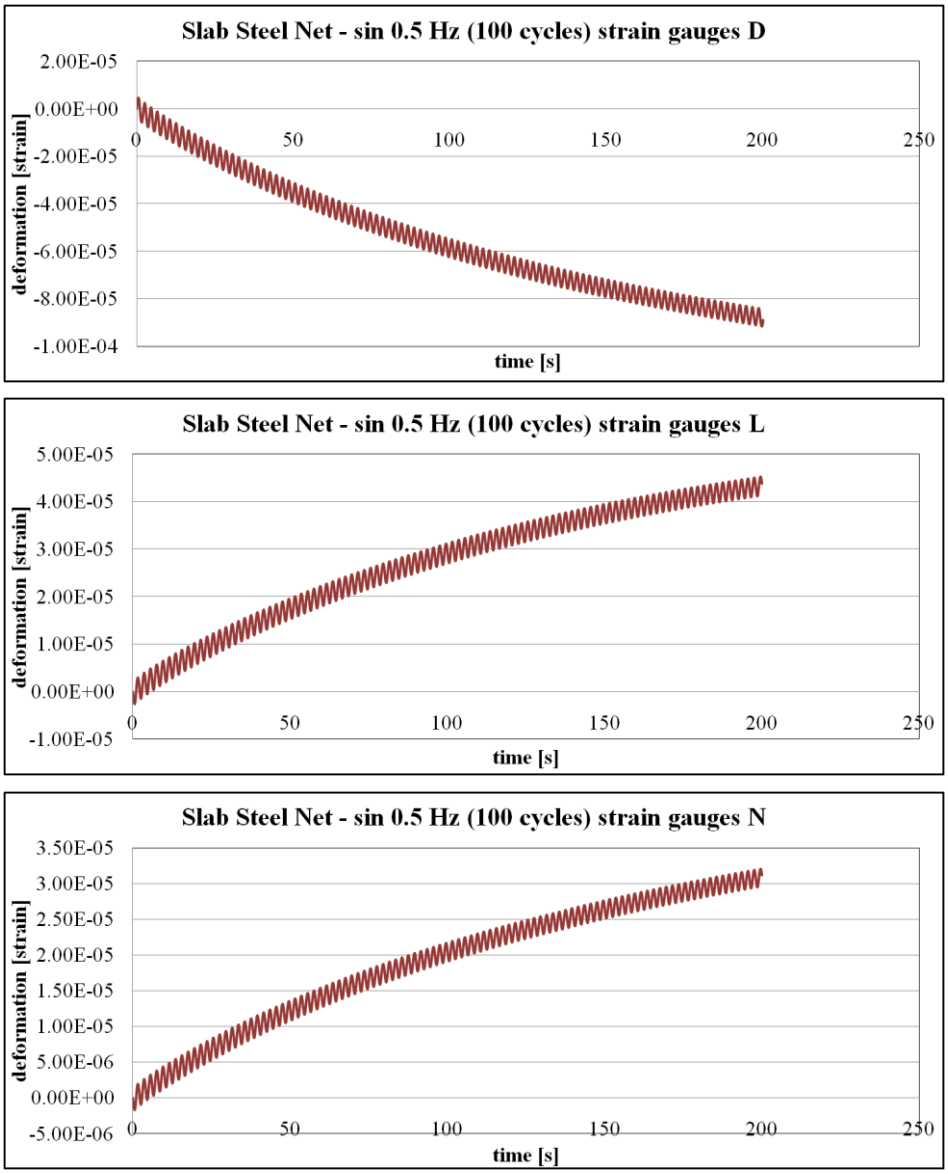

Figure 2.22 Sinusoidal test (100cycles, 0.5Hz) on slab with steel net - strain gauges D, L and N.

Table 2.10 highlights the strain peak values and the wave amplitude of the strain that were the output of Abaqus during the modelling investigations in those areas which corresponded to the laboratory strain gauges in position D, L and N.

Table 2.10 Peak value and wave amplitude of slab steel net (sinusoidal test 100 cycles, 0.5 Hz).

SIN 0.5Hz (100 cycles) – SLAB WITH STEEL NET			
Area corresponding to the Laboratory Strain Gauges Position	***D***	***L***	***N***
Peak value [μstrain]	-89	44	31
Wave amplitude [μstrain]	7.7	4.1	2.6

Figure 2.23 shows the strain response in different areas close to the loading mark of the control slabs and applying a sinusoidal load at 0.5 Hz for 1000 seconds.

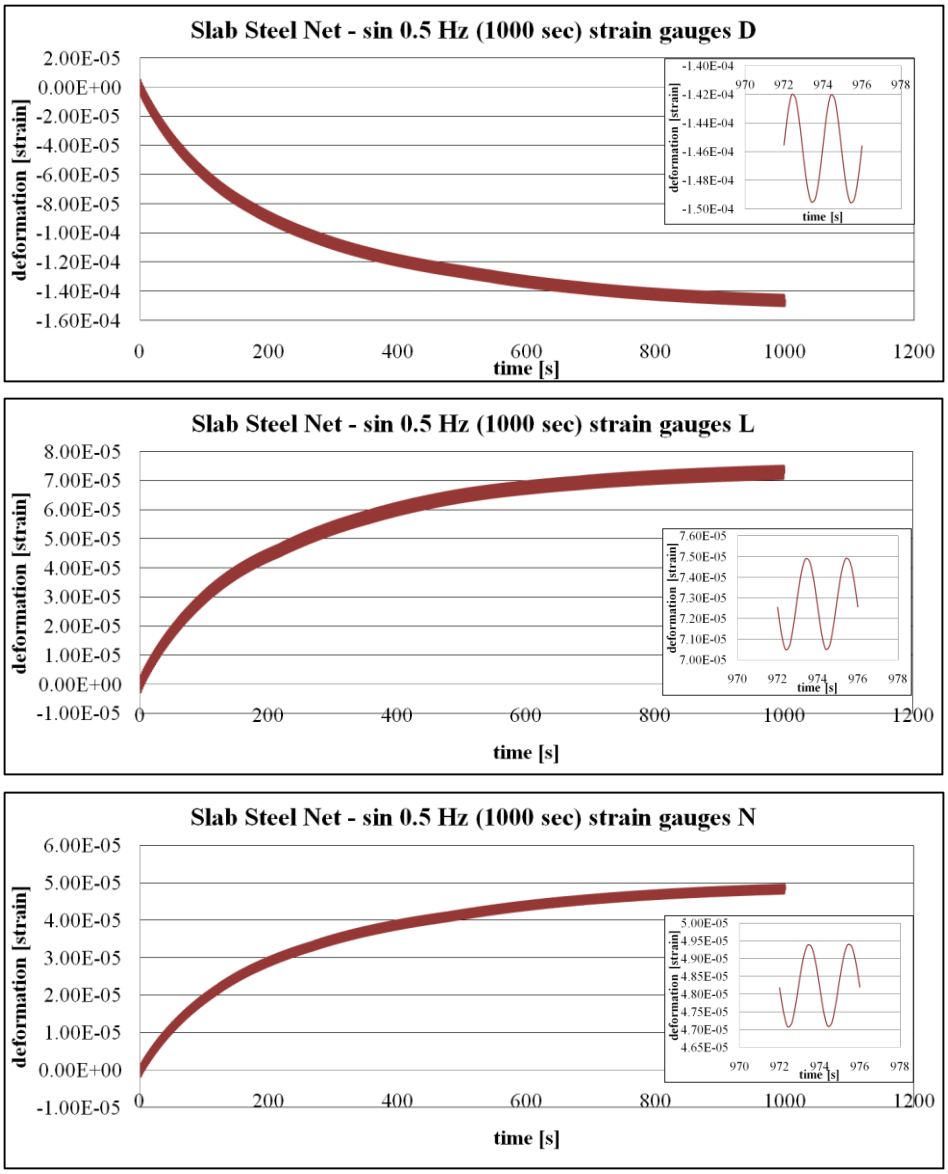

Figure 2.23 Sinusoidal test (1000 s, 0.5 Hz) on slab with steel net - strain gauges D, L and N.

Table 2.11 highlights the strain peak values and the wave amplitude of the strain that were the output of Abaqus during the modelling investigations in those areas which corresponded to the laboratory strain gauges in position D, L and N.

Table 2.11 Peak value and wave amplitude of slab steel net (sinusoidal test 1000 s, 0.5 Hz).

SIN 0.5Hz (1000 seconds) – SLAB WITH STEEL NET			
Area corresponding to the Laboratory Strain Gauges Position	***D***	***L***	***N***
Peak value [μstrain]	-147	73	49
Wave amplitude [μstrain]	7.5	4.4	2.3

Figure 2.24 shows the strain response in different areas close to the loading mark of the control slabs and applying 100 cycles of a sinusoidal load at 2 Hz.

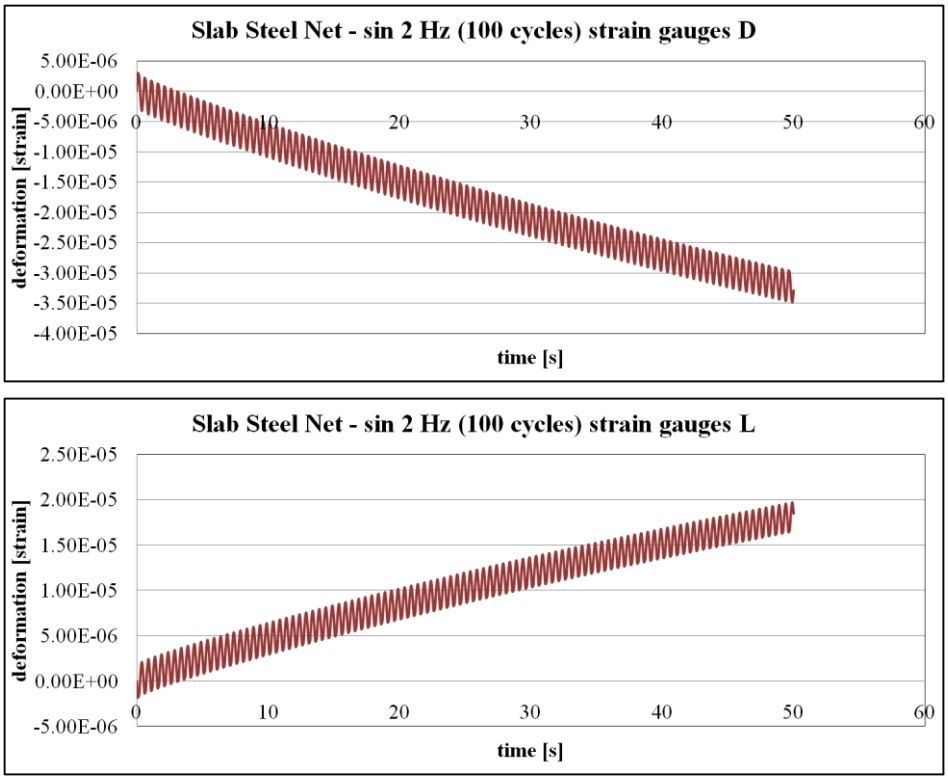

Figure 2.24 Sinusoidal test (100 cycles, 2 Hz) on slab with steel net - strain gauges D and L.

Table 2.12 highlights the strain peak values and the wave amplitude of the strain that were the output of Abaqus during the modelling investigations in those areas which corresponded to the laboratory strain gauges in position D and L.

Table 2.12 Peak value and wave amplitude of slab steel net (sinusoidal test 100 cycles, 2 Hz).

SIN 2Hz (100 cycles) – SLAB WITH STEEL NET		
Area corresponding to the Laboratory Strain Gauges Position	***D***	***L***
Peak value [μstrain]	-33	18
Wave amplitude [μstrain]	5.2	3.3

Figure 2.25 shows the strain response in different areas close to the loading mark of the control slabs and applying a sinusoidal load at 2 Hz for 1000 seconds.

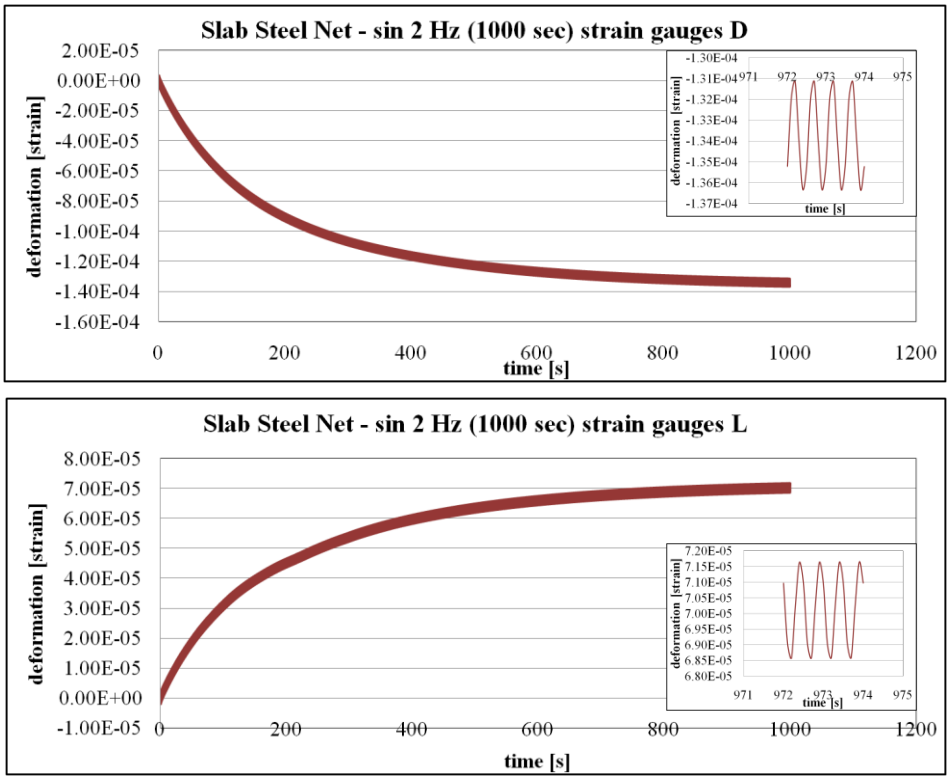

Figure 2.25 Sinusoidal test (100 cycles, 2 Hz) on slab with steel net - strain gauges D and L.

Table 2.13 highlights the strain peak values and the wave amplitude of the strain that were the output of Abaqus during the modelling investigations in those areas which corresponded to the laboratory strain gauges in position D and L.

Table 2.13 Peak value and wave amplitude of slab steel net (sinusoidal test 1000 s, 2 Hz).

SIN 2Hz (1000 seconds) – SLAB WITH STEEL NET		
Area corresponding to the Laboratory Strain Gauges Position	***D***	***L***
Peak value [μstrain]	-135	71
Wave amplitude [μstrain]	5.2	3.1

- ***Slabs reinforced with Glass Grid***

Figure 2.26 shows the strain response of the slab modelled with a glass grid between binder layer and base course in two different areas close to the loading mark while a creep test was simulated.

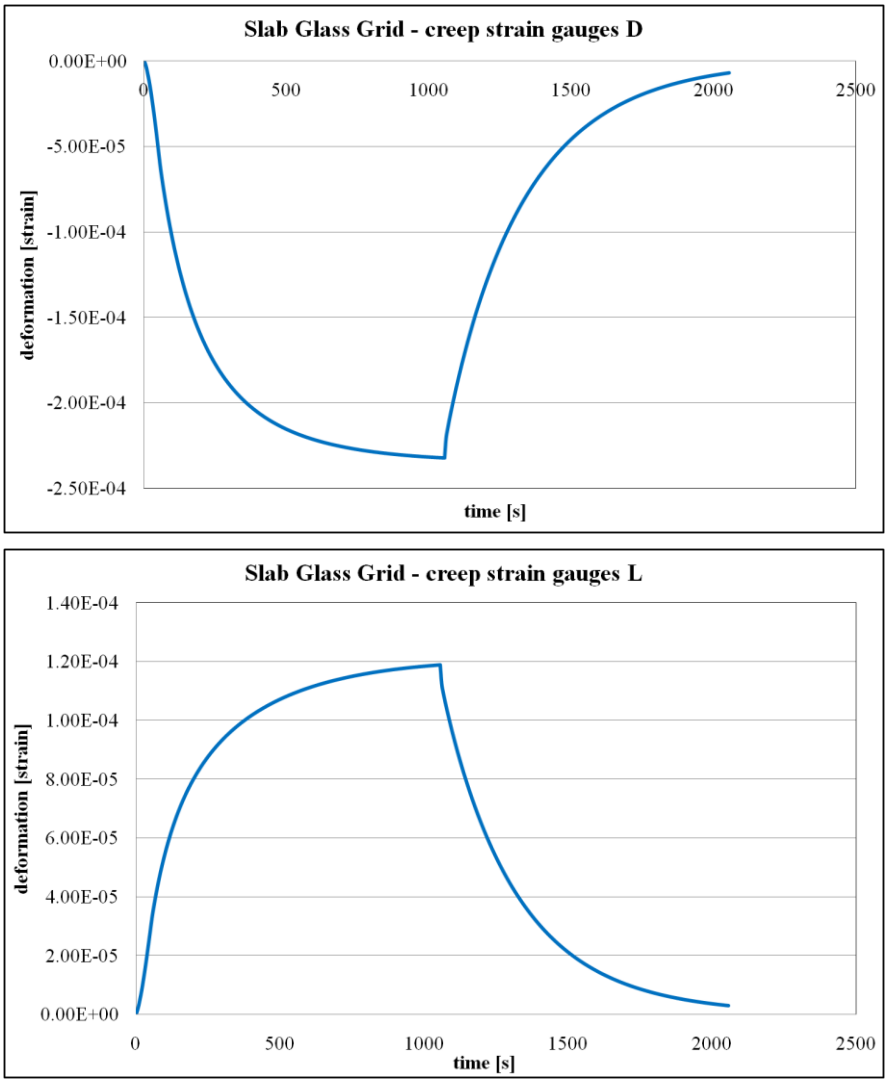

Figure 2.26 Creep test on slab with glass grid - strain gauges D and L.

Table 2.14 highlights the strain peak values and the percentages of the recovered strain, which were the output of Abaqus during the modelling investigations in those areas which corresponded to the laboratory strain gauges in position D and L.

Table 2.14 Peak value and recovery of slab with glass grid during the simulation of creep test.

CREEP – SLAB WITH GLASS GRID		
Area corresponding to the Laboratory Strain Gauges Position	***D***	***L***
Peak value [μstrain]	-232	119
Recovery [%]	97	98

Figure 2.27 shows the strain response in different areas close to the loading mark of the control slabs and applying 100 cycles of a sinusoidal load at 0.5 Hz.

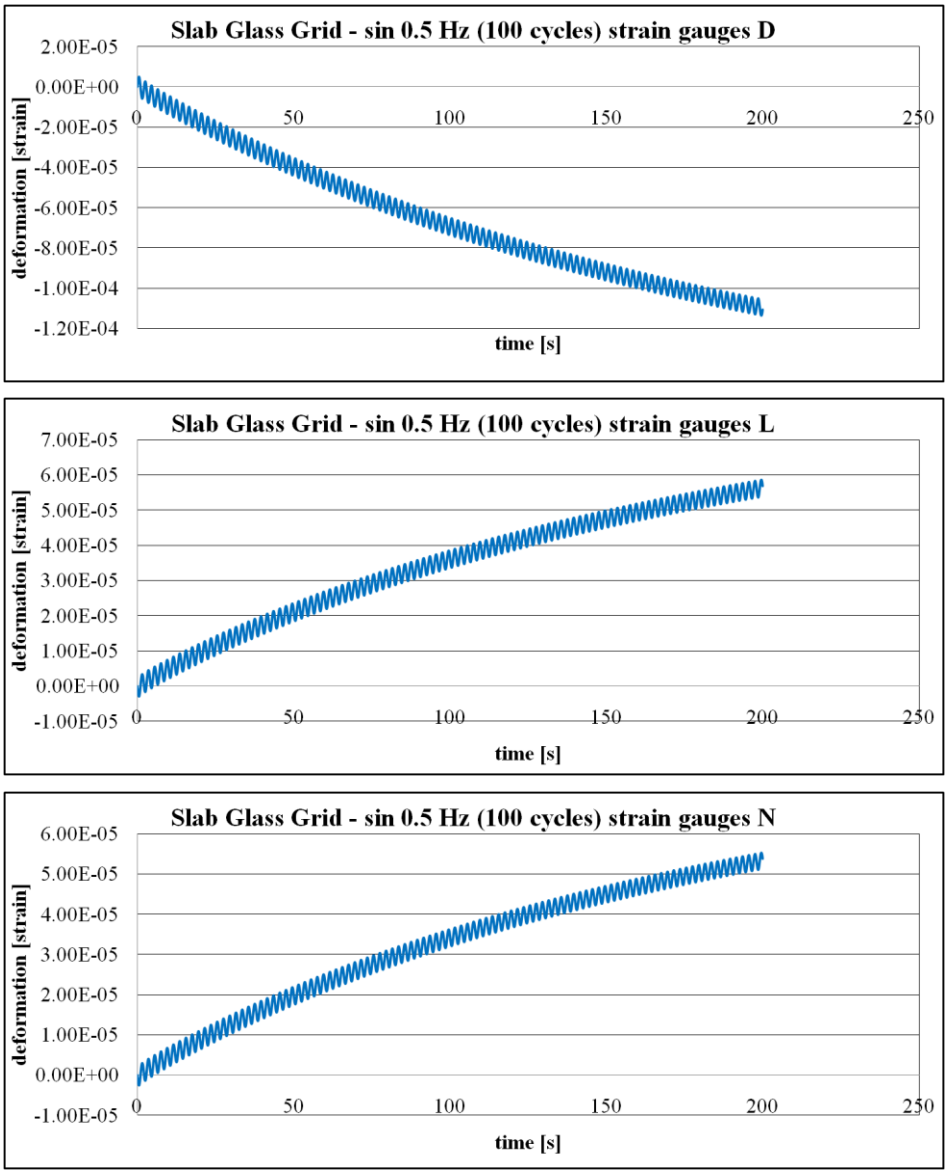

Figure 2.27 Sinusoidal test (100cycles,0.5Hz) on slab with glass grid-strain gauges D, L and N.

Table 2.15 highlights the strain peak values and the wave amplitude of the strain that were the output of Abaqus during the modelling investigations in those areas which corresponded to the laboratory strain gauges in position D, L and N.

Table 2.15 Peak value and wave amplitude of slab glass grid (sinusoidal test 100cycles, 0.5Hz).

SIN 0.5Hz (100 cycles) – SLAB WITH GLASS GRID			
Area corresponding to the Laboratory Strain Gauges Position	***D***	***L***	***N***
Peak value [μstrain]	-114	59	55
Wave amplitude [μstrain]	8.5	5.0	4.2

Figure 2.28 shows the strain response in different areas close to the loading mark of the control slabs and applying a sinusoidal load at 0.5 Hz for 1000 seconds.

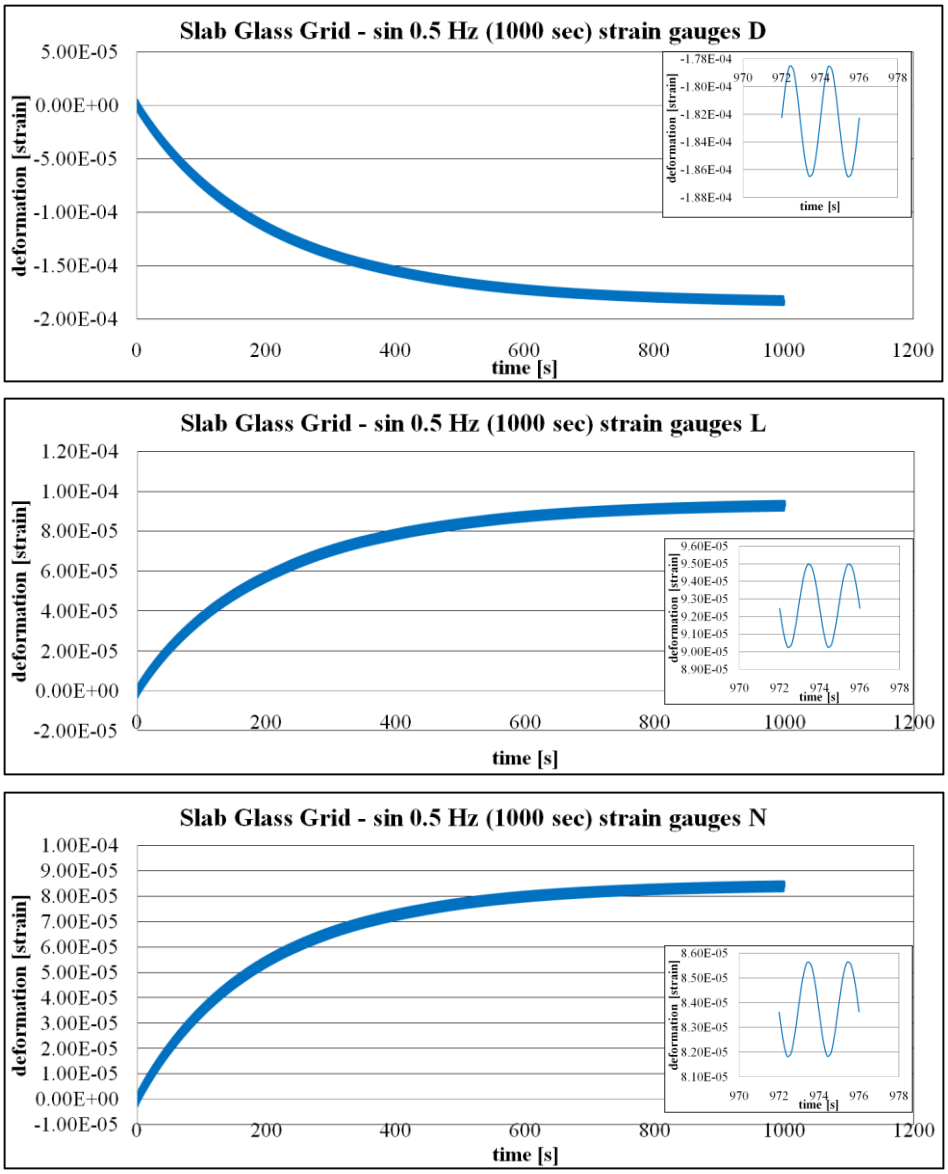

Figure 2.28 Sinusoidal test (1000 s, 0.5 Hz) on slab with glass grid - strain gauges D, L and N.

Table 2.16 highlights the strain peak values and the wave amplitude of the strain that were the output of Abaqus during the modelling investigations in those areas which corresponded to the laboratory strain gauges in position D, L and N.

Table 2.16 Peak value and wave amplitude of slab glass grid (sinusoidal test 1000 s, 0.5 Hz).

SIN 0.5Hz (1000 seconds) – SLAB WITH GLASS GRID			
Area corresponding to the Laboratory Strain Gauges Position	***D***	***L***	***N***
Peak value [μstrain]	-184	93	85
Wave amplitude [μstrain]	7.9	4.7	3.8

Figure 2.29 shows the strain response in different areas close to the loading mark of the control slabs and applying 100 cycles of a sinusoidal load at 2 Hz.

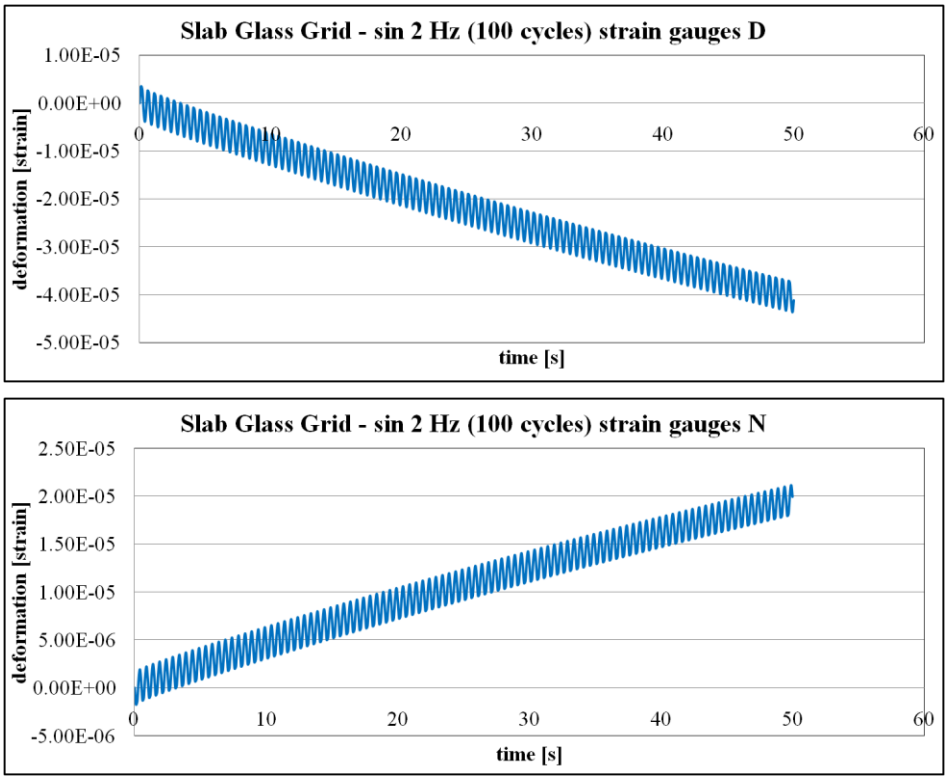

Figure 2.29 Sinusoidal test (100 cycles, 2 Hz) on slab with glass grid - strain gauges D and N.

Table 2.17 highlights the strain peak values and the wave amplitude of the strain that were the output of Abaqus during the modelling investigations in those areas which corresponded to the laboratory strain gauges in position D and N.

Table 2.17 Peak value and wave amplitude of slab glass grid (sinusoidal test 100 cycles, 2 Hz).

SIN 2Hz (100 cycles) – SLAB WITH GLASS GRID		
Area corresponding to the Laboratory Strain Gauges Position	***D***	***N***
Peak value [μstrain]	40	19
Wave amplitude [μstrain]	6.5	3.2

Figure 2.30 shows the strain response in different areas close to the loading mark of the control slabs and applying a sinusoidal load at 2 Hz for 1000 seconds.

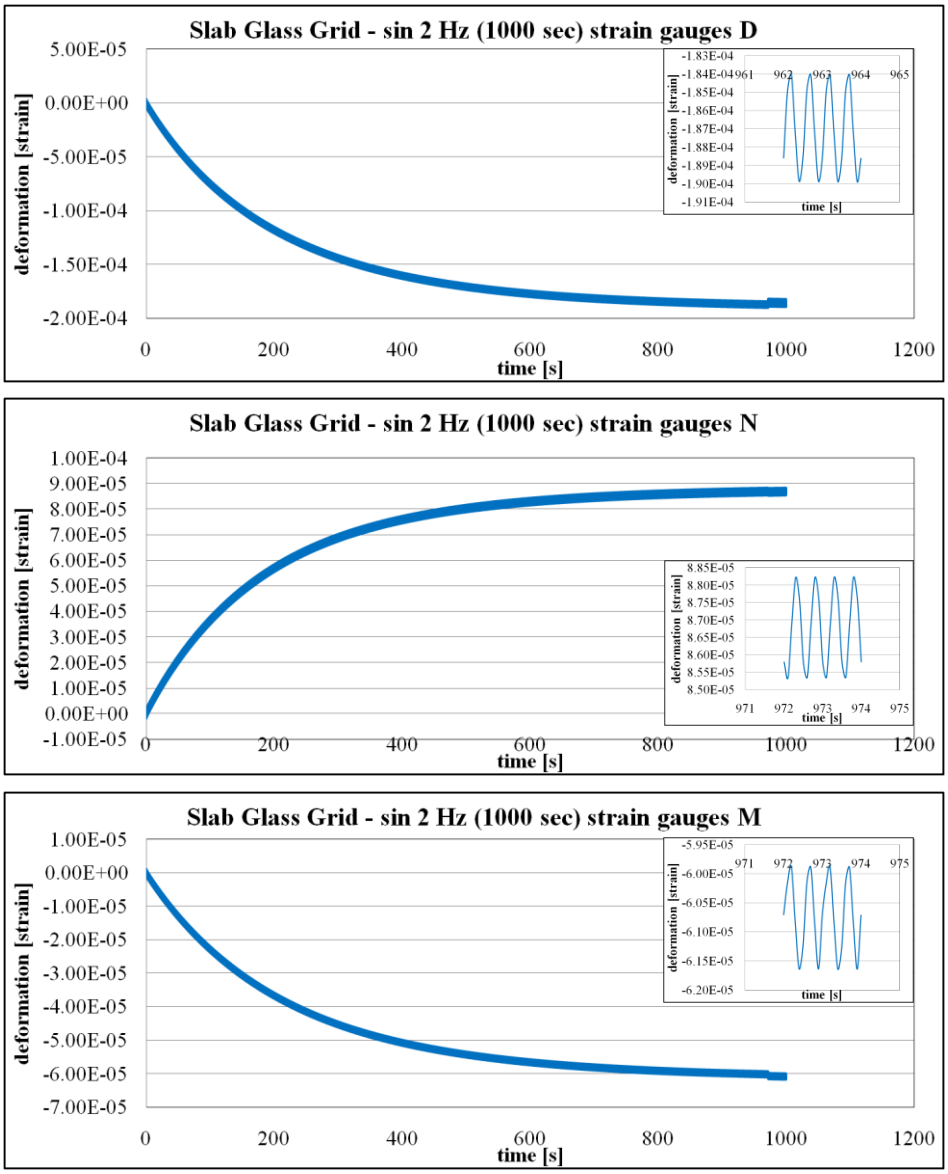

Figure 2.30 Sinusoidal test (1000 s, 2 Hz) on slab with glass grid - strain gauges D, N and M.

Table 2.18 highlights the strain peak values and the wave amplitude of the strain that were the output of Abaqus during the modelling investigations in those areas which corresponded to the laboratory strain gauges in position D, N and M.

Table 2.18 Peak value and wave amplitude of slab glass grid (sinusoidal test 1000 s, 2 Hz).

SIN 2Hz (1000 seconds) – SLAB WITH GLASS GRID			
Area corresponding to the Laboratory Strain Gauges Position	***D***	***N***	***M***
Peak value [μstrain]	-186	85	-61
Wave amplitude [μstrain]	6.0	2.9	1.8

The graphs and tables in the previous paragraphs showed the results coming from the simulations of the three different typologies of slabs and modelling different scenarios. It is possible to draw conclusions similar to the ones explained in the Chapter 1 related to the laboratory investigations. In fact, the static creep tests accumulated a higher level of strains compared to the dynamic tests. Moreover, the tests which applied a sinusoidal load at 2 Hz showed a lower level of strains accumulated, than the same output get from the analogous tests simulated at 0.5 Hz. Equivalent considerations could be drawn for the amplitude of the waves of the sinusoidal strain responses. Finally, the analyses of the strain responses in analogous positions showed a similar trend. In fact, the graphs related to the creep tests simulated on the slabs reinforced with steel net highlighted a comparable behaviour in those areas corresponding to the strain gauges I and L (figure 2.21).

After these preliminary considerations, the data got from the modelling permitted to compare the different behaviours of the three typologies of slabs, checking the dissimilarities between the reinforced and unreinforced samples through the analysis of the singular test simulated. The following Figures showed the data collected from strain gauges positioned in the same area close to the loading mark, which correspond to the position of the strain gauges D in the laboratory, but placed on the three different kinds of specimens.

Figure 2.31 shows the data coming from the strain in the area close to the loading mark of the three kinds of slabs, which correspond to the strain gauges in position D (laboratory) and running a creep test.

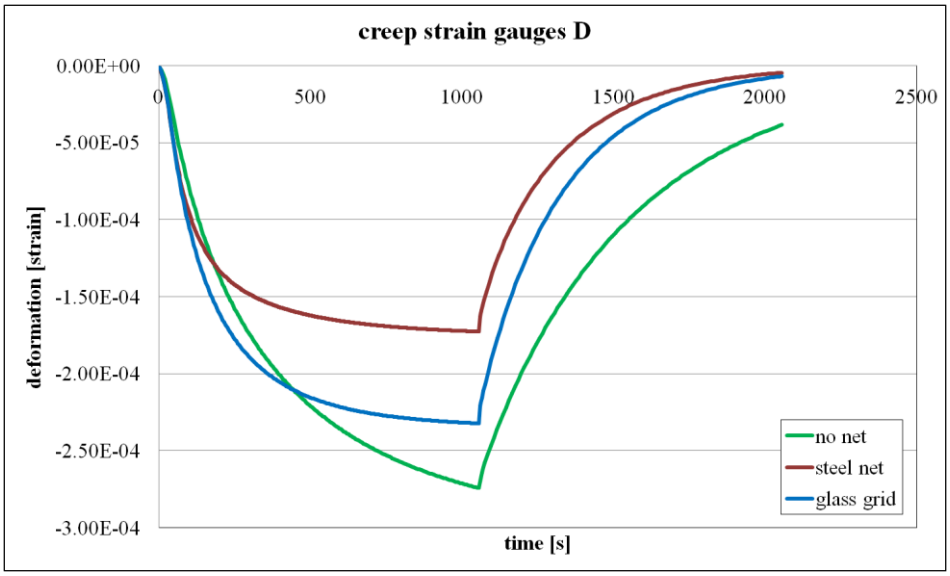

Figure 2.31 Comparison of the creep test simulated on the three typologies of slabs (with no net, steel net and glass grid - strain gauges D.

Table 2.19 highlights the strain peak values and the percentages of the recovered strain that were the output of Abaqus during the modelling investigations in those areas which corresponded to the laboratory strain gauges in position D on the three different kinds of slabs.

Table 2.19 Peak values and recovery of the three typologies of slabs during creep test.

CREEP – STRAIN GAUGES D			
Typology of Modelled Slab	***No Net***	***Steel Net***	***Glass Grid***
Peak value [μstrain]	-274	-173	-232
Recovery [%]	86	97	97

Figure 2.32 shows the strain response in the same area close to the loading mark of the three kinds of slabs which correspond to the laboratory strain gauges in position D and applying 100 cycles of a sinusoidal load at 0.5 Hz.

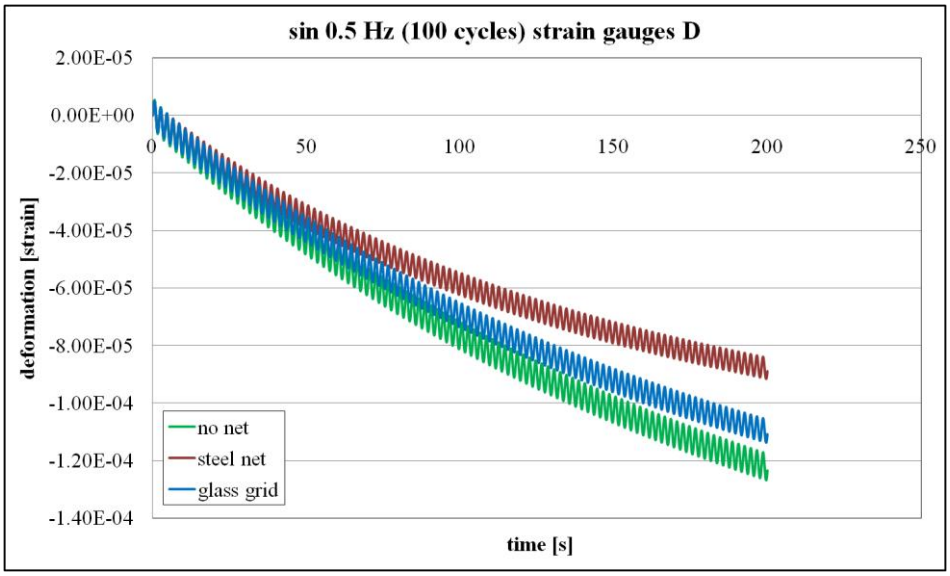

Figure 2.32 Comparison of the sinusoidal test (100 cycles, 0.5 Hz) simulated on the three typologies of slabs (with no net, steel net and glass grid - strain gauges D.

Table 2.20 highlights the strain peak values and the wave amplitude of the strain that were the output of Abaqus during the modelling investigations in those areas which corresponded to the laboratory strain gauges in position D on the three different kinds of slabs.

Table 2.20 Peak value and wave amplitude of the three kinds of slabs (sin 100 cycles, 0.5 Hz).

SIN 0.5Hz (100 cycles) – STRAIN GAUGES D			
Typology of Modelled Slab	***No Net***	***Steel Net***	***Glass Grid***
Peak value [μstrain]	-122	-89	-114
Wave amplitude [μstrain]	10.0	7.7	8.5

Figure 2.33 shows the strain response in the same area close to the loading mark of the three kinds of slabs which correspond to the laboratory strain gauges in position D and applying a sinusoidal load at 0.5 Hz for 1000 seconds.

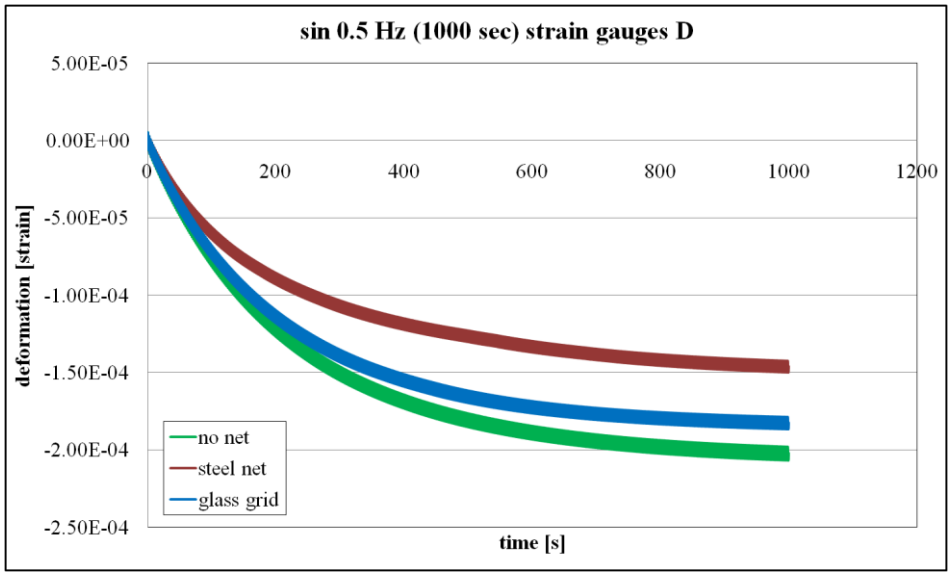

Figure 2.33 Comparison of the sinusoidal test (1000 s, 0.5 Hz) simulated on the three typologies of slabs (with no net, steel net and glass grid - strain gauges D.

Table 2.21 highlights the strain peak values and the wave amplitude of the strain that were the output of Abaqus during the modelling investigations in those areas which corresponded to the laboratory strain gauges in position D on the three different kinds of slabs.

Table 2.21 Peak value and wave amplitude of the three kinds of slabs (sin 1000 s, 0.5 Hz).

SIN 0.5Hz (1000 seconds) – STRAIN GAUGES D			
Typology of Modelled Slab	***No Net***	***Steel Net***	***Glass Grid***
Peak value [μstrain]	-203	-147	-184
Wave amplitude [μstrain]	8.9	7.5	7.9

Figure 2.34 shows the strain response in the same area close to the loading mark of the three kinds of slabs which correspond to the laboratory strain gauges in position D and applying 100 cycles of a sinusoidal load at 2 Hz.

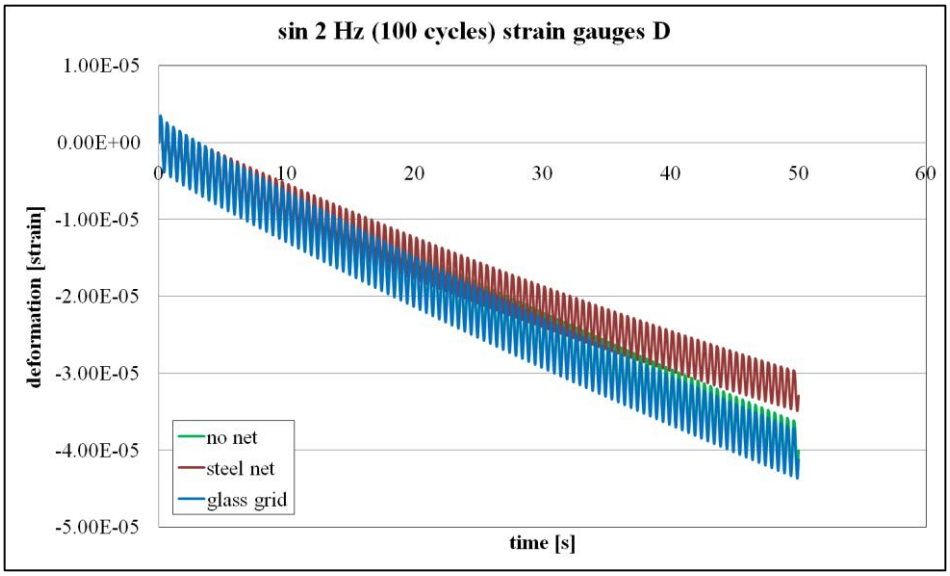

Figure 2.34 Comparison of the sinusoidal test (100 cycles, 2 Hz) simulated on the three typologies of slabs (with no net, steel net and glass grid - strain gauges D.

Table 2.22 highlights the strain peak values and the wave amplitude of the strain that were the output of Abaqus during the modelling investigations in those areas which corresponded to the laboratory strain gauges in position D on the three different kinds of slabs.

Table 2.22 Peak value and wave amplitude of the three kinds of slabs (sin 100 cycles, 2 Hz).

SIN 2Hz (100 cycles) – STRAIN GAUGES D			
Typology of Modelled Slab	***No Net***	***Steel Net***	***Glass Grid***
Peak value [μstrain]	-40	-33	-40
Wave amplitude [μstrain]	6.3	5.2	6.5

Figure 2.35 shows the strain response in the same area close to the loading mark of the three kinds of slabs which correspond to the laboratory strain gauges in position D and applying a sinusoidal load at 2 Hz for 1000 seconds.

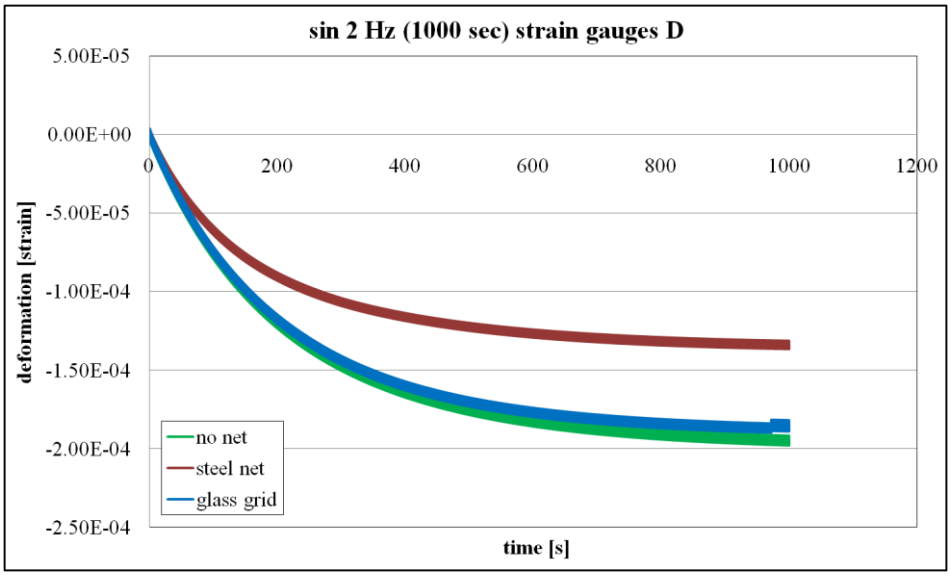

Figure 2.35 Comparison of the sinusoidal test (1000 s, 2 Hz) simulated on the three typologies of slabs (with no net, steel net and glass grid - strain gauges D.

Table 2.23 highlights the strain peak values and the wave amplitude of the strain that were the output of Abaqus during the modelling investigations in those areas which corresponded to the laboratory strain gauges in position D on the three different kinds of slabs.

Table 2.23 Peak value and wave amplitude of the three kinds of slabs (sin 1000 s, 2 Hz).

SIN 2Hz (1000 seconds) – STRAIN GAUGES D			
Typology of Modelled Slab	***No Net***	***Steel Net***	***Glass Grid***
Peak value [μstrain]	-195	-135	-186
Wave amplitude [μstrain]	6.2	5.2	6.0

The analyses of the results presented in the Figures and tables above highlighted a trend similar to the one underlined in the Chapter 1 for the laboratory investigations. In fact, the slabs modelled with a reinforcing system showed better performance than the unreinforced ones and the tendency was to accumulate fewer amounts of deformations when reinforcing systems were placed at the interface of binder layer and base course. Moreover, the amplitude of the waves of

the dynamic tests run at 2 Hz (both 100 cycles and 1000 seconds) was smaller for reinforced samples that the control slabs.

An important final remark has to underline that these Finite Element analyses were not an average of several simulations. In fact, the models were set and defined (as it was showed in the previous paragraphs) and the output were analysed and presented in this paragraph. Software like Abaqus cannot give changeable responds and its reliability consisted in a strict preliminary work on the design of the model step by step.

CHAPTER 3

Comparison.

The following step of this research work was the comparison of the data collected in the laboratory with the results of the Finite Element Analyses. In fact, the experimental investigations could be considered the validation of the simulations, in order to build models which could recreate real conditions. These modelling works could be a useful tool to investigate road pavements in real condition. This study focused the aim on the flexible pavements composed by a multilayer asphalt concrete with reinforcing system, but, once a real model would be validate, it would be possible to simulate any situation and analyse the performance of any road pavement. Finite Element Analyses can save money and time comparing to the analogous investigations in laboratory or in-situ. Therefore, the comparison between data collected in laboratory and running computational analyses permitted to verify the reliability of the Finite Element Modelling.

1.1 Comparison.

The results presented in the two previous chapters were compared, in order to evaluate the similarity of the data collected in the laboratory with the ones coming from the simulations. Obviously, the comparisons were divided into three sections: the multilayer flexible pavement with steel net, the ones with glass grid and the specimens without any kind of reinforcing systems (control samples). The results showed the behaviour of the samples in the area close to

the loading mark (Figure 3.1) and drew the attention on the shapes of the curves and the level of the strains accumulated.

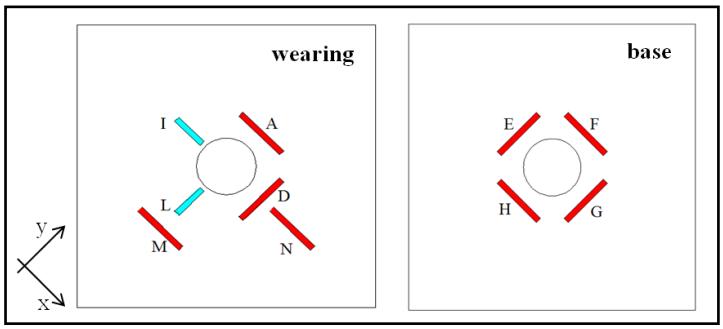

Figure 3.1 Position strain gauges on wearing surface and on base course.

- ***Control slabs (without any reinforcing system)***

In the following Figures the results of the control samples (without any reinforce) are presented starting from the creep tests and ending with the repeated sinusoidal cycles. Then, the data collected in the laboratory with the ones coming from modelling were compared. In fact, Figure 3.2 shows the strain response in two different positions close to the loading mark and running a creep test.

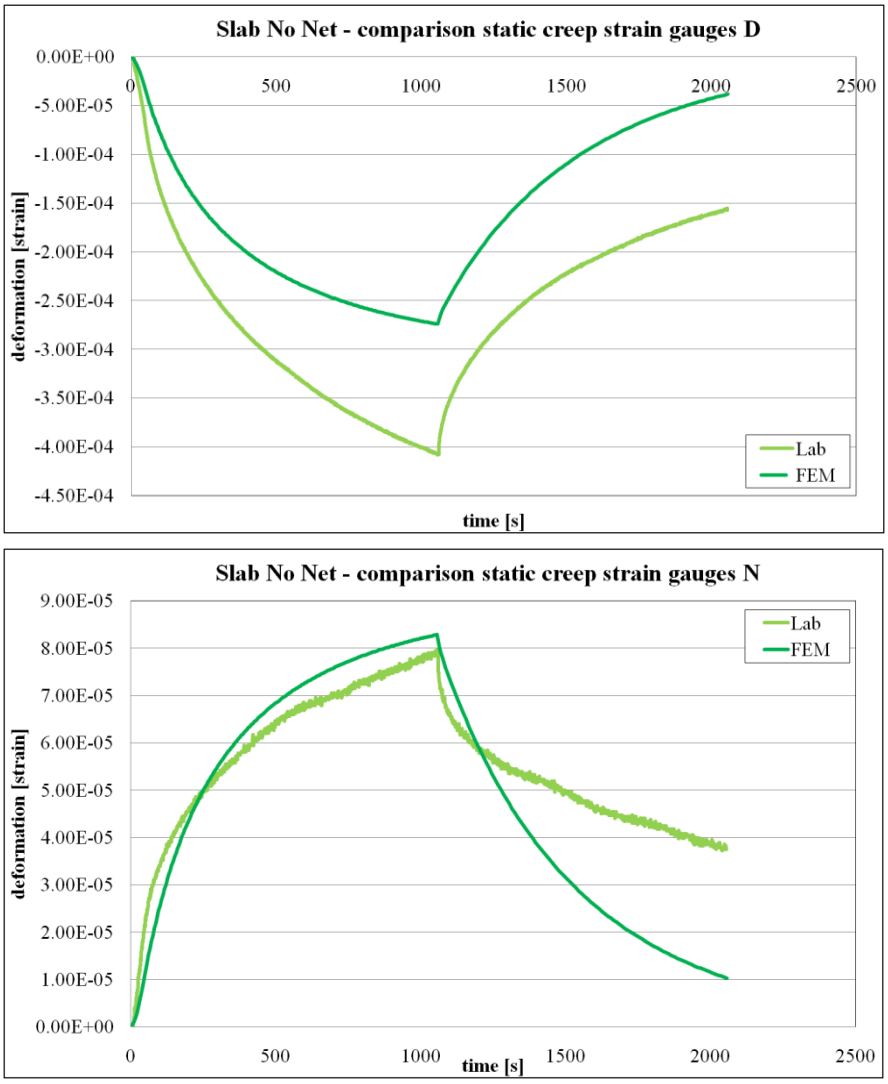

Figure 3.2 Creep test on control slab - strain gauges D and N.

Table 3.1 compares the strain peak values and the recovery percentages of the strain collected by the strain gauges in position D and N in the laboratory with the analogous data got from the Finite Element analyses, highlighting the percentage of difference between the two results.

Table 3.1 Peak value and recovery of control slab during creep test.

CREEP – CONTROL SLAB							
Peak value [μstrain]				***Recovery [%]***			
Position Monitored	**Lab**	**FEM**	**Difference**	***Position Monitored***	**Lab**	**FEM**	**Difference**
D	-408	-274	33 %	**D**	60	86	26 %
N	79	83	5 %	**N**	50	88	38 %

Figure 3.3 shows the strain response of the control samples applying 100 cycles of a sinusoidal load at 0.5 Hz.

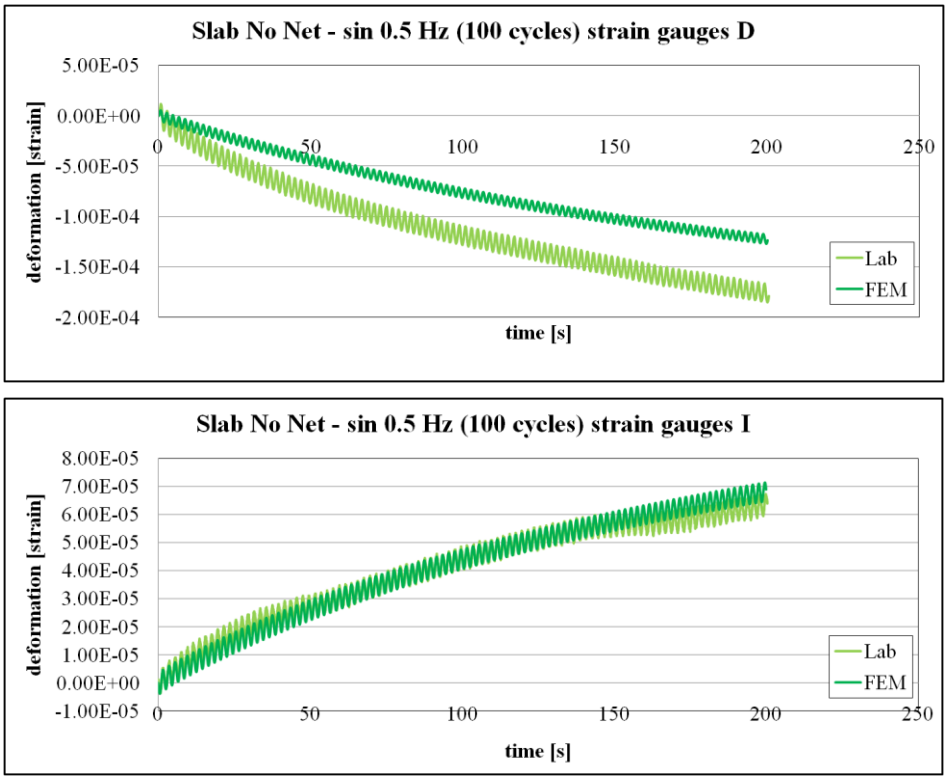

Figure 3.3 Sinusoidal test (100 cycles, 0.5 Hz) on control slab - strain gauges D and I.

Table 3.2 compares the strain peak values and the wave amplitudes of the strain collected by the strain gauges in position D and I in the laboratory with the analogous data got from the Finite Element analyses, highlighting the percentage of difference between the two results.

Table 3.2 Peak value and wave amplitude of control slab (sinusoidal test 100 cycles, 0.5 Hz).

SIN 0.5Hz (100 Cycles) – CONTROL SLAB							
Peak value [µstrain]				***Wave amplitude [µstrain]***			
Position Monitored	**Lab**	**FEM**	**Difference**	***Position Monitored***	**Lab**	**FEM**	**Difference**
D	-173	-122	9 %	**D**	18.6	9.7	48 %
I	62	68	29 %	**I**	8.2	7.0	16 %

Figure 3.4 shows the strain response of the control samples applying a sinusoidal load at 0.5 Hz for 1000 seconds.

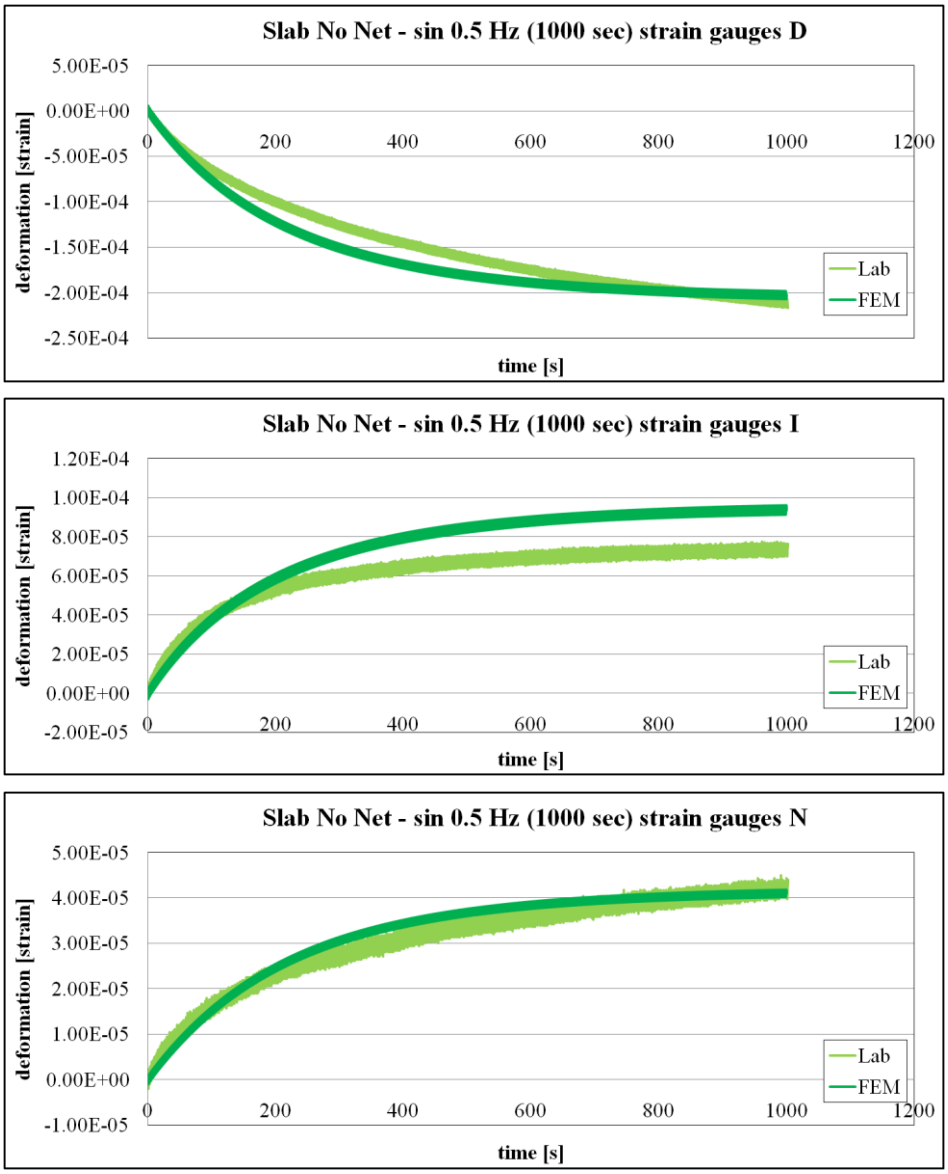

Figure 3.4 Sinusoidal test (1000s, 0.5 Hz) on control slab - strain gauges D, I and N.

Table 3.3 compares the strain peak values and the wave amplitudes of the strain collected by the strain gauges in position D, I and N in the laboratory with the analogous data got from the Finite Element analyses, highlighting the percentage of difference between the two results.

Table 3.3 Peak value and wave amplitude of control slab (sinusoidal test 1000s, 0.5 Hz).

SIN 0.5Hz (1000 seconds) – CONTROL SLAB							
Peak value [µstrain]				***Wave amplitude [µstrain]***			
Position Monitored	**Lab**	**FEM**	**Difference**	***Position Monitored***	**Lab**	**FEM**	**Difference**
D	-214	-203	5 %	**D**	9.8	8.9	9 %
I	73	94	30 %	**I**	7.1	4.8	32 %
N	42	41	2 %	**N**	3.9	1.6	59 %

Figure 3.5 shows the strain response of the control samples applying 100 cycles of a sinusoidal load at 2 Hz.

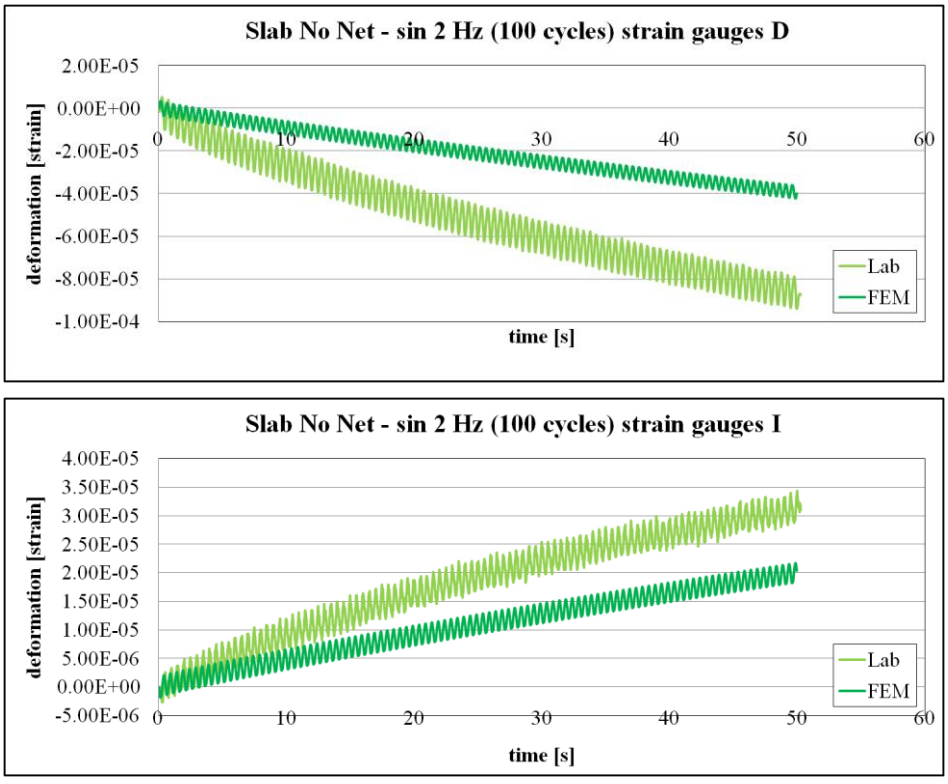

Figure 3.5 Sinusoidal test (100 cycles, 2 Hz) on control slab - strain gauges D and I.

Table 3.4 compares the strain peak values and the wave amplitudes of the strain collected by the strain gauges in position D and I in the laboratory with the analogous data got from the Finite Element analyses, highlighting the percentage of difference between the two results.

Table 3.4 Peak value and wave amplitude of control slab (sinusoidal test 100 cycles, 2 Hz).

SIN 2Hz (100 Cycles) – CONTROL SLAB							
Peak value [µstrain]				***Wave amplitude [µstrain]***			
Position Monitored	**Lab**	**FEM**	**Difference**	***Position Monitored***	**Lab**	**FEM**	**Difference**
D	-82	-40	51 %	**D**	15.3	6.3	60 %
I	31	20	36 %	**I**	6.0	3.5	42 %

Figure 3.6 shows the strain response of the control samples applying a sinusoidal load at 2 Hz for 1000 seconds.

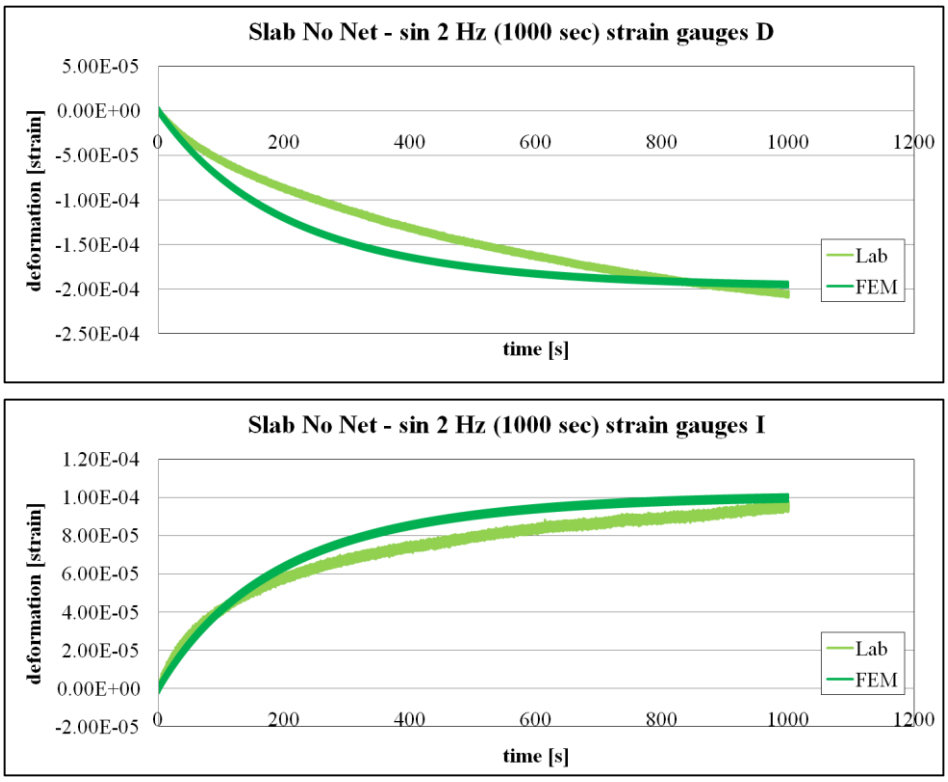

Figure 3.6 Sinusoidal test (1000s, 2 Hz) on control slab - strain gauges D and I.

Table 3.5 compares the strain peak values and the wave amplitudes of the strain collected by the strain gauges in position D and I in the laboratory with the analogous data got from the Finite Element analyses, highlighting the percentage of difference between the two results.

Table 3.5 Peak value and wave amplitude of control slab (sinusoidal test 1000s, 2 Hz).

SIN 2Hz (1000 seconds) – CONTROL SLAB							
Peak value [µstrain]				***Wave amplitude [µstrain]***			
Position Monitored	**Lab**	**FEM**	**Difference**	***Position Monitored***	**Lab**	**FEM**	**Difference**
D	-204	-195	4 %	**D**	7.5	6.2	17 %
I	93	100	7 %	**I**	4.9	3.8	22 %

- ***Slabs reinforced with Steel Net***

The next series of Figures compared the results collected with the laboratory slabs reinforced with the steel net and the corresponding FE simulations. Figure 3.7 show the data which came from creep tests monitored in three different positions close to the loading mark.

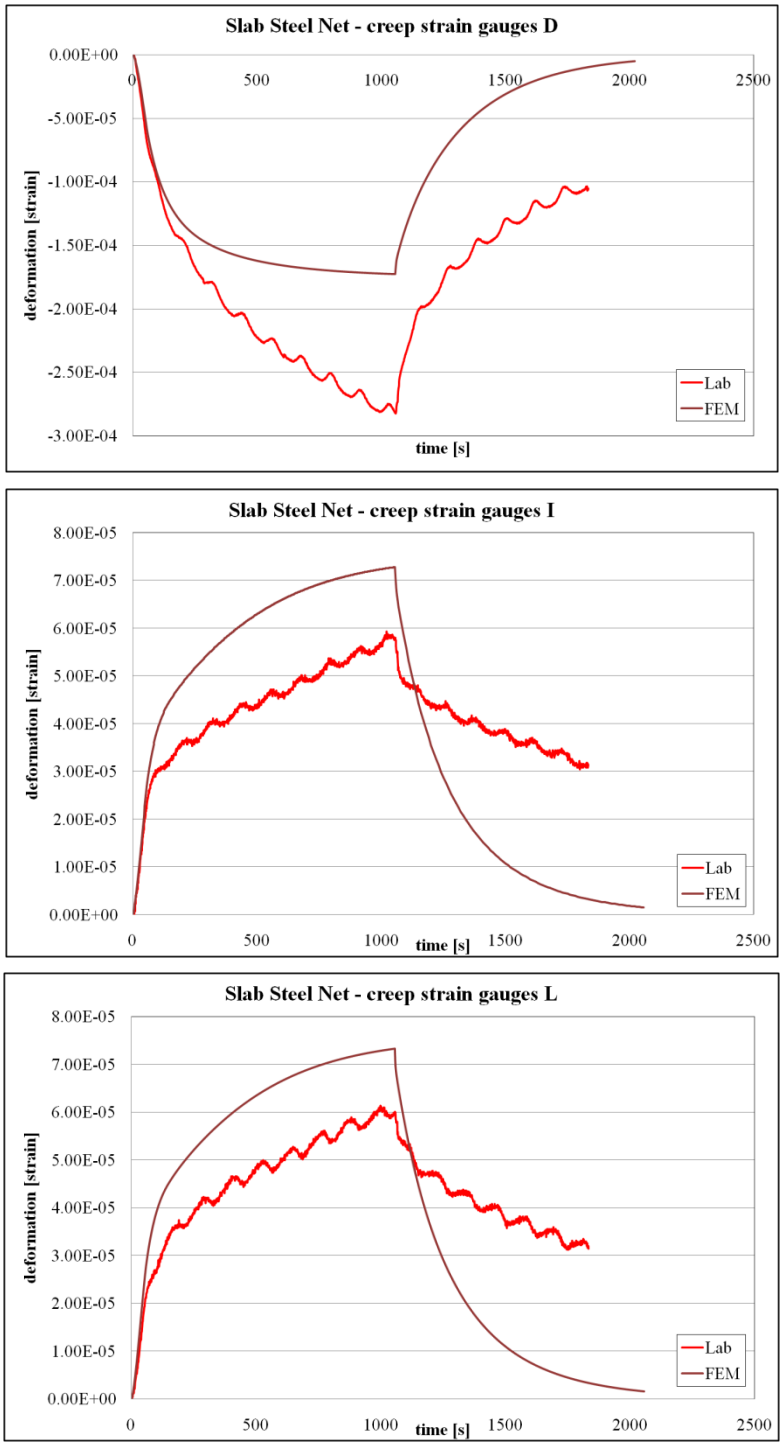

Figure 3.7 Creep test on slab with steel net - strain gauges D, I and L.

Table 3.6 compares the strain peak values and the recovery percentages of the strain collected by the strain gauges in position D, I and L in the laboratory with the analogous data got from the Finite Element analyses, highlighting the percentage of difference between the two results.

Table 3.6 Peak value and recovery of slab with steel net during creep test.

CREEP – SLAB WITH STEEL NET							
Peak value [μstrain]				***Recovery [%]***			
Position Monitored	**Lab**	**FEM**	**Difference**	***Position Monitored***	**Lab**	**FEM**	**Difference**
D	-283	-173	39 %	**D**	63	97	34 %
I	59	73	19 %	**I**	47	98	51 %
L	61	73	16 %	**L**	49	98	49 %

Figure 3.8 shows the strain response of the samples reinforced with the steel net applying 100 cycles of a sinusoidal load at 0.5 Hz.

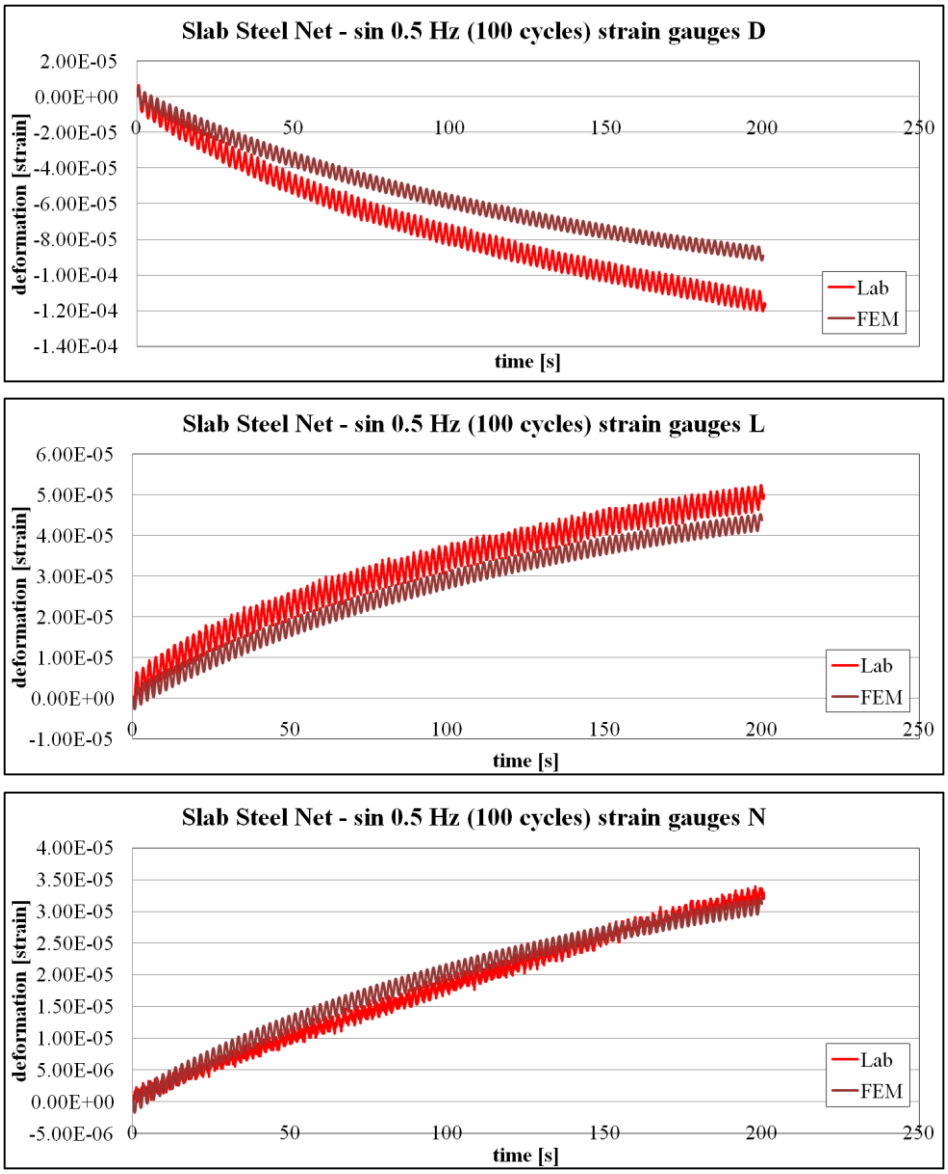

Figure 3.8 Sinusoidal test (100 cycles, 0.5 Hz) on slab with steel net - strain gauges D, L and N.

Table 3.7 compares the strain peak values and the wave amplitudes of the strain collected by the strain gauges in position D, L and N in the laboratory with the analogous data got from the Finite Element analyses, highlighting the percentage of difference between the two results.

Table 3.7 Peak value and wave amplitude of slab steel net (sinusoidal test 100 cycles, 0.5 Hz).

SIN 0.5Hz (100 Cycles) – SLAB WITH STEEL NET							
Peak value [µstrain]				***Wave amplitude [µstrain]***			
Position Monitored	**Lab**	**FEM**	**Difference**	***Position Monitored***	**Lab**	**FEM**	**Difference**
D	-115	-89	23 %	**D**	11.7	7.7	34 %
L	48	44	8 %	**L**	6.7	4.1	39 %
N	31	31	0 %	**N**	2.9	2.6	10 %

Figure 3.9 shows the strain response of the samples reinforced with the steel net applying 100 cycles of a sinusoidal load at 2 Hz.

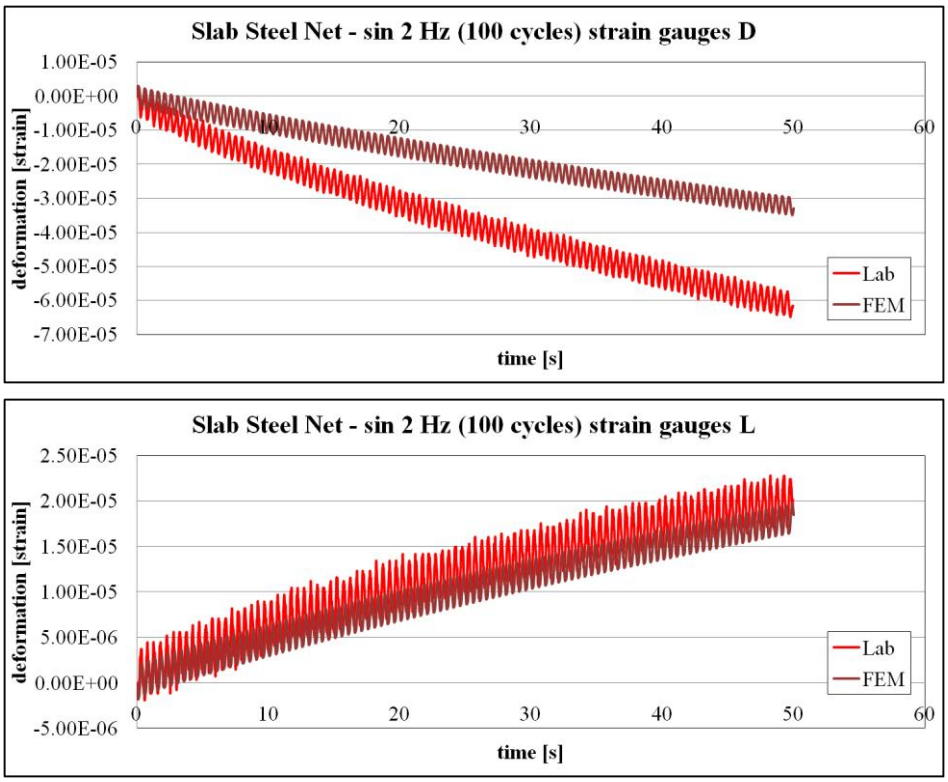

Figure 3.9 Sinusoidal test (100 cycles, 2 Hz) on slab with steel net - strain gauges D and L.

Table 3.8 compares the strain peak values and the wave amplitudes of the strain collected by the strain gauges in position D and L in the laboratory with the analogous data got from the Finite Element analyses, highlighting the percentage of difference between the two results.

Table 3.8 Peak value and wave amplitude of slab steel net (sinusoidal test 100 cycles, 2 Hz).

SIN 2Hz (100 cycles) – SLAB WITH STEEL NET							
Peak value [µstrain]				***Wave amplitude [µstrain]***			
Position Monitored	**Lab**	**FEM**	**Difference**	***Position Monitored***	**Lab**	**FEM**	**Difference**
D	-56	-33	41 %	**D**	8.8	5.2	41 %
L	17	18	6 %	**L**	5.6	3.3	42 %

Figure 3.10 shows the strain response of the samples reinforced with the steel net applying a sinusoidal load at 2 Hz for 1000 seconds.

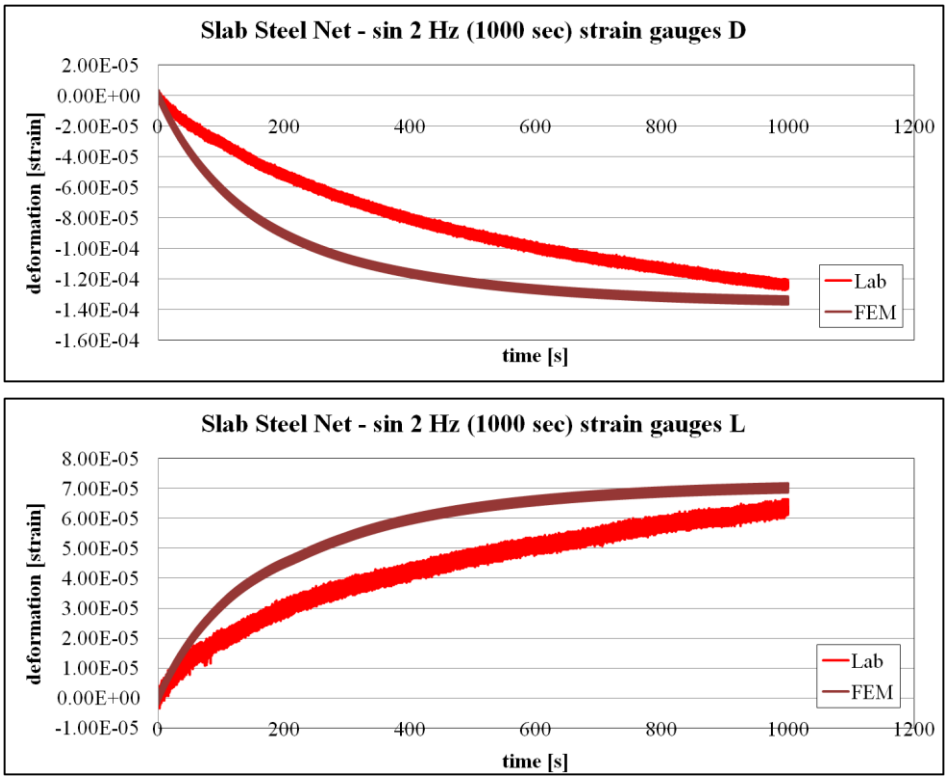

Figure 3.10 Sinusoidal test (1000s, 2 Hz) on slab with steel net - strain gauges D and L.

Table 3.9 compares the strain peak values and the wave amplitudes of the strain collected by the strain gauges in position D and L in the laboratory with the analogous data got from the Finite Element analyses, highlighting the percentage of difference between the two results.

Table 3.9 Peak value and wave amplitude of slab steel net (sinusoidal test 1000s, 2 Hz).

SIN 2Hz (1000 seconds) – SLAB WITH STEEL NET							
Peak value [μstrain]				***Wave amplitude [μstrain]***			
Position Monitored	**Lab**	**FEM**	**Difference**	***Position Monitored***	**Lab**	**FEM**	**Difference**
D	-123	-135	9 %	**D**	6.0	5.2	16 %
L	65	71	8 %	**L**	6.2	3.1	50 %

- ***Slabs reinforced with Glass Grid***

Finally the subsequent charts present the compared results collected with samples reinforced with the glass grid and Figure 3.11 show the data which came from creep tests monitored in two different positions close to the loading mark.

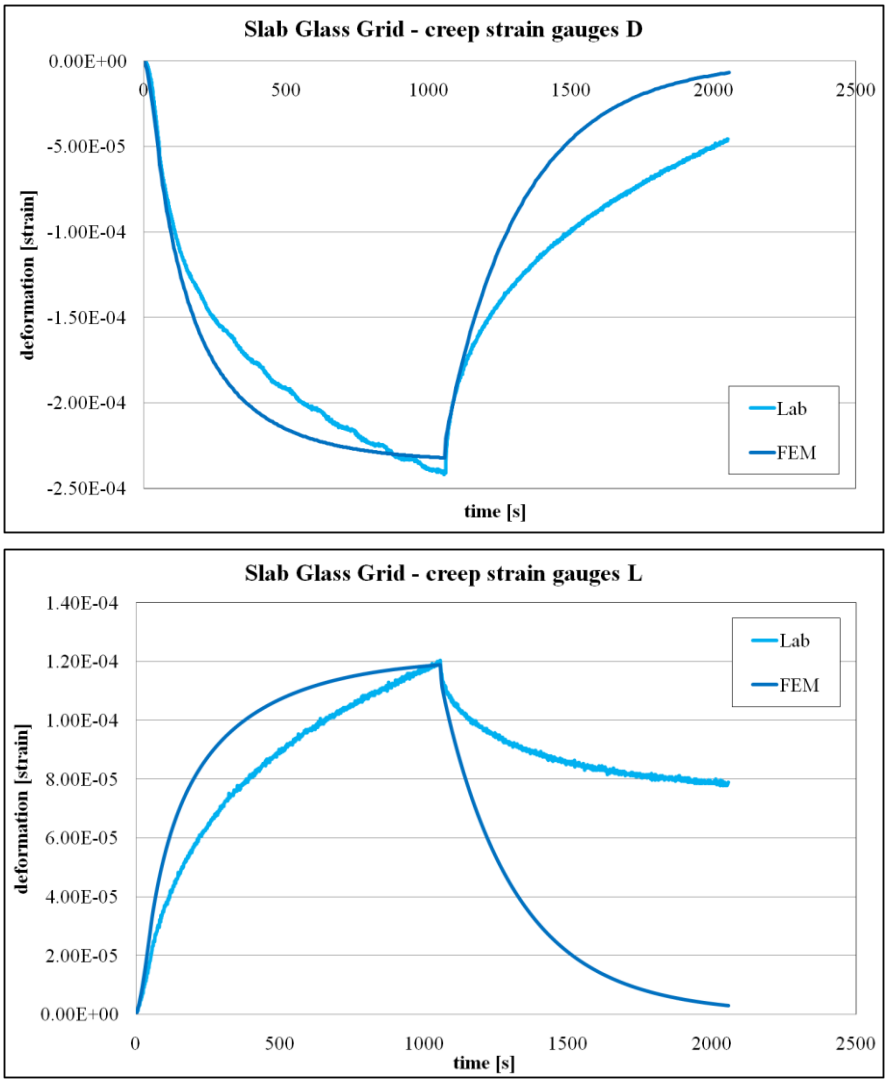

Figure 3.11 Creep test on slab with glass grid - strain gauges D and L.

Table 3.10 compares the strain peak values and the recovery percentages of the strain collected by the strain gauges in position D and L in the laboratory with the analogous data got from the Finite Element analyses, highlighting the percentage of difference between the two results.

Table 3.10 Peak value and recovery of slab with glass grid during creep test.

CREEP – SLAB WITH GLASS GRID							
Peak value [μstrain]				***Recovery [%]***			
Position Monitored	**Lab**	**FEM**	**Difference**	***Position Monitored***	**Lab**	**FEM**	**Difference**
D	-242	-232	4 %	**D**	84	97	13 %
L	120	119	1 %	**L**	35	98	63 %

Figure 3.12 shows the strain response of the samples reinforced with the glass grid applying 100 cycles of a sinusoidal load at 2 Hz.

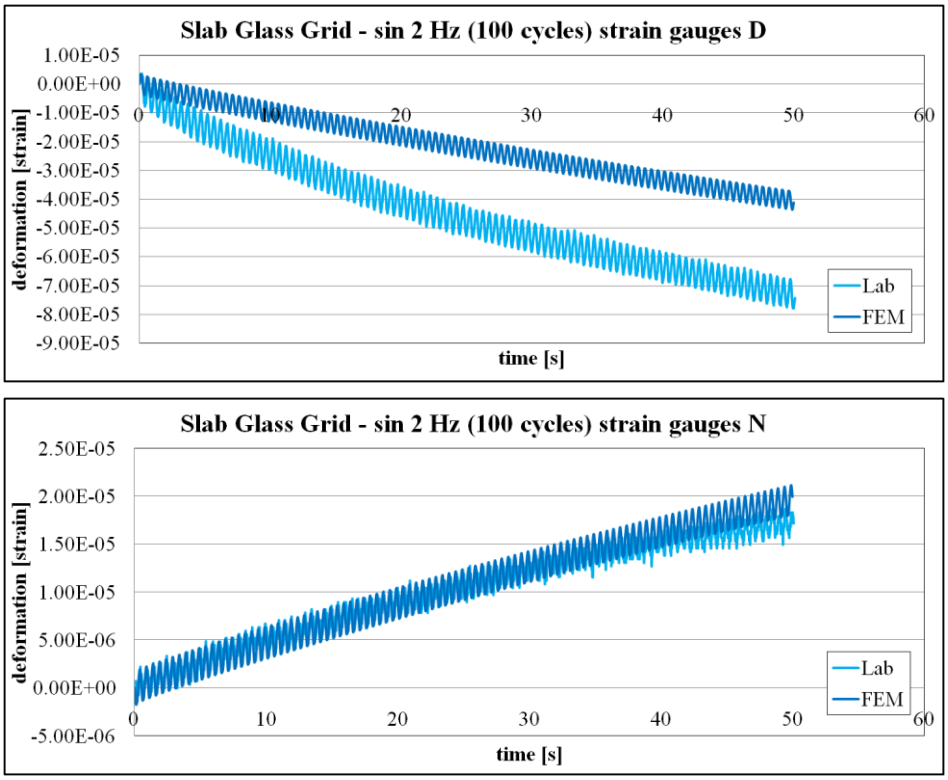

Figure 3.12 Sinusoidal test (100 cycles, 2 Hz) on slab with glass grid - strain gauges D and N.

Table 3.11 compares the strain peak values and the wave amplitudes of the strain collected by the strain gauges in position D and N in the laboratory with the analogous data got from the Finite Element analyses, highlighting the percentage of difference between the two results.

Table 3.11 Peak value and wave amplitude of slab glass grid (sinusoidal test 100 cycles, 2 Hz).

SIN 2Hz (100 cycles) – SLAB WITH GLASS GRID							
Peak value [μstrain]				***Wave amplitude [μstrain]***			
Position Monitored	**Lab**	**FEM**	**Difference**	***Position Monitored***	**Lab**	**FEM**	**Difference**
D	-68	-40	41 %	**D**	10.0	6.5	35 %
N	16	19	19 %	**N**	1.6	3.2	50 %

Figure 3.13 shows the strain response of the samples reinforced with the glass grid applying a sinusoidal load at 2 Hz for 1000 seconds.

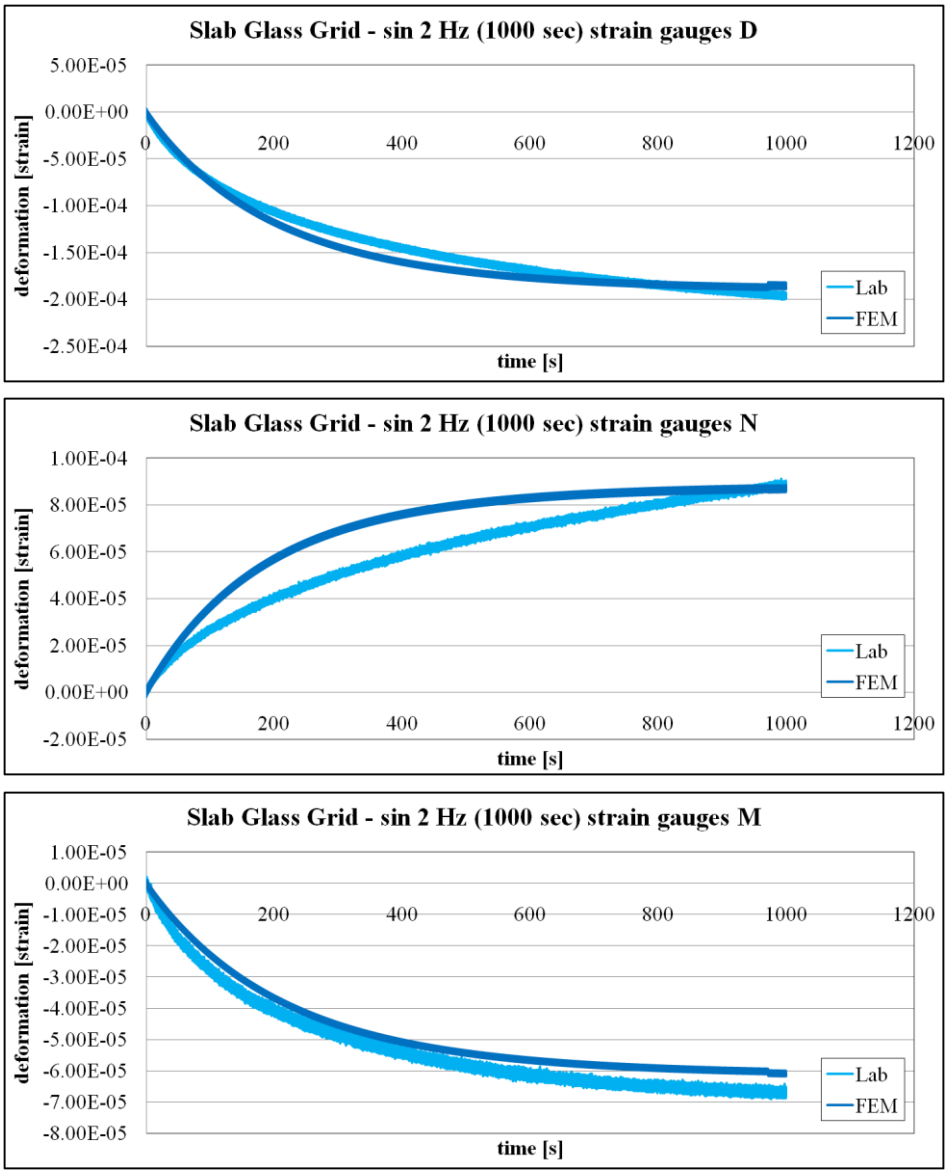

Figure 3.13 Sinusoidal test (1000s, 2 Hz) on slab with glass grid - strain gauges D, N and M.

Table 3.12 compares the strain peak values and the wave amplitudes of the strain collected by the strain gauges in position D, N and M in the laboratory with the analogous data got from the Finite Element analyses, highlighting the percentage of difference between the two results.

Table 3.12 Peak value and wave amplitude of slab glass grid (sinusoidal test 1000s, 2 Hz).

SIN 2Hz (1000 seconds) – SLAB WITH GLASS GRID							
Peak value [µstrain]				***Wave amplitude [µstrain]***			
Position Monitored	**Lab**	**FEM**	**Difference**	***Position Monitored***	**Lab**	**FEM**	**Difference**
D	-195	-186	5 %	**D**	7.1	6.0	15 %
N	88	85	4 %	**N**	2.6	2.9	9 %
M	-67	-61	9 %	**M**	2.6	1.8	31 %

The graphs in the previous Figures illustrated a good agreement between the data collected in laboratory and running Finite Element Analyses. The dynamic analyses carried out on the three typologies of samples showed curves with similar shapes. Moreover, the waves at different frequencies had form and amplitude comparable, especially considering the longest test (1000 seconds), where the material responses could be considered more stable and reliable than the same test run for 100 cycles. The amount of deformations at the end of the dynamic analyses was similar for laboratory data and the simulated ones. Furthermore, it is important to highlight that the comparisons involved the strain responses of the real scale samples in the area close to the load mark, but in two directions, since strain gauges were positioned in perpendicular positions. This choice permitted to investigate the whole scenario of the deformations highlighting the compressed areas and the tensile zones. A further note has to be related to the creep tests. These investigations showed that the trends of the laboratory curves were different from the modelling ones in the recovery phase of the test (after the removing of the load). In fact, in most of the case the Finite Element software Abaqus could totally recover the deformations accumulated in the first 1000 seconds. On the other hand, the laboratory investigations highlighted a different behaviour, since the recovery phase was longer than the simulated one. In fact, the slabs in the laboratory could completely recover the deformations, but this phase was longer than 1000 seconds.

The results presented were divided into the three typologies of samples tested, comparing the different tests carried out. In fact, the final aim of this research work was not only to make proper comparisons among the reinforced road pavements. But it was the creation of a reliable Finite Element model useful to study the behaviours of multilayer infrastructures, starting from a preliminary investigation in the laboratory as a validation tool.

It is important to underline that the laboratory results presented in this research work were an average among several tests carried out on different samples and using strain gauges in analogous positions. It is well known that experimental studies have to be repeated several times, in order to obtain reliable data and this means a great effort in terms of time and money. However, the simulations were created step by step trying to build a model comparable to those specimens tested in the laboratory. The most important phase was the preliminary calibration of the data inserted in the software to simulate the asphalt mixture constitutive law. Beside this fundamental step, the creation of the models was straightforward and the only tool necessary was a common personal computer. These preliminary remarks want to highlight the substantial difference between a laboratory investigation and a computational analysis and underline the advantages of this second testing method, which is worldwide acknowledged. This research work demonstrated the possibility of replacing the laboratory investigations with simulations. In fact, the Finite Element Analyses suggested the possibility to limit the work in the laboratory as a validation tool, in order to provide reliable results. It would be possible to study the performance of road pavements in diverse conditions or scenarios, just taking cores of the asphalt mixtures from a test section. In fact, this study started collecting dynamic moduli related to the mixes on cylindrical samples, in order to calculate Prony series parameters to insert in the software Abaqus. Moreover, using the same specimens, those parameters were validated and, following this strict procedure, it was possible to present the agreement between the laboratory and modelling results.

This research work promoted the possibility to study road pavements using Finite Element Analyses, in order to investigate their different aspects or performance. In fact, it would be a powerful toll to predict the in-service life or to check the consistency of the design. This kind of analysis show its versatility as well as the possibility to save money in the preliminary

investigations, which are necessary before building any new infrastructures or even during the maintenance works.

CHAPTER 4

Conclusions and Future Tasks.

This research work laid the bases for a new investigation method of road pavements and their performance. The simulations evaluated in this job could provide useful information for the design steps and could avoid problems during the in-service life of the infrastructures. In fact, a preliminary modelling section would permit to consider different technical solutions before the setting of the final execution project. The infrastructures have diverse characteristics, such as different level of traffic or need to maintain specific qualities according to the rendering of services. For these reasons, the possibility of testing various design solutions could be considered a proper way to save money and time, as well as the possibility to keep higher level of service.

The presented results could show that the Finite Element Analyses could behave as a real pavement, just passing through a simple laboratory procedure. The first step of the modelling section worked on the constitutive laws of the asphalt mixtures and this could be considered a fundamental phase. In fact, the geometry of the model as well as the interactions between layers was an important aspect, but definite and clear. On the other hand, the characteristics of the asphalt concretes could strongly change the output in terms of stress and strain and could influence the outputs of the modelling. In fact, Hot Mix Asphalt can be usually considered as a visco-elasto-plastic material. However, in this research work a preliminary assumption considered the asphalt concretes as a linear visco-elastic mixture. Hence, the modelling was built step by step, starting from the setting of the constitutive laws, in order to collect reliable results. Moreover, the Finite Element Analyses were supported by a strict laboratory study, which was considered the validation procedure. The laboratory investigation was carried out on real scale samples with the same characteristics of the simulations created with the Finite

Element software (Abaqus). The analyses were run at low/medium temperature (10°C), since in that condition the asphalt mixtures can be considered a linear visco-elastic material. Moreover, the tests carried out were the reproduction of the in-service life of a real pavement, as well as the analogous simulations run in Abaqus. A further important aspect of this research work was the typology of the samples tested. In fact, the whole study worked on reinforced flexible pavements with different kind of net (steel net or glass grid) and a parallel investigation was conducted either with Finite Element modelling or in the laboratory. These analyses permitted to understand the behaviours of the multilayer pavements, when these kinds of reinforcing systems are positioned in a superficial position, which meant between binder layer and base course. This research field cannot be considered a brand-new area and the undoubted effectiveness of the reinforcing systems inserted in road pavements were proved by several worldwide research works. However, this study emphasized the benefits of reinforcing nets, trying to create a new investigation method. In fact, this work could be summarized into two different phases (laboratory and modelling), where both investigations kept the same characteristics, in order to make proper comparisons. The presented results demonstrated that it would be possible to realise Finite Element models to analyse road pavements performance, setting a suitable laboratory investigation and considering the percentage of error which usually is implied in these works.

However, this study focused its efforts on asphalt multilayer flexible pavements, which are typically adopted in Italy. In fact the laboratory investigations and the corresponding Finite Element Analyses took advantages from previous research works run at the University of Parma, which were based on this kind of roadways (see Introduction and Literature Review). Therefore, taking advantage of the results obtained in this work with flexible pavements, new laboratory investigations were organized, in order to extend this analysis to different scenarios. In fact, new real scale samples were built trying to reproduce a small portion of a rigid pavement with structural joint and a reinforced asphalt overlay. This kind of roadways are typically adopted in North America or Europe, where climate is severe during the winter or for those infrastructures which need to support heavy loads, such as the airports. These new specimens were prepared following the same procedure explained in Chapter 1. In fact, three different typologies of slabs were built using two reinforcing systems (steel net and glass grid) and adding a control sample without any kind of reinforce. Analogously to the flexible slabs,

these specimens were manufactured in layers starting from the bottom neoprene stratum, to the upper asphalt surface (Table 4.1).

Table 4.1 Features of rigid slabs with an asphalt concrete overlay.

MULTILAYER RIGID SLABS	
Stratum	**Thickness [mm]**
Surface layer	40
Leveling layer	20
Slurry Seal	10
Portland Cement Concrete	200
Neoprene	40

The asphalt upper layers (surface and leveling) were mixed using Italian aggregates and natural bitumen as well as the same asphalt mixer mentioned in Chapter 1. Moreover the particle size curves of the surface and leveling layer are respectively shown in Chapter 1 (Figure 1.1 (b) and (a)). In addition to the volumetric and mechanical characteristics are shown in Table 1.2 and Figure 1.7. The slurry seal was a mix of fine aggregate (maximum aggregate size 4 mm), bituminous emulsion, cement and water and it had the function to embed the reinforcing net, besides to connect the asphalt mixtures and the Portland Cement Concrete (PCC) base. In fact, the asphalt overlay was laid on a 200 mm thick layer of PCC (R_{ck} = 250) with a structural transversal joint of 6 mm. The bottom layer of neoprene could simulate 150 mm of sub-base layer with a Deformation Modulus (M_d) of 500 kN/mm^2. These multilayer slabs were a square with 50 cm side length (Figure 4.1), since these investigations were analogous to the ones carried out on the flexible samples. The two reinforcing systems were the same mentioned in Chapter 1: hexagonal steel net and a squared glass grid covered with a thin bituminous film (Figure 1.8 – 1.9 and Table 1.4 – 1.5).

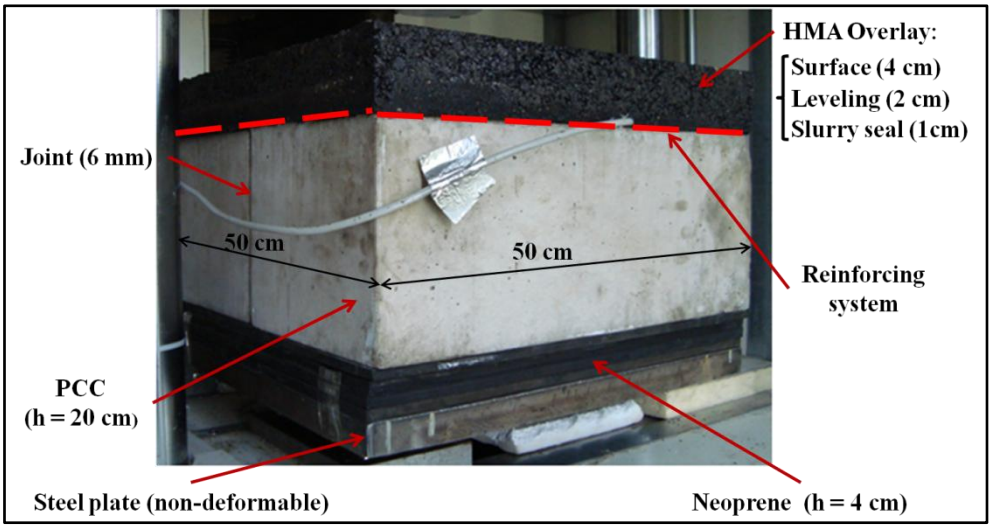

Figure 4.1 Rigid multiplayer sample with an asphalt overlay.

These multilayer slabs were built in two phases. In the first one the PCC was cast in formworks divided into two areas, in order to recreate a 6 mm joint in the middle of the slab. After 28 days the cement material could reach the perfect maturation and the slabs were removed from the formworks. In the second phase, the asphalt layers were compacted one upon the other using the heavy compactor available at the University of Parma (Chapter 1, Paragraph 1.1). At the bottom of the formwork, the reinforcing system was positioned and covered with a thin layer of slurry seal (1 cm). In this way, it was possible to obtain a perfect interlock between the net and the slurry seal, since this heterogeneous stratum was placed at the bottom of the formwork and compacted with the upper asphalt strata. The subsequent compaction procedure was the same one explained in Chapter 1, which was followed to realize the multilayer flexible samples. After these two phases, the two halves samples were put together, in order to obtain a proper adhesion between the PCC slabs and the asphalt layers. However, before this "fixing procedure", strain gauges were positioned at the bottom of the slurry seal stratum. In fact, these devices permitted to investigate the strain distribution at the interface between slurry seal and PCC layer, in the same central area where the structural joint created a discontinuity in the PCC base layer (Figure 4.2 (a)). Moreover, additional strain gauges were position on the top of the surface layer, in the area close to the loading mark, as shown in Figure 4.2 (b).

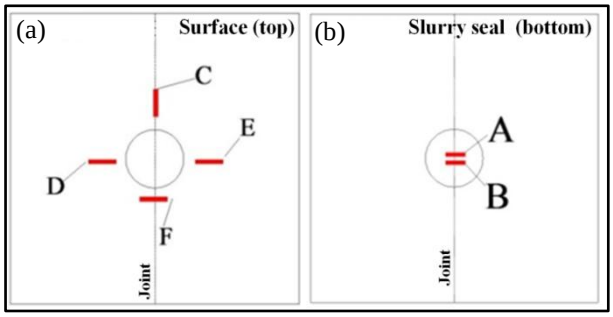

Figure 4.2 Position of the strain gauges on the overlay (a) and on bottom of slurry seal (b).

The proper adhesion between asphalt layers and PCC was achieved running a shear test analogous to the ones explained in Chapter 1. The test was carried out using two kind of sample that could recreate the two different layers in contact (PCC and slurry seal). The test set-up was similar to the one adopted for flexible pavements even if the specimens had squared shape (10 cm length side) with a thickness of 3 cm. They were cut from a slab (50 cm x 50 cm) appropriately compacted and composed by the slurry seal stratum (without any kind of reinforce) and the leveling layer. The second part of the shear specimens was a Portland Cement prism with a squared base of 10 cm length and a thickness around 4 cm. The two halves were put in contact with an amount of natural bitumen equal to 0.46 l/m^2 and following the same "fixing procedure" explained in Chapter 1. Shear tests were run using a MTS machine, setting the displacement control rate at 0.042 mm/s and the normal pressure at 0.0016 MPa (Figure 4.3).

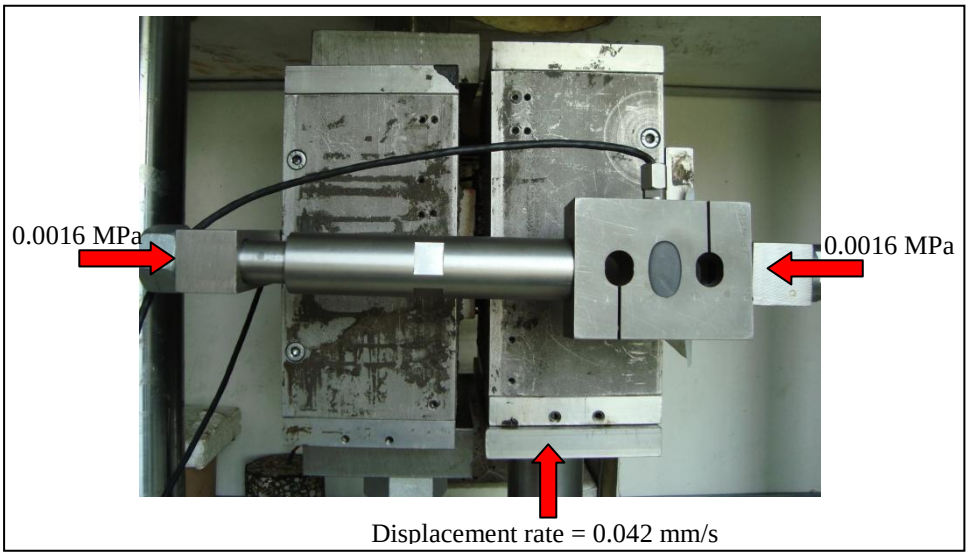

Figure 4.3 Set-up configuration of the shear test.

The tests were carried out at 10°C, in order to keep the asphalt mixtures in a range of viscoelasticity. In Figure 4.4 (a) the interface shear strength between PCC and slurry seal is shown with respect to the displacement rate in mm. Moreover, Figure 4.4 (b) highlights the analogous value calculated with the software BISAR simulating a semi-indefinite pavement with linear elastic characteristics and checking the horizontal shear stress between PCC and slurry seal. This further investigation was analogous to the one run for flexible slabs (Chapter 1, Paragraph 1.3).

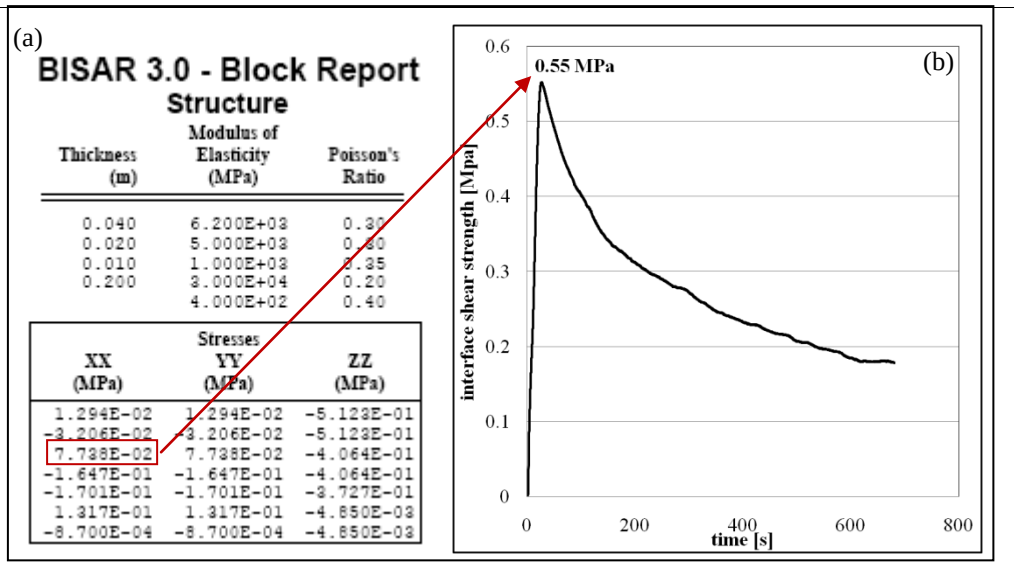

Figure 4.4 Results collected during shear test and the maximum interface shear strength (a) and Bisar report with the horizontal stress between slurry seal and PCC base highlighted (b).

The interface shear strength obtained in the laboratory was 7 time higher than the value obtained with BISAR. These further investigations laid the bases for the creation of real scale slabs composed by PCC and asphalt concrete layers, which could be work and respond as an in-continuum system.

After these preliminary shear tests, three different kinds of slabs were built following a "fixing procedure" analogous to the one explained in Chapter 1 to fix the asphalt mixture layers on the top of the PCC base. Subsequently, the slabs were tested in order to simulate the real passing of a heavy wheel in correspondence to the structural joint. The investigations were analogous to the ones explained in Chapter 1 and were run on the reinforced slabs (with steel net or glass grid) and on the specimens without any kind of reinforcing system. The load applied could simulate a tire with an inflate pressure of 7 bar and it was positioned on a circular loading mark (10 cm diameter) on the central area of the squared slabs. Moreover, the test set-up was the same explained in Chapter 1 and the distribution of the strain was collected in the area around the loading mark as well as at the interface between PCC and slurry seal. The investigations carried out were examined and the data collected were analyzed checking the differences

between the reinforced slabs and the unreinforced ones. However, a preliminary analysis was conducted taking into consideration each typology of slab and permitted to draw conclusions analogous to Chapter 1 and 2. These introductory examinations highlighted that each kind of slab could accumulate a higher level of strain applying a static load. Therefore, the creep tests showed a bigger deformation compared to the dynamic tests. Moreover, the tests run at lower frequency (0.5 Hz) highlighted a trend to accumulate more deformations compared to the corresponding investigations run at higher frequency (2 Hz). Analogously, the analysis of the amplitudes of the strain sinusoidal waves showed the same tendency. Furthermore, the behaviour of the three different slabs was compared analysing static and dynamic tests. The following charts could show an unexpected behaviour of the reinforcing systems with respect to the data collected in the laboratory or running Finite Element analyses. Moreover, the strain gauges positioned at the interface between asphalt overlay and PCC base did not collect any reliable results, since the data did not show any consistent trend. Any results will be presented despite the equipments were placed following a strict procedure.

Figure 4.5 shows the data collected from strain gauges placed in position D and F running a creep test on the three kinds of slabs.

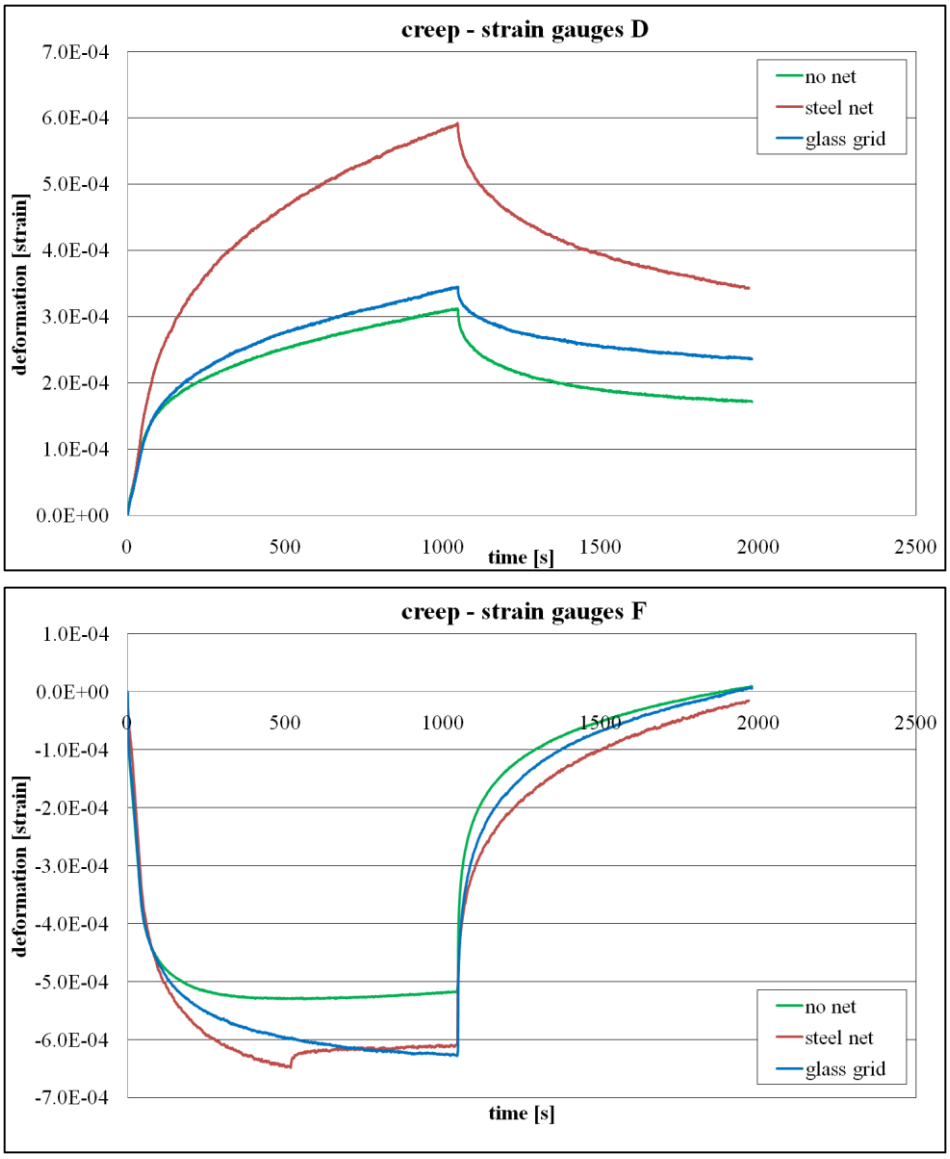

Figure 4.5 Comparison of the creep test carried out on the three typologies of slabs (with no net, steel net and glass grid - strain gauges D and F.

Table 4.2 highlights the strain peak values and the percentages of the recovered strain collected by the strain gauges in position D and F on the three different kinds of slabs.

Table 4.2 Peak values and recovery of the three typologies of slabs during creep test.

CREEP – STRAIN GAUGES D			
Typology of Slab	***No Net***	***Steel Net***	***Glass Grid***
Peak value [μstrain]	312	592	354
Recovery [%]	45	42	33
CREEP – STRAIN GAUGES F			
Typology of Slab	***No Net***	***Steel Net***	***Glass Grid***
Peak value [μstrain]	-530	-648	-628
Recovery [%]	100	98	100

Figure 4.6 shows the data collected by strain gauges placed in the same area close to the loading mark (position D and F) on the three kinds of slabs and applying 100 cycles of a sinusoidal load at 2 Hz.

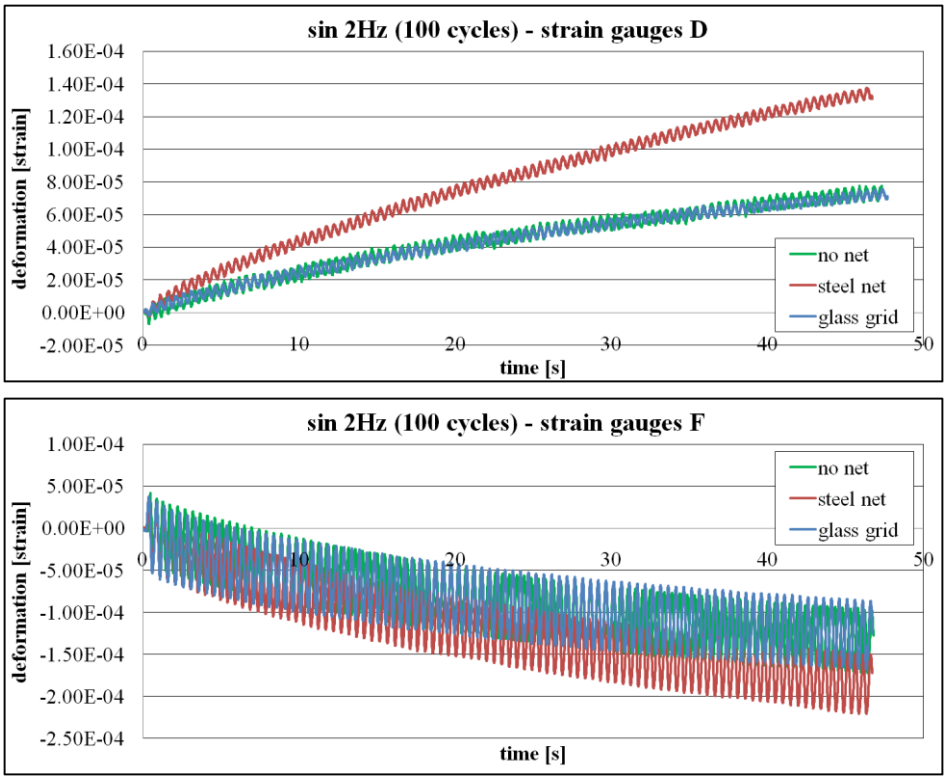

Figure 4.6 Comparison of the sinusoidal test (100 cycles, 2 Hz) carried out on the three typologies of slabs (with no net, steel net and glass grid - strain gauges D and F.

Table 4.3 highlights the strain peak values and the wave amplitude of the strain collected by the strain gauges in position D and F on the three kinds of slabs.

Table 4.3 Peak value and wave amplitude of the three kinds of slabs (sin. test 100 cycles, 2 Hz).

SIN 2Hz (100 cycles) – STRAIN GAUGES D			
Typology of Slab	***No Net***	***Steel Net***	***Glass Grid***
Peak value [μstrain]	75	133	71
Wave amplitude [μstrain]	9.4	7.1	6.0
SIN 2Hz (100 cycles) – STRAIN GAUGES F			
Typology of Slab	***No Net***	***Steel Net***	***Glass Grid***
Peak value [μstrain]	-139	-181	-125
Wave amplitude [μstrain]	75.1	70.6	82.0

Figure 4.7 shows the data collected by strain gauges placed in the same areas close to the loading mark (position D and F) of the three kinds of slabs and applying a sinusoidal load at 2 Hz for 1000 seconds.

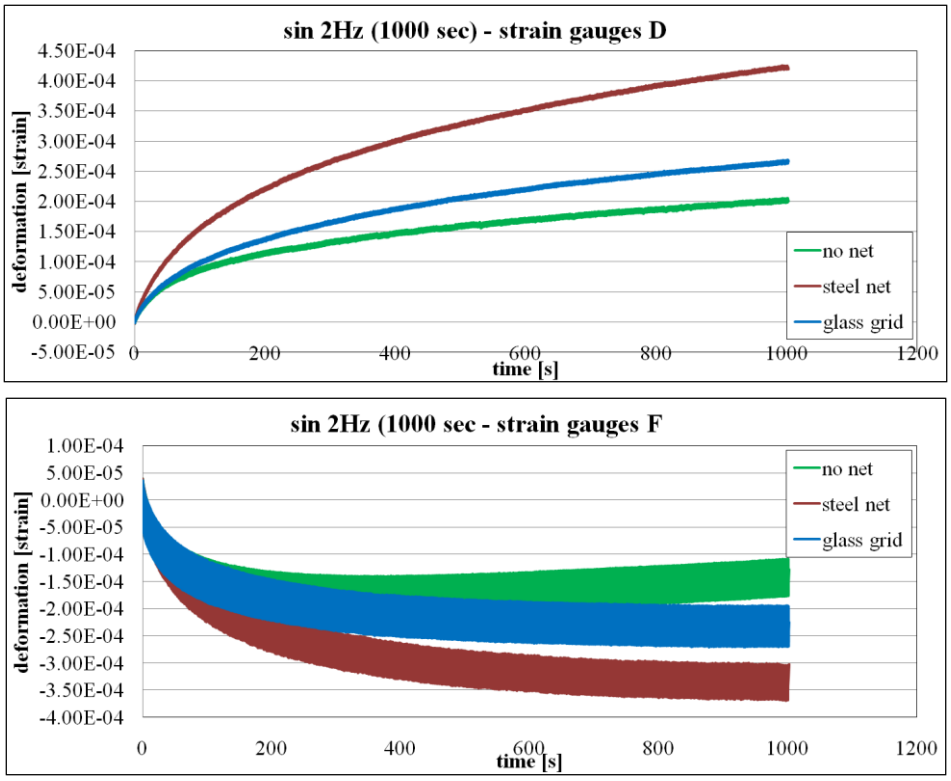

Figure 4.7 Comparison of the sinusoidal test (1000 s, 2 Hz) carried out on the three typologies of slabs (with no net, steel net and glass grid - strain gauges D and F.

Table 4.4 highlights the strain peak values and the wave amplitude of the strain collected by the strain gauges in position D and F on the three kinds of slabs.

Table 4.4 Peak value and wave amplitude of the three kinds of slabs (sin. test 1000s, 2 Hz).

SIN 2Hz (1000 seconds) – STRAIN GAUGES D			
Typology of Slab	***No Net***	***Steel Net***	***Glass Grid***
Peak value [μstrain]	203	422	266
Wave amplitude [μstrain]	0.7	1.9	1.1
SIN 2Hz (1000 seconds) – STRAIN GAUGES F			
Typology of Slab	***No Net***	***Steel Net***	***Glass Grid***
Peak value [μstrain]	-101	-277	-233
Wave amplitude [μstrain]	11.6	11.9	12.0

The analyses of the results were managed similarly to the one conducted on flexible pavements. In particular the data collected showed that the steel net could not highlight any benefit. These results were different from the ones collected during the laboratory investigations carried out on flexible real scale samples. These analyses could be evaluated and read considering different point of views. First of all, it is important to underline that this research work started at the University of Parma several years ago on flexible pavements and the laboratory investigations were set based on the results collected in-situ (see Introduction and Literature Review). This preliminary stage permitted to evaluate the shape of the real scale samples, the set-up of the test and the characteristic of the load, in order to carry out a reliable laboratory investigation. These further studies on rigid pavements with an asphalt concrete overlay were arranged following an analogous procedure, but they were not preceded by any studies in-situ on real pavements. The rigid slabs were not only different for the thickness of the layers or the material which composed the strata, but a discontinuity was set on the PCC base. In fact, a structural 6 mm joint split the bottom layer into two parts and the slabs were not homogeneous like the flexible ones. This fundamental detail could be considered a possible reason to explain the differences checked between the data collected in the laboratory with flexible slabs and the rigid ones. It is reasonable to presume that a bigger dimension of the multilayer slabs which comprehend a discontinuity could help the real scale samples to exhibit the effect of the reinforcing systems during the in service life. Obviously, this interpretation of the results collected could not be considered the unique one. In fact, it would be possible to simply state that the data collected did not show any benefits of the net positioned at the interface of asphalt overlay and PCC base.

This last consideration could be useful to criticize not only the shape of the slabs adopted, but also the position of the reinforce, or the use of the slurry seal layer in order to embed the net, or the test set-up itself. It is reasonable to state that further investigations that would reach the end of the in-service life, would have exhibited more clearly the benefits or the disadvantages of the reinforcing systems. In fact, on these rigid slabs with asphalt concrete overlay any preliminary analyses were not conducted, such as three point bending tests, in order to highlight the macroscopic effects of the nets. On the contrary, these kinds of investigations were carried out on flexible multilayer samples before setting the work of this research work (see Chapter 1, Paragraph 1.5).

However, the laboratory investigation explained in this chapter could be considered a starting point for further studies related to rigid pavement with an asphalt concrete overlay, starting from these criticisms. The first results collected in laboratory could represent the basis to organize a research in the field, in order to set a proper laboratory investigation, which could represent the suitable validation step for a possible Finite Element Analysis.

References.

[1] "Conto Nazionale del Ministero delle Infrastrutture e dei Trasporti" (www.mti.gov.it).

[2] Brown S. F., Thom N. H., Sanders P. J., (2001). "*A Study of Grid Reinforced Asphalt to Combat Reflection Cracking"*, Journal of the Association of Asphalt Paving Technologists, Vol. 70, pp 543-569.

[3] Rowe G. M., Lewandowski L. H., Grzybowski K. F., Rasche J., (2009). *"Development of the Beam on Elastic Foundation for the Evaluation of Geo-Synthetic Materials for Reinforcing of Asphalt Layers"*, Transportation Research Board, Washington D. C. (USA).

[4] Al-Qadi I.L., Appea A. K., (2003). *"Eight-Year of Field Performance of a Secondary Road Incorporating Geosynthetics at the Subgrade-Base Interface"*, Transportation Research Board, Washington D. C. (USA).

[5] Powell R. B., (2008). "*Installation and Performance of a Fiberglass Geogrid Interlayer on the NCAT Pavement Test Track"*, Pavement Cracking - Al-Qadi, Scarpas & Loizos Eds., Taylor & Francis Group, London.

[6] Al-Qadi I. L., Dessouky S. H., Kwon J., Tutumluer E., (2008). *"Geogrid in Flexible Pavements: Validated Mechanism"*, Transportation Research Board, Washington D. C. (USA).

[7] Perkins S., Cortez E. R., (2004). *"Evaluation of Base-Reinforced Pavements Using a Heavy Vehicle Simulator"*, Transportation Research Board, Washington D. C. (USA).

[8] Cox B. R., McCartney J. S., Wood C. M., Curry B., (2010). *"Performance Evaluation of Full-Scale Geosynthetic-Reinforced Flexible Pavements Using Field Cyclic Plate Load Tests"*, Transportation Research Board, Washington D. C. (USA).

[9] Antunes M. L., Fontul S., Pinelo A. M., (2008). *"Anti-reflective Cracking Solutions for Asphalt overlays: 8 years Performance Monitoring"*, Pavement Cracking - Al-Qadi, Scarpas & Loizos Eds., Taylor & Francis Group, London.

[10] Al-Qadi I. L., Elseifi M. A., Leonard D., (2003). *"Development of an Overlay Design Model for reflective Cracking with and without Steel Reinforcing Nettings"*. Journal of the Association of Asphalt Paving Technologists, Vol. 72, pp 388-423.

[11] Kwon J., Tutumluer E., Kim M., (2005). *"Development of a Mechanistic Model for Geogrid Reinforced Flexible Pavements"*, Transportation Research Board, Washington D. C. (USA).

[12] Kwon J., Tutumluer E., Kim M., (2005). "*Mechanistic Analysis of Geogrid Base Reinforcement in Flexible Pavement Considering Unbound Aggregate Quality"*, 5th International Conference on road and airfield Pavement and Technology (ICPT), Seoul, Korea.

[13] Kwon J., Tutumluer E., (2009). *"Geogrid Base Reinforcement with Aggregate Interlock and Modeling of the Associated Stiffness Enhancement in Mechanistic Pavement Analysis"*, Transportation Research Board, Washington D. C. (USA).

[14] Doh Y. S., Cho S. H., Lee K. H., Kim B. C., Kim K. W., (2005). *"Laboratory Evaluation of Geo-grid Effect on Reflection Cracking Control"*, 5th International Conference on road and airfield Pavement and Technology (ICPT), Seoul, Korea.

[15] Vervaecke F., Maeck J., Vanelstraete A., (2008). *"On Site Validation and Long Term Performance of Anti-cracking Interfaces"*, Pavement Cracking - Al-Qadi, Scarpas & Loizos Eds., Taylor & Francis Group, London.

[16] Kuo C. M., Hsu T. R., (2003). *"Traffic Induced Reflective Cracking on Pavements with Geogrid-Reinforced Asphalt Concrete Overlay"*, Transportation Research Board, Washington D. C. (USA).

[17] Baek J., Al-Qadi I. L., (2006). *"FE Modeling of Reflective Cracking Initiation and Propagation: Investigation of the Effect of Steel Reinforcement Interlayer on Retarding Reflective Cracking in HMA Overlay"*, Transportation Research Board, Washington D. C. (USA).

[18] Baek J., Al-Qadi I. L., (2009). *"Reflective Cracking: Modeling Fracture Behavior of Hot-Mix Asphalt Overlay with Interlayer System"*, Journal of the Association of Asphalt Paving Technologists, Vol. 78, pp 638-673.

[19] Baek J., (2010). *"Modeling Reflective Cracking Development in Hot-Mix Asphalt Overlays and Quantification of Control Techniques"*, PhD thesis, University of Illinois at Urbana-Champaign.

[20] Montepara A., Tebaldi G., Costa A., (2005). *"Performance Evaluation of a Surface Pavement Steel Reinforcement"*, 5th International Conference on road and airfield Pavement and Technology (ICPT), Seoul, Korea.

[21] Montepara A., Tebaldi G., Costa A., (2005). *"Study of a Rehabilitation Method with a Pavement Reinforcement System for Low Volume Roads"*, 7th International Conference on the Bearing Capacity of Roads, Norway.

[22] Montepara A., Tebaldi G., Costa A., (2007). *"A Surface Steel Reinforcement for Pavement Rehabilitation"*, special International Conference on road and airfield Pavement and Technology (ICPT) Symposium, Road Construction and Maintenance Technology in China, Baijing, China.

[23] Montepara A., Al-Qadi I. L., Tebaldi G., Costa A., Baek J., Rota V., (2007). *"Loading Responses Comparison Between Laboratory Testing and Numerical Modelling for Hot-Mix Asphalt Specimens"*, IV Convegno Internazionale Società Italiana Infrastrutture Viarie (SIIV), Palermo, Italy.

[24] Montepara A., Tebaldi G., Costa A., (2009). *"Pavement Rehabilitation Using Steel Reinforcement"*, The Sixth International Conference on Maintenance and Rehabilitation of Pavements and Technological Control (MAIREPAV 6), Torino, Italy.

[25] Centro Interuniversitario di Ricerca Stradale (CIRS). *"Norme tecniche di tipo prestazionale per capitolati speciali d'appalto"*, Ministero delle Infrastrutture e dei Trasporti, Ispettorato per la Circolazione e la Sicurezza Stradale.

[26] Montepara A., Rastelli, S. and Rota V. (abstract accepted and paper submitted on December 2010). *"Laboratory Compaction of Asphalt Mixtures: the Use of a Slab Heavy Compactor"*, 5th International Conference Bituminous Mixtures and Pavements, Thessaloniki, Greece.

[27] Al-Qadi I. L., Carpenter S. H., Leng Z., Ozer H., Trepanier J. S. (2008). *"Tack Coat Optimization for HMA Overlay"*, Research Report FHWA-ICT-08-023, Illinois Center for Transportation, USA.

[28] Santagata F. A., Partl M. N., Ferrotti G., Canestrari F., Flisch A., (2008). *"Layer Characteristics Affecting Interlayer Shear Resistance in Flexible Pavements"*, Journal of the Association of Asphalt Paving Technologists, Vol. 77, pp 221-256.

[29] Read J. M., Collop A. C., (1997). *"Practical Fatigue Characterization of Bituminous*

Paving Mixtures", Journal of the Association of Asphalt Paving Technologists, Vol. 66, pp 74-108.

[30] Ferrari P., Giannini F., (1996). *"Corpo Stradale e Pavimentazioni"*, (Vol. 2), Ed. ISEDI.

[31] Khalid H. A.,(2003). *"Assessing the Potential in Fatigue of a Dense Wearing Course Emulsified Bitumen Macadam"*, 6th RILEM Symposium - Performance Testing and Evaluation of Bituminous Materials, Zurich, Swiss.

[32] Walubita L. F., Martin A. E., Jung S. H., Glover C. J., Cleveland G. S., Lytton R. L., (2005). *"Two Approaches to Predict Fatigue Life of Hot Mix Asphalt Concrete Mixtures"*, Transportation Research Board, Washington D. C. (USA).

[33] Di Benedetto H., De la Roche C., Baaj H., Pronk A., Lundström R., (2004). *"Fatigue of Bituminous Mixtures"*, Material and Structures, Vol. 37, pp 202-216.

[34] Abaqus. (2009). Abaqus /Standard User's Manual Version 6.9, ABAQUS, Inc., Palo Alto, CA, (USA).

[35] Von Quintus H. L., (1994). *"Performance Prediction Models in the Superpave Mix Design System"*, Strategic Highway Research Program (SHRP - A - 699).

[36] Park S. W., (2001). *"Analytical Modeling of Viscoelastic Dampers for Structural and Vibration Control"*, International Journal of Solids and Structures, Vol. 38, pp 8065-8092.

[37] Christensen D. W. Jr., Pellinen T., Bonaquist R. F., (2003). *"Hirsh Model for Estimating the Modulus of Asphalt Concrete"*, Journal of the Association of Asphalt Paving Technologists, Vol. 72, pp 97-121.

[38] Ferry J. D.(1980). *"Viscoelastic Properties of Polymers"*, John Wiley & Sons Eds.

[39] Jacobs M. M. J., (1995). *"Crack Growth in Asphaltic Mixes"*, PhD thesis Delft University of Technology.

[40] Francken L., Vanelstraete A., (1996). *"Complex Moduli of Bituminous Binder and Mixes Interpretation and Evaluation"*, Eurasphalt & Eurobitume Congress, Strasbourg, France.

[41] Pellinen T. K., Witczak M. W., (2002). *"Stress Dependent Master Curve Construction for Dynamic (Complex) Modulus"*, Journal of the Association of Asphalt Paving Technologists, Vol. 71, pp 281-309.

[42] Francken L., Vanelstraete A., (1997). *"Complex Moduli of Bituminous Materials: a*

Rational Method for the Interpretation of test results", Mechanical Tests for Bituminous Materials, Di Benedetto & Francken Eds., RILEM.

[43] Antonakakis J. N., Bhargava P., Chuang K. C., Zehnder A. T., (2006). *"Linear Viscoelastic Properties of HFPE-II-52 Polyimide"*, Journal of Applied Polymer Science, Vol. 100, pp3255-3263.

[44] Gibson N. H., Schwartz C. W., Schapery R. A., Witczak M. W., (2003). *"Viscoelastic, Viscoplastic, and Damage Modeling of Asphalt Concrete in Unconfined Compression"*, Transportation Research Board, Washington D. C. (USA).

[45] Elseifi M. A., Dessouky S. H., Al-Qadi I. L., Yang S. H., (2006). *"A Viscoelastic Model to Describe the Mechanical Responses of Bituminous Sealants at Low Temperature"*, Transportation Research Board, Washington D. C. (USA).

[46] Yoo P. J., Al-Qadi I. L., (2007). *"Effect of Transient Dynamic Loading on Flexible Pavements"*, Transportation Research Board, Washington D. C. (USA).

Acknowledgement.

At the end of this work, I would like to express my gratitude to my advisor Prof. Antonio Montepara and to Dr. Gabriele Tebaldi, who introduce me Prof. Imad L. Al-Qadi. His contribution was fundamental to achieve this objective and my experience at the University of Illinois was very important from different points of view. Special thanks go to Dr. Arianna Costa, who helped me a lot through this long route. Our long discussions were precious to me and she never stopped to motivate me.

I would like to thank my colleagues, first of all my office mate Dr. Silvia Rastelli, the students who worked with me and all the people I could meet all over the world.

Finally, I am very grateful to my family, who always supported me.